USGS
science for a changing world

Studies by the U.S. Geological Survey in Alaska, Volume 15

# Facies Variation within Outcrops of the Triassic Shublik Formation, Northeastern Alaska

Professional Paper 1814–H

U.S. Department of the Interior
U.S. Geological Survey

**Cover.** Photograph of Shublik Formation at its type section along Fire Creek, North Slope, Alaska. Photograph by D.W. Houseknecht, U.S. Geological Survey.

# Facies Variation within Outcrops of the Triassic Shublik Formation, Northeastern Alaska

By Julie A. Dumoulin, Katherine J. Whidden, William A. Rouse, and Christina DeVera

Studies by the U.S. Geological Survey in Alaska, Volume 15

Professional Paper 1814–H

**U.S. Department of the Interior**
**U.S. Geological Survey**

U.S. Geological Survey, Reston, Virginia: 2024



Suggested citation:
Dumoulin, J.A., Whidden, K.J., Rouse, W.A., and DeVera, C., 2024, Facies variation within outcrops of the Triassic Shublik Formation, northeastern Alaska, *in* Dumoulin, J.A., ed., Studies by the U.S. Geological Survey in Alaska, v. 15: U.S. Geological Survey Professional Paper 1814-H, 49 p., https://doi.org/10.3133/pp1814H.

Associated data for this publication:
Dumoulin, J.A., Whidden, K.J., Rouse, W.A., and DeVera, C., 2023, Geochemical data from selected Triassic rock samples in northeastern Alaska: U.S. Geological Survey data release, https://doi.org/10.5066/P9FAGE8O.

ISSN 2330-7102 (online)

# Contents

## Figures

## Tables

# Conversion Factors

U.S. customary units to International System of Unit

| Multiply | By | To obtain |
|---|---|---|
| | Length | |
| inch (in.) | 2.54 | centimeter (cm) |
| inch (in.) | 25.4 | millimeter (mm) |
| foot (ft) | 0.3048 | meter (m) |
| mile (mi) | 1.609 | kilometer (km) |

International System of Units to U.S. customary units

| Multiply | By | To obtain |
|---|---|---|
| | Length | |
| centimeter (cm) | 0.3937 | inch (in.) |
| millimeter (mm) | 0.03937 | inch (in.) |
| meter (m) | 3.281 | foot (ft) |
| kilometer (km) | 0.6214 | mile (mi) |

Temperature in degrees Celsius (°C) may be converted to degrees Fahrenheit (°F) as follows:

$$°F = (1.8 \times °C) + 32.$$

Temperature in degrees Fahrenheit (°F) may be converted to degrees Celsius (°C) as follows:

$$°C = (°F - 32) / 1.8.$$

# Datum

Horizontal coordinate information is referenced to the North American Datum of 1927 (NAD27)

# Abbreviations

| | |
|---|---|
| CAI | color alteration index |
| GR | gamma-ray |
| HPS | highly phosphatic strata |
| ICP-OES-MS | inductively coupled plasma-optical emission spectroscopy-mass spectroscopy |
| LC | lower clastic unit |
| LC1 | lower clastic unit 1 |
| loc. | locality |
| MCC | middle carbonate-chert unit |
| MCC1 | middle carbonate-chert unit 1 |
| MCC2 | middle carbonate-chert unit 2 |
| MCC3 | middle carbonate-chert unit 3 |
| mfs | maximum flooding surface |
| µm | micrometer |
| ppm | parts per million |
| p-XRF | portable X-ray fluorescence |
| REE | rare earth element |
| RST | regressive systems tract |
| S1 | transgressive-regressive (T-R) sequence 1 |
| S2 | transgressive-regressive (T-R) sequence 2 |
| S3 | transgressive-regressive (T-R) sequence 3 |
| S4 | transgressive-regressive (T-R) sequence 4 |
| S5 | transgressive-regressive (T-R) sequence 5 |
| TOC | total organic carbon |
| T-R | transgressive-regressive |
| TST | transgressive systems tract |
| UCC | upper clastic-carbonate unit |
| UCC1 | upper clastic-carbonate unit 1 |
| USGS | U.S. Geological Survey |

**Studies by the U.S. Geological Survey in Alaska, volume 15**
Edited by Julie A. Dumoulin
U.S. Geological Survey Professional Paper 1814–H
[Also see https://pubs.usgs.gov/AK_studies/]

# Facies Variation within Outcrops of the Triassic Shublik Formation, Northeastern Alaska

By Julie A. Dumoulin, Katherine J. Whidden, William A. Rouse, and Christina DeVera

## Abstract

The Shublik Formation (Middle to Upper Triassic) is a heterogeneous unit that is a major hydrocarbon source rock in northern Alaska and the largest known Triassic phosphate accumulation in the world. This formation, which occurs in the subsurface and crops out within the Arctic Alaska basin, was deposited on a gently sloping ramp along the northwestern Laurentian margin. In this study, we document spatial and temporal facies variations within the Shublik and the overlying Karen Creek Sandstone (Upper Triassic) through 19 outcrop localities in the northeastern Brooks Range. New organic and inorganic geochemical data from these localities support and extend our sedimentologic and petrographic findings. The petrographic data come from an analysis of more than 900 thin sections, whereas age constraints come mainly from species of the pelecypod genera *Daonella*, *Halobia*, *Eomonotis*, and *Monotis*. Thirteen sites make up a main outcrop belt within which facies of the Shublik are spatially consistent but show marked vertical changes. Six additional outcrops located south of the main belt contain more distal facies of the Shublik that accumulated farther from land.

Exposures of the Shublik Formation in its main outcrop belt are divisible into five informal lithologic units, each of which formed during a distinct transgressive to regressive sequence. The basal unit of the Shublik (Anisian? to Ladinian; Middle Triassic) is quartz siltstone to very fine grained sandstone that is locally phosphatic. The three middle units (Ladinian to middle Norian; Middle to Upper Triassic) contain various proportions of siliciclastic, carbonate, phosphatic, and organic material. The uppermost unit (middle to upper Norian; Upper Triassic) is mainly shale and mudstone. Highly phosphatic strata (10–34 percent phosphorus pentoxide) are chiefly Ladinian and lower to middle Norian. Highly phosphatic Ladinian strata have been transported, are granular, and formed during transgression and early regression. In contrast, highly phosphatic Norian strata include event beds and hardgrounds, contain displaced and in situ phosphate peloids and nodules, and cap regressive parasequences. The total organic content reaches 4.97 weight percent in the main belt and is highest in muddy beds, which are found mainly in the lower parts of the three middle units. Distal sections of the Shublik are typically finer grained, more organic-rich (total organic content as high as 6.33 weight percent), and less fossiliferous than those in the main belt.

Both temporal and spatial factors shaped facies in the Shublik Formation. Shublik strata accumulated at a time of reduced tectonic activity in Arctic Alaska, resulting in diminished siliciclastic input. Marine upwelling along the northwestern Laurentian margin facilitated the development of heterozoan carbonates, as well as local concentrations of phosphatic and organic matter. Large- and small-scale eustatic cycles also affected this margin and provided further controls on Shublik facies distribution.

## Introduction

The Shublik Formation (Middle to Upper Triassic) is a mixed siliciclastic-carbonate-phosphatic unit extending widely across the subsurface of the North Slope of Alaska and cropping out chiefly in the northeastern Brooks Range (fig. 1). The Shublik is a major source rock for the Prudhoe Bay Oil Field and other hydrocarbon accumulations in northern Alaska (Peters and others, 2006), and is also a potential self-sourced resource play (Houseknecht and others, 2012; Hosford Scheirer and Bird, 2020). In addition, this formation is the largest known Triassic phosphate accumulation in the world (Cathcart, 1991; Trappe, 1994). The thickness of the Shublik ranges regionally from <15 meters (m) to >180 m (Bird, 1988; Kupecz, 1995; Hulm, 1999; Parrish and others, 2001a; Kelly, 2004; Kelly and others, 2007; Hutton, 2014; Whidden and others, 2018; Houseknecht, 2019; Rouse and others, 2020). The formation was deposited on a shallowly dipping ramp (part of the Arctic rifted margin of Laurentia) at a paleolatitude of ~45–60° (Scotese, 2002; Colpron and Nelson, 2011; Houseknecht, 2019).

This study is part of a broader U.S. Geological Survey (USGS) research project to examine Mesozoic and Cenozoic depositional systems and petroleum resources across northern Alaska. In this report, we summarize outcrop facies variations of the heterogeneous Shublik Formation using the stratigraphic framework of Whidden and others (2018). This framework, along with spectral gamma-ray (GR) correlations (Rouse and others, 2020), indicates that the Middle and Upper Triassic strata of northern Alaska represent six transgressive-regressive sequences. These sequences correlate well with those recognized in other Arctic basins, implying regional and perhaps global significance (fig. 2) (Whidden and others, 2018). Identifying detailed patterns of facies variation within the Shublik in northeastern Alaska allows us to better

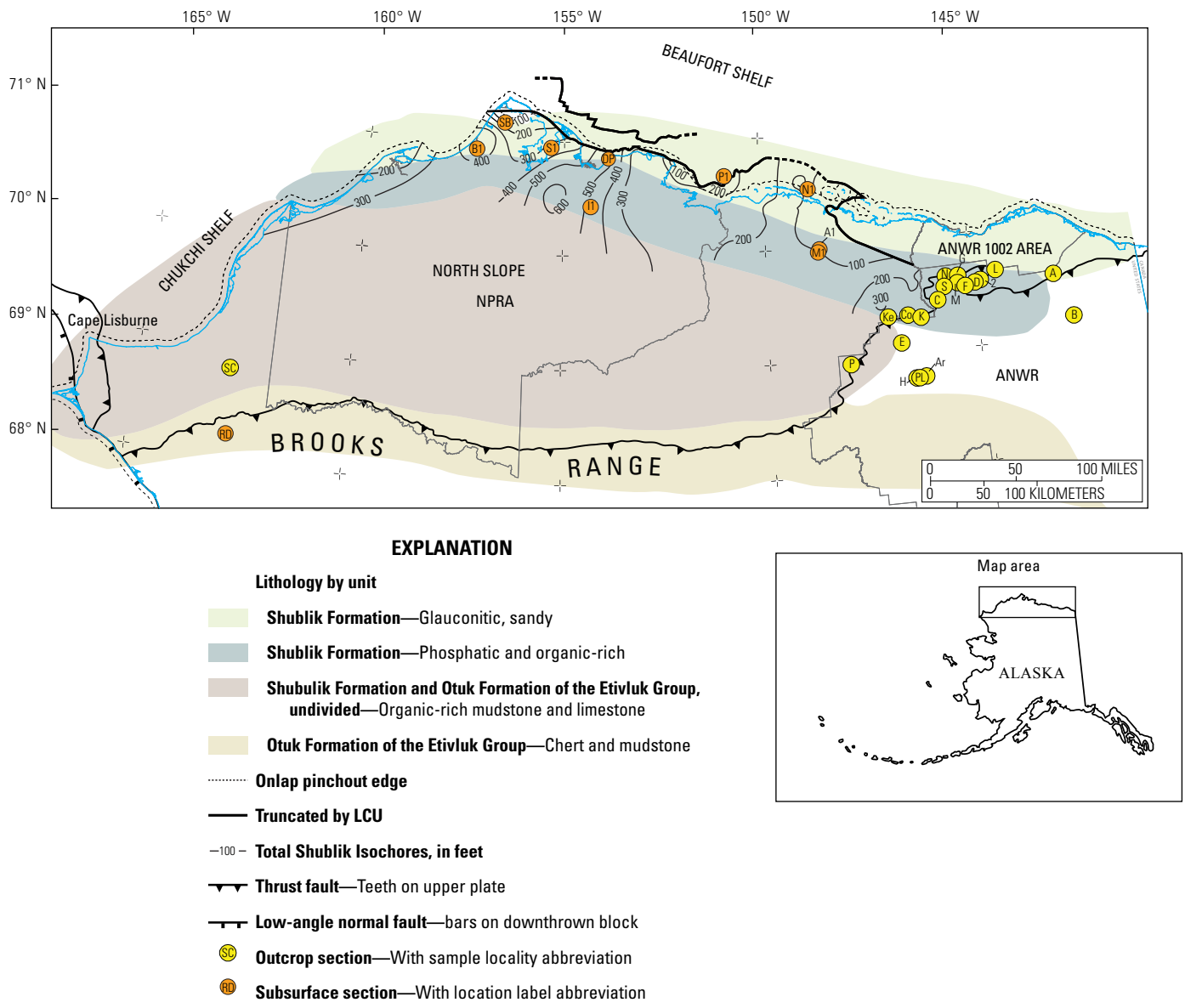


**Figure 1.** Map of generalized lithologies and isochores of selected Triassic rocks across northern Alaska. Outcrop and subsurface sections are discussed in the text (see table 1 for additional data). The Shublik Formation crops out mainly in the northeastern Brooks Range but is widely distributed in the subsurface of the North Slope. The Otuk Formation of the Etivluk Group crops out from Cape Lisburne to the southeastern Brooks Range. The transition between the two formations has not been precisely located. Lithologies modified from Kelly and others (2007); isochores, pinch-out lines, and truncation lines from Rouse and others (2020). The Arctic Alaska basin extends from north of the front of Brooks Range across the Chukchi and Beaufort Shelves (see fig. 1 of Houseknecht, 2019). Outcrop section names: A, Aichilik River; Ar, Arctic D–4 quadrangle; B, Bathtub ridge; C, Cache Creek; Co, Cobble Creek; D, Dodo Creek; E, Echooka River; F, Fire Creek; G, Golden Eagle; H, Helicopter ridge; K, Kavik River; Ke, Kemik Creek; L, Last Creek; M, Mesa; N, North Sadlerochit; P, Philip Smith Mountains; PL, Porcupine Lake West; S, Spire; SC, Surprise Creek; 2, Camp 263 Creek. Main outcrop belt extends from Ke east to A and north to G. Strata at Surprise Creek are transitional between the Shublik and Otuk Formations (Dumoulin and others, 2022). Subsurface section names: A1, Alcor 1 well; B1, Brontosaurus 1 well; DP, Drew Point 1 well; I1, Ikpikpuk 1 well; M1, Merak 1 well; N1, Northstar 1 well; P1, Phoenix 1 well; RD, Red Dog Mine district; S1, Simpson 1 well; SB, South Barrow 3 well. Other abbreviations: ANWR, Arctic National Wildlife Refuge; LCU, Lower Cretaceous unconformity; NPRA, National Petroleum Reserve in Alaska.

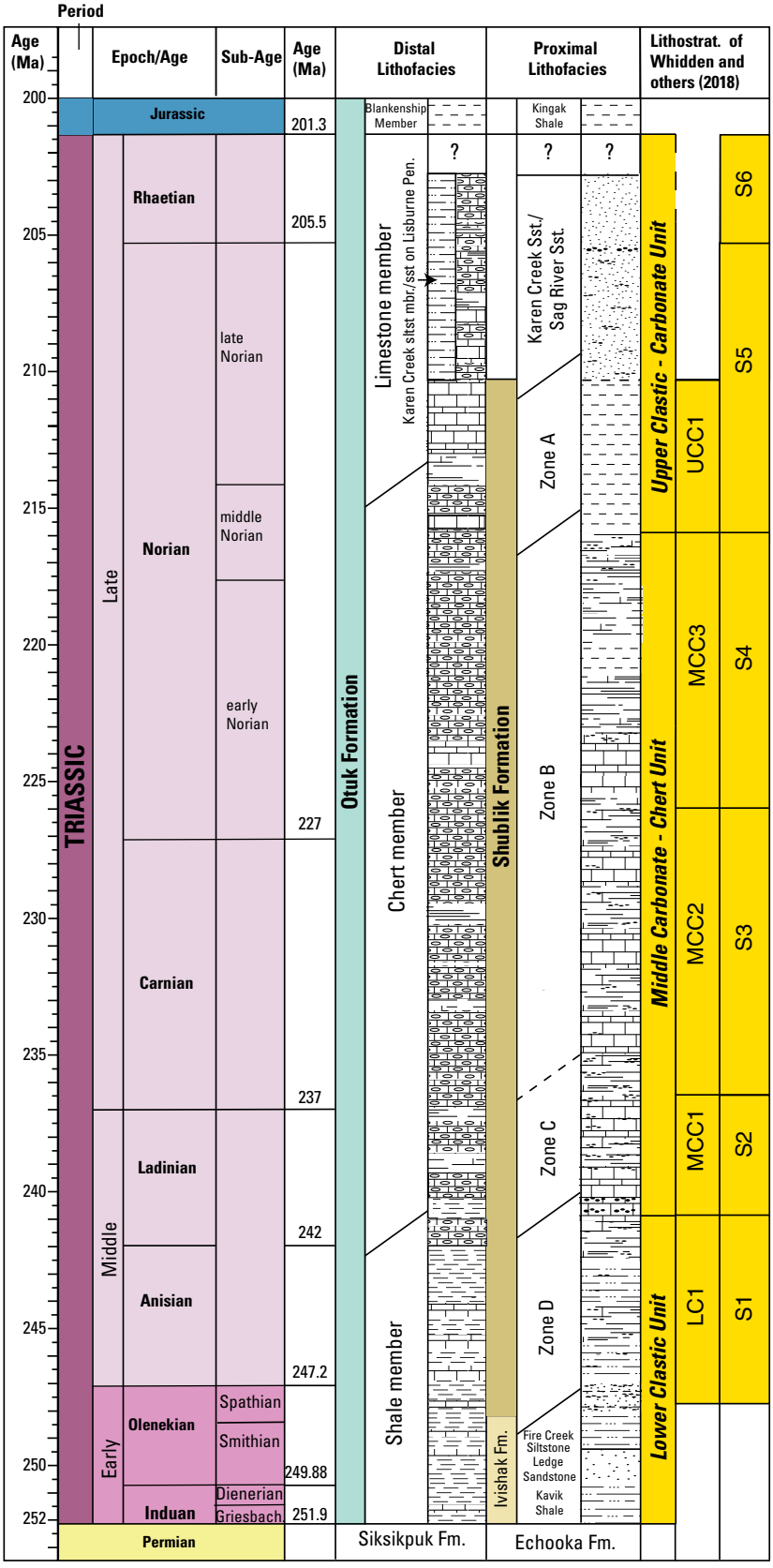


**EXPLANATION**

- Phosphatic layer
- Mudstone and siltstone
- Calcareous mudstone and siltstone
- Limestone
- Chert
- Sandstone

**Figure 2.** Stratigraphic section and nomenclature for Triassic strata in northern Alaska, modified from Whidden and others (2018). The age of the base of the Shublik Formation is considered to be earliest Middle Triassic (Detterman and others, 1975) but it is poorly constrained and could be older; see text for discussion. Absolute ages of boundaries between Ages are from Walker and Geissman (2022), except for the boundary between the Norian and Rhaetian Ages, which is based on data from Wotzlaw and others (2014), and the boundary between the Induan and Olenekian Ages, which is from Ogg and others (2020). Only selected subages are shown. Boundaries between subages in the Norian based on data in McRoberts (2010) and Ogg and others (2020); boundaries between subages in the Early Triassic are from Ogg and others (2020). Zone A–D designations are from Kupecz (1995). Informal Karen Creek siltstone member of the Otuk Formation of Bodnar (1984) is found in the central Brooks Range, and informal sandstone member of the Otuk Formation of Dumoulin and others (2022) is found at Cape Lisburne. Angled lines represent possible time-transgressive unit boundaries; dashed lines indicate positional uncertainty. Boundaries between transgressive-regressive sequences are transgressive surfaces. Queried where unknown or uncertain. Ma, mega-annum; Griesbach, Griesbachian; Fm., Formation; sltst, siltstone; mbr., member; Pen., Peninsula; sst, sandstone; Lithostrat., lithostratigraphy; LC, lower clastic unit; MCC, middle carbonate-chert unit; UCC, upper clastic-carbonate unit; S, sequence.

constrain the distribution of source-rock facies and highly phosphatic strata, and to relate these patterns to geographic, paleoenvironmental, and tectonic causal factors.

## Geologic Setting

The Shublik Formation and its distal (deposited farther offshore) partial-equivalent, the Otuk Formation of the Etivluk Group (fig. 2), form the upper part of the Mississippian to Triassic Ellesmerian tectonostratigraphic sequence (for example, Hubbard and others, 1987; Moore and others, 1994; Houseknecht, 2019). This sequence accumulated within the Arctic Alaska basin, which constitutes the eastern part of the Arctic Alaska-Chukotka microplate (Houseknecht, 2019, and references therein). The Ellesmerian sequence was deposited along the rifted margin of Laurentia, which faced south in present-day coordinates, during the opening of the Angayucham Ocean basin; subsequent rift-opening of the Canada Basin in the Jurassic to Early Cretaceous terminated Ellesmerian sequence deposition (Houseknecht, 2019). Topographic features within the Arctic Alaska basin include the Hanna Trough (a failed rift system initiated during the Devonian [Sherwood and others, 2002]) and areas of positive relief such as the Barrow high (equivalent to the basement arch of Homza and others [2020]) (see also Houseknecht, 2019; Rouse and others, 2020).

Geographic variation of lithologies within the Shublik Formation was recognized by Parrish and others (2001a, b), who delineated five lithologic zones oriented roughly parallel to the northern Alaska coastline: Three main zones, from north to south, contain chiefly glauconitic, phosphatic, and organic-rich lithologies; two additional transitional zones separate these main zones. Figure 1 shows these lithologic zones as modified by Kelly (2004) and Kelly and others (2007), who simplified the original scheme by eliminating the transitional zones (fig. 1). Our studies found additional complexities of lithologic variation within the Shublik Formation that are described herein.

Vertical lithologic changes within outcrop sections of the Shublik Formation were noted by Detterman and others (1975), who divided the formation into two informal siliciclastic-dominated members separated by a carbonate-rich middle member. Following Whidden and others (2018), this report further refines that scheme into five informal lithostratigraphic units (fig. 2).

The transgressive-regressive (T-R) sequences of the Shublik Formation, as defined by Whidden and others (2018) and Rouse and others (2020), each span ~5 to 10 million years (fig. 2), suggesting the cycles are second order (Haq and Schutter, 2008). These sequences generally consist of a thin transgressive systems tract (TST) and a thicker regressive systems tract (RST) separated by a maximum flooding surface (mfs); the RSTs comprise one or more coarsening- and (or) thickening-upward parasequence(s).

The Shublik Formation outcrop sections discussed herein have thermal indices indicative of temperatures above the window for oil preservation. Vitrinite reflectance values of 1.71 and 2.94 are reported from the Shublik Formation at the Last Creek and Fire Creek localities (fig. 1), respectively (Bird and others, 1999). Conodonts from Shublik sections at Cobble Creek (fig. 1) and Fire Creek have color alteration index (CAI) values of 3.5 and 4, respectively (J.E. Repetski, USGS, written commun., 2014), indicating temperatures of 150–250 degrees Celsius (Watts and others, 1994). These CAIs are slightly lower than the CAI of 4.5 reported from a sample in the Fire Creek area by Bird and others (1999), but still equate to overmature conditions for petroleum (see fig. VR1 of Bird and others, 1999).

## Materials, Methods, and Terminology

The focus of this study is the Shublik Formation, but for comparative purposes, we also provide information on the upper part of the underlying Ivishak Formation of the Sadlerochit Group (the Fire Creek Siltstone Member) and the overlying Karen Creek Sandstone (fig. 2). Data were collected from 19 outcrop localities in the northeastern Brooks Range (fig. 1; table 1). Sections were measured with measuring tape, Jacob's staff, and Brunton compass at 12 of these sites; the other 7 sections were described and sampled but were not measured due to time constraints and (or) poor exposure. However, a suite of representative lithologic samples was taken from sections at all 19 study localities. Petrographic data come from an analysis of more than 900 thin sections. Selected samples from many of the outcrop localities (table 1) were analyzed for total organic carbon (TOC) and for major and trace elements using inductively coupled plasma-optical emission spectroscopy-mass spectroscopy (ICP-OES-MS). Major and trace element values for some elements in samples from Fire Creek were also determined using a Thermo Niton handheld portable X-ray fluorescence (p-XRF) unit. Some samples, mainly from the Last Creek, Mesa, and Cache Creek sections (fig. 1), were analyzed only for TOC. Selected geochemical data are summarized and discussed in the text and compared to previously reported data (Detterman, 1970; Kelly, 2004). TOC, ICP-OES-MS, and p-XRF data are published in an accompanying data release by Dumoulin and others (2023). TOC data are reported in weight percent. Aluminum, calcium, silicon, phosphorus, iron, and sulfur concentrations are reported in percent. Molybdenum, uranium, and cesium concentrations are reported in parts per million (ppm). Unpublished reports on fossils mentioned herein, as well as field notes that contain additional details on the measured and spot-sampled sections we describe, are reposited in the Technical Data Unit (https://www.usgs.gov/centers/alaska-science-center/science/alaska-technical-data-unit-field-records-archives) of the USGS Alaska Science Center, Anchorage, Alaska, and copies can be made available upon

**Table 1.** Triassic Shublik Formation localities in northeastern Alaska.

[See figure 1 for locality map. Total organic carbon (TOC) and inductively coupled plasma-optical emission spectroscopy-mass spectroscopy (ICP) data available in Dumoulin and others (2023); additional details on measured and spot-sampled sections available upon request in field notes reposited in the U.S. Geological Survey (USGS) Technical Data Unit of the Alaska Science Center, Anchorage, Alaska (https://www.usgs.gov/centers/alaska-science-center/science/alaska-technical-data-unit-field-records-archives). Units from oldest to youngest: FC, Fire Creek Siltstone of Ivishak Formation; LC1, lower clastic unit 1; MCC1, middle carbonate-chert unit 1; MCC2, middle carbonate-chert unit 2; MCC3, middle carbonate-chert unit 3; UCC1, upper clastic-carbonate unit 1; KC, Karen Creek Sandstone. Queries indicate uncertainty. Data sources: B, Bergquist (1966); Br, Brosgé and others (2001); C, Camber (1994); D1, Detterman (1970); D2, Detterman and others (1975); Df, Detterman (USGS, unpub. data, 1970); H, Hutton (2014); Ke, Kelly (2004) and Kelly and others (2007); Kn, Knox (2018); L, Leffingwell (1919); P, Parrish and others (2001a, b); R, Rouse and others (2020); S, Sable (USGS, unpub. data, 1948); T, Tourtelot and Tailleur (1971); Wd, Whidden and others (2018); Wt, Whittington (USGS, unpub. data, 1952). Other abbreviations: l, lower; LCU, Lower Cretaceous unconformity; MS, measured section; Paleo, paleontologic sample; spot, spot samples; TS, thin section; u, upper; —, not applicable]

| Locality [letter or number designation] | Latitude N., longitude W. | Unit(s) studied | Study method | Data | Other studies | Remarks |
|---|---|---|---|---|---|---|
| North Sadlerochit [N] | 69°38.28’, 145°38.79’, | MCC2 (u) | Spot | TOC, TS | — | — |
| Golden Eagle [G] | 69°38.03’, 145°20.73’ | LC1 (u)–MCC2 (l) | MS | ICP, Paleo, TOC, TS | — | LCU is top of section |
| Last Creek [L] | 69°37.81’–37.90’, 144°26.06’–26.52’ | FC, LC1–MCC2 (l) | MS | ICP, Paleo, TOC, TS | Kn, P | LCU is top of section |
| Mesa (lower) [M] | 69°33.86’–33.90’, 145°23.55’–23.60’ | MCC2 (u)–MCC3 (l) | MS | Paleo, TOC, TS | — | — |
| Mesa (upper) [M] | 69°33.55’, 145°21.75’ | UCC1?, KC | Spot | Paleo, TOC, TS | — | — |
| Camp 263 Creek [2] | 69°33.76’, 144°49.25’ | MCC2–3 | MS (MCC2), spot (MCC3) | ICP, TOC, TS | L | Both units only partly exposed |
| Dodo Creek1 [D] | 69°33.22’–33.85’, 144°57.33’–57.93’ | FC, LC1–UCC1, KC | Spot | ICP, TOC, TS | B, S, Wt | — |
| Spire [S] | 69°33.08’, 145°42.54’ | FC, LC1–UCC1 (l) | MS | ICP, Paleo, TOC, TS | — | — |
| Fire Creek1 [F] | 69°32.12’, 145°12.20’ | FC, LC1–UCC1, KC | MS (MCC1–3), spot (other units) | ICP, Paleo, TOC, TS | D1, D2, H, Ke, Kn, P, R, T, Wd | — |
| Aichilik River1 [A] | 69°31.40’, 143°02.67’ | FC, LC1–UCC1, KC | MS | ICP, TOC, TS | T | — |
| Cache Creek [C] | 69°26.33’, 145°54.29’ | MCC2 (u)–KC | MS | ICP, Paleo, TOC, TS | T | — |
| Kemik Creek [Ke] | 69°20.22’–20.23’, 147°07.78’–07.89’ | LC1–MCC2 | Spot | ICP, TOC, TS | — | — |
| Cobble Creek [Co] | 69°19.77’–19.82’, 146°39.44’–39.56’ | FC, LC1–MCC3 (l) | MS (LC1), spot (other units) | ICP, Paleo, TOC, TS | — | — |
| Kavik River [K] | 69°18.26’, 146°21.21’ | LC1–MCC1 | Spot | ICP, Paleo, TOC, TS | Kn, P | Structurally disturbed |
| Bathtub Ridge (lower) [B] | 69°07.71’, 142°41.61’ | FC, LC1, MCC3? | Spot | ICP, TOC, TS | C | Structurally disturbed |
| Bathtub Ridge (upper) [B] | 69°07.69’, 142°45.84’ | MCC3 | Spot | ICP, TOC, TS | C | Unit partly exposed |
| Echooka River [E] | 69°06.04’–06.17’, 146°52.60’–52.78’ | FC, LC1–MCC3, KC | MS | ICP, TOC, TS | D2, Df | — |
| Philip Smith Mountains [P] | 68°56.76’, 148°07.30’ | LC1, MCC | Spot | TS | — | Deformed, foliated |
| Arctic D–4 Quadrangle [Ar] | 68°46.84’, 146°23.06’ | MCC3 | Spot | TS | Fossil locality 26 in Br | Deformed, foliated |
| Helicopter Ridge [H] | 68°46.55’–46.59’, 146°36.54’–36.72’ | FC, MCC | MS | TOC, TS | Fossil locality 22 in Br | Deformed, foliated |
| Porcupine Lake West [PL] | 68°46.52’, 146°32.30’ | MCC | MS | TS | Fossil locality 15 in Br | Deformed, foliated |

request (Dumoulin, USGS, unpub. data, 2012, 2014, 2015, 2018, 2019; Whidden, USGS, unpub. data, 2012, 2014, 2015).

We define highly phosphatic strata (HPS) as strata with ≥10 weight percent phosphorus pentoxide (≥4.4 percent phosphorus), and we follow Patton and Matzko (1959) and Trappe (1998) in using the term "phosphorite" for rocks having ≥18 weight percent phosphorus pentoxide (≥7.86 percent phosphorus). Phosphate in the Shublik Formation occurs as (1) peloids and nodules that formed in situ; (2) firmgrounds and hardgrounds that preserve multiple cycles of phosphatization, erosion, and redeposition; and (3) silt- to cobble-sized clasts that have been transported (fig. 3). The nodules typically have an elongate shape parallel to bedding, an internal texture like that of the surrounding matrix, and (or) diffuse boundaries that indicate in situ formation (fig. 3*A–C*) (see also the pristine phosphate of Föllmi, 1996). Other phosphate masses appear to have been transported; these are generally rounded, have internal textures that differ from both the surrounding matrix and adjacent phosphate clasts, and (or) occur in laminated to cross-laminated or graded beds along with similar-sized clasts of quartz or chert (fig. 3*D–G*) (see also the condensed and allochthonous phosphatic sediments of Föllmi, 1996). Complex intermixtures of these end-member phosphate types are commonly observed (fig. 3*C*, *F*) (see also the hybrids of Föllmi, 1996).

Many beds in the Shublik Formation have sedimentary structures (cross-lamination or scours) and (or) textural features (broken or rounded clasts) that indicate the effects of energetic depositional processes. The term "event bed" is used herein to refer to such strata, which may have formed through a variety of mechanisms including storms or turbidity currents (for example, Whidden and others, 2019b).

## Stratigraphic and Structural Framework

Whidden and others (2018) divided the Triassic strata of northern Alaska into three informal units: a lower clastic unit (LC), a middle carbonate-chert unit (MCC), and an upper clastic-carbonate unit (UCC) (fig. 2). LC consists of an informal lower clastic unit 1 (LC1) (comprising the lower part of the Shublik Formation) and all the underlying Ivishak Formation (fig. 2). Three informal subdivisions are recognized within MCC: middle carbonate-chert unit 1 (MCC1), middle carbonate-chert unit 2 (MCC2), and middle carbonate-chert unit 3 (MCC3), in ascending order. UCC encompasses an informal upper clastic-carbonate unit 1 (UCC1) (the upper part of the Shublik Formation) and overlying siliciclastic strata of the Karen Creek and Sag River Sandstones (fig. 2). The definitions of these Shublik Formation units are based chiefly on the sections at Fire Creek and the Tenneco Phoenix 1 well (fig. 1) (Whidden and others, 2018). Recognition of these units in other sections relies on lithostratigraphy augmented by fossil data.

Triassic facies patterns were altered by tectonic events of the Brooks Range orogeny during the Jurassic, Cretaceous, and Cenozoic (for example, Moore and others, 1994; Houseknecht, 2019). The Shublik Formation in most of the subsurface is autochthonous and essentially undeformed, but Shublik outcrops in the northeastern Brooks Range are parautochthonous and have been thrust tens of kilometers northward during contractional deformation associated with this orogeny (for example, Cole and others, 1999; Moore, 1999).

**Figure 3 (page 7).** Images of phosphate in the Triassic Shublik Formation, northeastern Alaska. *A*, Thin section scan from the Helicopter ridge locality showing an elongate, in situ phosphate nodule parallel to bedding within a fine-grained limestone containing sparse flat-clam fragments; unit uncertain (likely the middle carbonate-chert unit). *B*, Thin section scan from the Aichilik River locality of incipient, in situ phosphate nodules with diffuse boundaries (i); lower clastic unit 1 (LC1). *C*, Thin section scan from the Spire locality of displaced phosphate clasts (p) in an event bed that also contains incipient, in situ phosphate masses with diffuse boundaries (i); middle carbonate-chert unit 2. *D*, Thin section scan from the Kavik River locality of displaced phosphate clasts (p) that contain rare to abundant white quartz silt. Other clasts are mainly chert, several of which have dark, pyritic rims. Sample is from conglomerate at the base of LC1. *E*, Thin section scan from the Last Creek locality showing irregular layers of phosphate silt and sand (ps) that have been transported alternating with limy siltstone layers (c); middle carbonate-chert unit 1. Calcite is stained pink on right side of image. *F*, Photomicrograph from the Mesa locality of displaced (and some possibly in situ) phosphate peloids in an event bed that also contains a displaced phosphate clast (p), a phosphate-filled gastropod steinkern (g), and bioclasts, including a belemnoid rostrum (b); middle carbonate-chert unit 3. *G*, Photomicrograph from the Cobble Creek locality of displaced phosphate peloids and phosphate-coated quartz grains in a very fine grained quartz sandstone bed (phosphatic sandstone); LC1. See figure 1 and table 1 for locality information. Geochemical data (Dumoulin and others, 2023) shown in inset box where available. %, percent; P, phosphorus; mm, millimeter; µm, micrometer. Photographs by J.A. Dumoulin, U.S. Geological Survey.

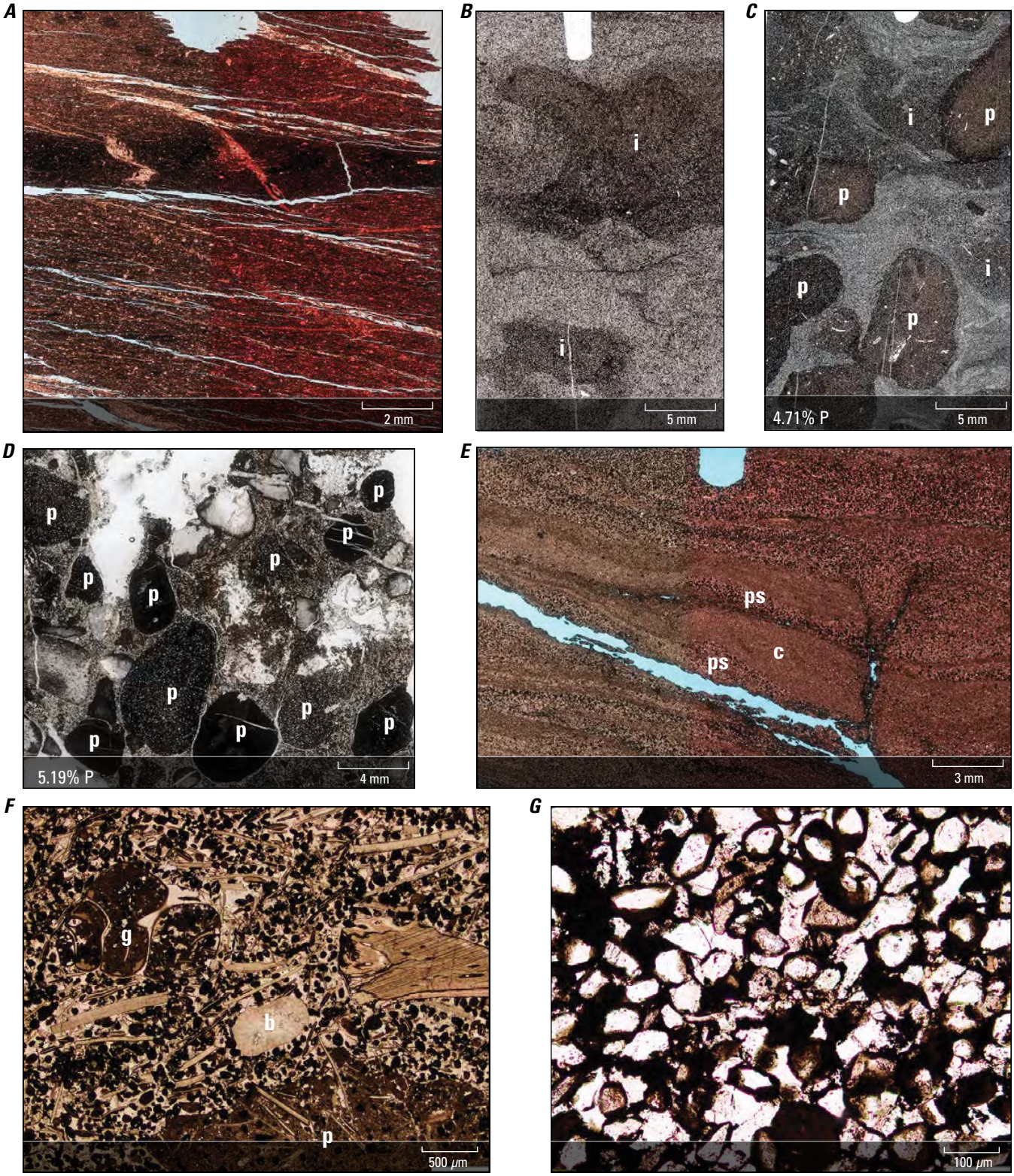
A
2 mm
B
i
i
5 mm
C
i
p
p
i
p
p
4.71% P
5 mm
D
p
p
p
p
p
p
p
p
p
p
5.19% P
4 mm
E
ps
c
ps
3 mm
F
g
b
p
500 μm
G
100 μm

Our study localities are discussed using geographic groupings that reflect depositional controls and other factors affecting facies patterns (fig. 1; table 1). The main outcrop belt, which contains 13 localities, extends over 180 kilometers (km) east to west and 45 km north to south. Shublik Formation strata at the Bathtub ridge locality, ~46 km southeast of the easternmost point of the main belt (fig. 1), were first described by Camber (1994) and represent a condensed and (or) structurally attenuated section in which only LC1 and MCC3 are exposed; these rocks have similarities to equivalent strata in the main belt and are generally discussed with them throughout the text. The Echooka River section, located 28 km south of the westernmost point of the main belt (fig. 1), has many distinctive features that warrant separate discussion for most of its units. Strata at four additional outcrops have undergone considerable deformation and some recrystallization. Three of these outcrops (Helicopter ridge, Porcupine Lake West, and Arctic D–4 quadrangle) are located ~40 km southeast of the Echooka River section; the Philip Smith Mountains locality is ~50 km to its southwest (fig. 1). Most subdivisions of the stratigraphic framework cannot be recognized at these four outcrops, so their rocks are discussed in a separate section, "Other Sections of the Shublik Formation."

# Lower Clastic Unit 1

LC1 (Whidden and others, 2018), which encompasses the lowest part of the Shublik Formation (fig. 2), is equivalent to the informal siltstone member of the Shublik of Detterman and others (1975) and partly equivalent to zone D of Kupecz (1995) (fig. 2). LC1 was studied and sampled at 11 outcrop localities (figs. 1, 4–6; table 1). It consists mainly of bioturbated quartz siltstone to very fine grained sandstone that contains lesser chert clasts and minor glauconite; beds are even to irregular and 2–20 centimeters (cm) thick (fig. 5*A–C*). Rare to abundant phosphate appears as sand-sized peloids, coatings on quartz sand grains, and millimeter (mm-) to cm-scale clasts and nodules that show various degrees of transport versus in situ growth (fig. 3*B–C*, *G*; fig. 5*A*, *E*, *F*; fig. 6*A*). Subordinate interbeds and partings of mudstone to muddy siltstone occur mainly in the lower half of the unit (fig. 4). LC1 includes three of the phosphatic facies described at Fire Creek by Kelly and others (2007): (1) phosphatic siltstone and fine-grained sandstone, (2) pebbly phosphorite, and (3) nodular phosphorite. Two coarsening- and thickening-upward intervals constitute the upper part of LC1 at Fire Creek (Whidden and others, 2018), as well as in other sections described herein (fig. 4).

The contact between the Shublik Formation and the underlying Ivishak Formation generally appears to be conformable and is marked by the first occurrence of notable phosphate—that is, phosphate that is easily visible in hand samples—at the base of the Shublik (for example, Detterman and others, 1975). Phosphate occurs in all the LC1 sections described herein, but phosphate type and abundance vary vertically and laterally within the unit.

LC1 has few age constraints, but the most age-diagnostic fossils have been found in the Fire Creek area (fig. 2) (Detterman and others, 1975; Whidden and others, 2018). These consist of a Smithian (late Early Triassic) ammonite from 7 m below the top of the Fire Creek Siltstone Member, an early Anisian (early Middle Triassic) ammonite from 8 m above the base of the Shublik Formation, and the Ladinian (late Middle Triassic) flat clam *Daonella frami* at the top of LC1. Poorly preserved palynomorphs of Middle to Late Triassic age occur in several mudstone beds in LC1 at the Last Creek section (J. Bujak, Bujak Research International, written commun., 2015). The onset of phosphate deposition in LC1 is approximately coeval with the Anisian first occurrence of radiolarian chert in distal facies of the Otuk Formation (Dumoulin and others, 2013; Whidden and others, 2018).

## Lithologies

The measured thickness of LC1 in our sections ranges from 7.3 to 26 m (fig. 4). The unit is thinnest at the Golden Eagle locality to the north and is thickest at the Aichilik River locality (the easternmost site in the main belt of the study area) (fig. 1). A layer of chert- and phosphate-clast conglomerate to pebbly sandstone, 0.5–1.75 m thick, forms the base of LC1 in the Kavik River, Aichilik River, and Last Creek sections (figs. 3*D*, 4, and 5*D*). Conglomerate clasts are rounded, mostly <2 cm in diameter (rarely as large as 7 cm), and tightly to loosely packed in a matrix of poorly sorted chert- and quartz-clast siltstone to coarse-grained sandstone. Many of the chert clasts contain siliceous sponge spicules and (or) radiolarians, and some chert clasts have pyritic rims as thick as 1.5 mm (figs. 3*D*, 5*D*). The phosphate clasts contain trace to very abundant quartz silt (figs. 3*D*, 5*D*). Subordinate clast types include quartz siltstone to fine-grained sandstone identical to that found in the underlying Fire Creek Siltstone Member of the Ivishak Formation.

In some sections, the contact between LC1 and the underlying Ivishak Formation is covered or marked by one or more layers of phosphatic nodules at the base of LC1. Such a phosphate nodule layer forms the base of the Shublik Formation in the Fire Creek section (Detterman and others, 1975; Kelly, 2004; Kelly and others, 2007; Whidden and others, 2018).

The main component of LC1 in all outcrop sections is quartz siltstone to very fine grained sandstone with subordinate chert grains. Undulatory bedforms are common, and some intervals display hummocky cross-stratification (see fig. 8*B* of Whidden and others, 2018). Beds typically appear coarsely to finely mottled as a result of partial bioturbation (fig. 5*C*). Discrete horizontal burrows are seen on bed bottoms; vertical to subvertical burrows (fig. 5*B*), a few millimeters wide and as long as 14 cm, were also noted locally. *Zoophycos* trace fossils are present on bedding surfaces in the LC1 section at Bathtub ridge (Camber, 1994), and similar spreite-filled burrows were seen in sections at Last Creek and Echooka River (fig. 5*G*). Minor clast types include feldspar, white mica, chlorite, tourmaline, and possible glauconite. Some samples

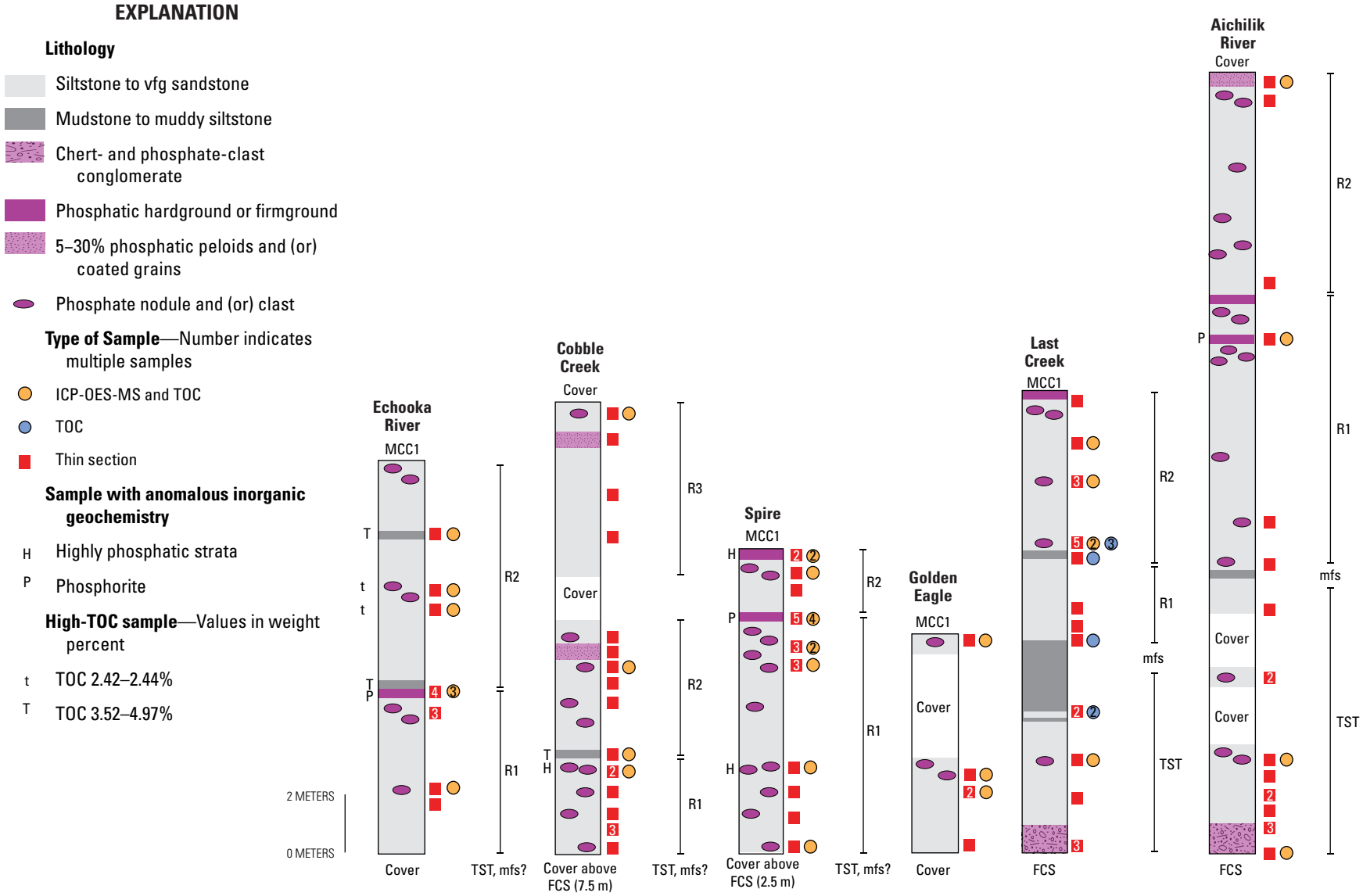


**Figure 4.** Stratigraphy of lower clastic unit 1 (LC1) of the Triassic Shublik Formation in sections measured for this study, northeastern Alaska. Sample labels P and H are based on inductively coupled plasma-optical emission spectroscopy-mass spectroscopy (ICP-OES-MS) analyses (Dumoulin and others, 2023). The term "cover" indicates a part of a section that is poorly exposed or covered. See figure 1 and table 1 for section localities. R1, R2, and R3 denote regressive parasequences within the regressive systems tract. Other abbreviations: vfg, very fine grained; TOC, total organic carbon; MCC1, middle carbonate-chert unit 1; TST, transgressive systems tract; mfs, maximum flooding surface (queried where uncertain); FCS, Fire Creek Siltstone Member of Ivishak Formation; %, percent; m, meter. The informal LC1 and MCC1 units are from Whidden and others (2018).

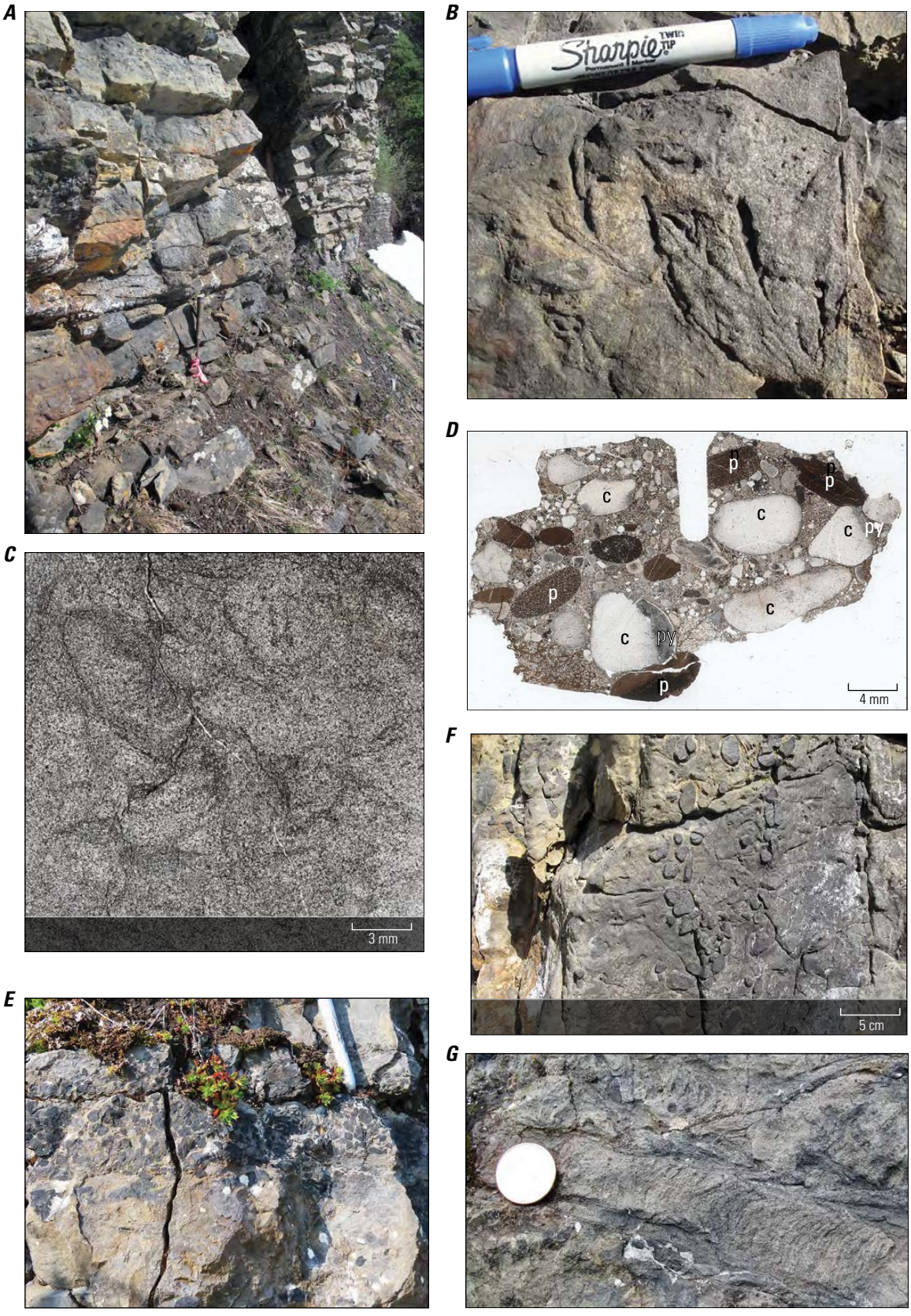
A
B
Sharpie
C
3 mm
D
p
c
py
4 mm
E
F
5 cm
G

**Figure 5 (page 10).** Images of sedimentary and biogenic features of lower clastic unit 1 (LC1) of Whidden and others (2018) in the Triassic Shublik Formation, northeastern Alaska. *A*, Outcrop at the Last Creek locality showing beds rich in phosphate clasts and nodules (visible above hammer handle) that make up the uppermost part of LC1. *B*, Close-up of outcrop at Last Creek showing subvertical burrows near the top of LC1. *C*, Thin section scan from the Echooka River locality of bioturbated quartz siltstone to very fine grained sandstone with negligible phosphate. *D*, Thin section scan from Last Creek showing conglomerate at the base of LC1; clast types include phosphate pebbles (p), which contain rare to abundant white quartz silt, and chert (c). Some chert clasts have dark pyritic rims (py). *E*, Outcrop at the Dodo Creek locality showing abundant phosphate clasts and nodules near the top of the lower parasequence in LC1. *F*, Outcrop at Last Creek showing abundant phosphate clasts and nodules near the top of the upper parasequence in LC1. *G*, Close-up of outcrop at Echooka River showing a spreite-filled burrow in the lower parasequence in LC1; coin is approximately 2 centimeters (cm) in diameter. See figure 1 and table 1 for locality information. mm, millimeter. Photographs by J.A. Dumoulin, U.S. Geological Survey.

have ≤10 percent calcite and (or) ferric dolomite, appearing as patchy cement and (or) disseminated grains, but silica cements other beds.

Phosphate is unevenly distributed through LC1. Small amounts of phosphate occur widely through this unit in most sections, but HPS are less common, and true phosphorites are rarer still. All our outcrop sections of LC1 include intervals one to a few meters thick that show negligible phosphate in thin section (fig. 5*C*) and geochemical analyses (table 2) (Dumoulin and others, 2023). Other beds have 5–30 percent sand-sized phosphatic peloids and (or) phosphate-coated quartz grains (fig. 3*G*). Some intervals contain sparse to common phosphate nodules and (or) clasts that are rounded, ellipsoidal, or irregular, and are generally ≤1 to 2 cm in size but rarely as large as 8 cm (fig. 5*A*, *E–F*; fig. 6*A*). Textural features, such as ellipsoidal forms parallel to bedding and diffuse boundaries (fig. 3*B*), indicate that many granule- to pebble-sized phosphate masses in LC1 formed in place and experienced little or no subsequent reworking. Some beds, especially notable at the Spire section, contain phosphate masses with diverse internal compositions and textures, which indicate these clasts have experienced transport and redeposition (fig. 6*A*). Sand-sized phosphate peloids locally occur within larger (cm-scale) phosphate clasts and nodules (fig. 6*B*, *E*). The highest phosphate concentrations in LC1 in the outcrop belt occur near the tops of the coarsening- and thickening-upward sequences, where phosphate nodules and clasts are most abundant (fig. 5*A*, *E–F*) and locally coalesce (fig. 6*E*) to form firmgrounds or hardgrounds that are typically ≤30 cm thick (fig. 6*D*, *F–G*). Small, vertical borings filled with calcite or phosphate occur locally in these beds (Kelly and others, 2007) along with phosphatized burrows (fig. 6*G*), fossil fragments (fig. 6*G*), and complex internal layering (fig. 6*F–G*).

Radiolarians are rare to abundant components of phosphate nodules in LC1 in most sections, and their test structures are locally well preserved (fig. 6*B–C*). The tests are filled with phosphate, fine-grained silica, or pyrite. Discrete, phosphate-filled radiolarians are also sparsely disseminated within some sandstone beds. Although megafossils are rare in LC1, phosphate nodules and hardgrounds found in several sections contain a few bivalve fragments (fig. 6*G*). In the Fire Creek and Cobble Creek sections, the upper part of LC1 also contains trace amounts of echinoderm and probable daonellid fragments.

## Geochemistry

### Total Organic Carbon Data

TOC is generally low in LC1 in the main outcrop belt. Published values from this interval at Fire Creek (Detterman, 1970; Kelly, 2004; Whidden and others, 2018) are all <1.5 weight percent, and most are <1 weight percent New data reported herein for Fire Creek and nine other

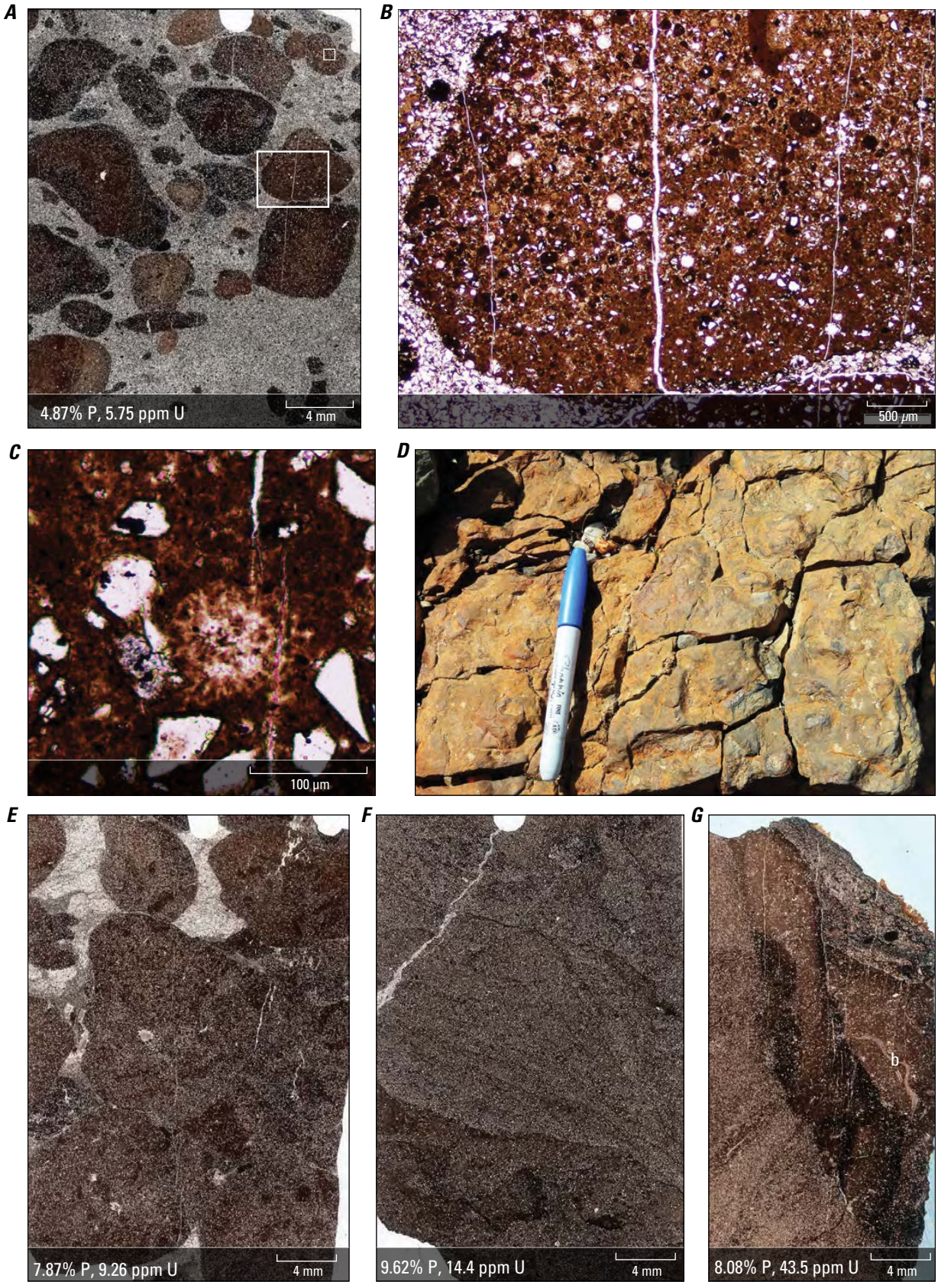
A
4.87% P, 5.75 ppm U
4 mm
B
500 µm
C
100 µm
D
E
7.87% P, 9.26 ppm U
4 mm
F
9.62% P, 14.4 ppm U
4 mm
G
b
8.08% P, 43.5 ppm U
4 mm

**Figure 6 (page 12).** Images of additional sedimentary and biogenic features of lower clastic unit 1 (LC1) of Whidden and others (2018) in the Triassic Shublik Formation, northeastern Alaska. *A*, Thin section scan from the Spire locality of phosphate clasts with irregular shapes and diverse internal compositions (phosphatic sandstone). Large and small boxes in part *A* show extents of parts *B* and *C*, respectively. *B*, Photomicrograph of a phosphate clast that contains abundant radiolarians. *C*, Photomicrograph of a phosphate clast showing a well-preserved radiolarian test structure. *D*, Outcrop at the Dodo Creek locality of the upper surface of the phosphatic hardground at the top of LC1. *E*, Thin section scan taken beneath the hardground at the top of the lower parasequence in LC1 at Spire, showing coalescing phosphate nodules. *F*, Thin section scan from a phosphatic hardground at the Aichilik River locality, showing a complexly layered texture. *G*, Thin section scan from a phosphatic hardground at the Echooka River locality, showing a complexly layered texture with phosphatized burrows and bivalve fragments (b). See figure 1 and table 1 for locality information. Geochemical data (Dumoulin and others, 2023) shown in inset box where available. %, percent; P, phosphorus; U, uranium; ppm, parts per million; mm, millimeter; µm, micrometer. Photographs by J.A. Dumoulin, U.S. Geological Survey.

main belt outcrops (number of samples [*n*]=65) are similarly low (<1.6 weight percent), with a few exceptions (table 2) (Dumoulin and others, 2023). Higher values were found in a muddy siltstone in the Cobble Creek section (4.97 weight percent) and in four mudstone and siltstone samples from the Echooka River section (2.42–4.32 weight percent) (fig. 4).

## Inorganic Geochemical Data

Inorganic geochemical data from LC1 support our petrographic observations. Silicon values are high (>23 percent in rocks with little to moderate phosphate; >17 percent in most HPS), whereas calcium values are low (generally <10 percent; ≤20 percent in most HPS) (table 2) (Dumoulin and others, 2023). Beds with little or no visible phosphate in thin section contain <1 percent phosphorus and are similar in overall petrographic and chemical composition to samples from the underlying Fire Creek Siltstone Member of the Ivishak Formation (table 2). Molybdenum values in all samples are low (≤12 parts per million [ppm]).

Nine phosphorites and 12 other samples of HPS were analyzed from nine sections (fig. 1; table 2). The highest phosphate values were found mainly in the upper part of the lower coarsening-upward sequence of LC1 (fig. 4) and, to a lesser extent, near the top of the unit, matching the pattern reported by Kelly (2004) for strata we assign to LC1 at Fire

**Table 2.** Geochemical data (Dumoulin and others, 2023) from the Triassic Fire Creek Siltstone Member of the Ivishak Formation and lower clastic unit 1 (LC1) of Whidden and others (2018) in the Shublik Formation, northeastern Alaska.

[See figure 1 for locality map and table 1 for locality details. See (Dumoulin and others, 2023) for complete geochemical data; samples from LC1 that were analyzed only for total organic carbon (TOC) (Fire Creek, number of samples [*n*]=2; Last Creek, *n*=7) are not included below. Localities: A, Aichilik River; B, Bathtub Ridge; Co, Cobble Creek; D, Dodo Creek; E, Echooka River; F, Fire Creek; G, Golden Eagle; K, Kavik River; Ke, Kemik Creek; L, Last Creek; S, Spire. Other abbreviations: Al, aluminum; Ca, calcium; HPS, highly phosphatic strata; m, mudstone; md, muddy; Mo, molybdenum; P, phosphorus; ph, phosphatic; ppm, parts per million; pte, phosphorite; Si, silicon; sltst, siltstone; sst, sandstone; U, uranium; %, percent; /, and]

| Lithology | Localities | TOC (weight percent) | Concentration | | | | | |
|---|---|---|---|---|---|---|---|---|
| | | | Al (%) | Ca (%) | Si (%) | P (%) | Mo (ppm) | U (ppm) |
| Fire Creek Siltstone Member | | | | | | | | |
| m to sltst/sst | L, S (*n*=8) | <0.2–1.28 | 1–7.69 | 0.19–9.09 | 24.2–35.8 | 0.09–1.48 | <2–3 | 1.97–8.39 |
| Lower clastic unit 1 | | | | | | | | |
| m to md sltst | B (*n*=4) | 0.34–1.01 | 4.75–11 | 0.69–3.02 | 28.5–36.7 | 0.1–0.29 | <2–2 | 3.19–3.93 |
| | Co, E (*n*=3) | 3.52–4.97 | 4.52–6.1 | 3.5–9.53 | 24.8–32.8 | 1.58–3.52 | 7–12 | 12.3–28.7 |
| sltst/sst | A, B, G, S (*n*=8) | <0.2–1.01 | 0.79–3.76 | 0.69–8.03 | 23.9–39.8 | 0.1–0.86 | <2–3 | 1.48–4.34 |
| | E (*n*=2) | 0.21, 2.42 | 2.69, 3.2 | 2.38, 11.01 | 26.6, 37.6 | 0.55, 0.72 | <2, 6 | 2.66, 7.3 |
| ph sltst/sst | A, B, Co, F, G, K, L, S (*n*=17) | 0.24–1.02 | 1.13–3.22 | 4.25–16.5 | 23.4–34.6 | 1.01–4.26 | <2–10 | 2.98–13.4 |
| | E (n=1) | 2.44 | 3.07 | 10.1 | 24.8 | 1.02 | 7 | 9.21 |
| HPS | B, Co, D, F, K, S (*n*=12) | 0.23–1.24 | 0.77–1.5 | 11.2–17.8 | 20–29.4 | 4.35–7.44 | <2–6 | 7.24–25.8 |
| pte | A, D, Ke, S (*n*=5) | 0.37–1.59 | 1.12–2.04 | 18.4–21.3 | 17.4–22.3 | 7.87–9.84 | <2–10 | 9.26–22.5 |
| | B, E (*n*=4) | 0.38–0.72 | 0.82–1.75 | 19.6–23.2 | 16.6–19.2 | 8.08–8.87 | <2–6 | 43.5–86.7 |

Creek. All but four HPS in our LC1 database have <26 ppm uranium (fig. 6*A*, *E–F*). Two phosphorites from the Bathtub ridge site and two from the Echooka River section have notably higher uranium values (43.5–86.7 ppm) (fig. 6*G*; table 2). Elevated rare earth element (REE) concentrations also occur in three of these uranium-rich samples, with values as high as 136 ppm for cerium, 50.4 ppm for dysprosium, and 432 ppm for yttrium; typical values for these elements in the Shublik Formation are <50, <20, and <100 ppm, respectively (Dumoulin and others, 2023).

## Depositional Setting

Our findings support previous interpretations (for example, Kelly, 2004; Kelly and others, 2007) that LC1 accumulated in an inner-ramp setting. Sedimentary structures such as hummocky cross-stratification are consistent with such a setting, and pervasive bioturbation and uniformly low molybdenum values (for example, Scott and Lyons, 2012) indicate an oxic environment. Intervals of increasing grain size and bed thickness in the upper part of the unit represent shallowing-upward successions. Abundant phosphate concentrated at the tops of these intervals (fig. 5*A*, *E–F*; fig. 6*A*, *D–G*) formed through a combination of in situ phosphatization and subsequent reworking and redeposition of phosphate during energetic events such as storms. Phosphatic hardgrounds, which develop during depositional hiatuses (for example, Strasser, 2015), occur in our sections both between successive shallowing-upward intervals and at the top of LC1. The presence of abundant phosphate and common radiolarians in LC1 suggests an environment characterized by high productivity, consistent with previous interpretations (for example, Parrish and others, 2001a, b) that the Shublik Formation accumulated in a coastal area affected by upwelling currents.

In contrast to other units within the Shublik Formation, LC1 in the Echooka River section is very similar to LC1 in the main outcrop belt. The major difference is that siltstone from Echooka River is more organic-rich than LC1 siltstone in other localities: four of five Echooka River siltstone samples contain >2.4 weight percent TOC, whereas virtually all siltstone samples from other localities contain ≤1 weight percent TOC (fig. 4; table 2) (Dumoulin and others, 2023). Elevated organic matter content in the Echooka River section likely reflects a slightly deeper water setting, in keeping with its more distal (southward) position within the Arctic Alaska basin.

## Sequence Stratigraphy

LC1 makes up T-R sequence 1 (S1) of Whidden and others (2018) and Rouse and others (2020) (fig. 2). Phosphate at the base of the Shublik Formation marks the transgressive surface at the base of S1. In many sections, the TST of this sequence consists mostly of a thin interval of recessive mudstone that is poorly exposed or covered, but a thicker TST is well-exposed in two northeastern sections (Last Creek and Aichilik River) (fig. 4). Fining-upward intervals measuring 7 and 9.5 m thick form the lower part of the Shublik at these two localities; each interval consists of phosphatic conglomerate and sandstone that grades up into quartz siltstone and is capped by mudstone, which we interpret to represent the mfs.

Two coarsening- and thickening-upward parasequences constitute the RST of S1 at the Fire Creek section (Whidden and others, 2018; Rouse and others, 2020). HPS, including local phosphatic hardgrounds (Kelly and others, 2007), cap both parasequences, though the highest phosphorus contents are at the top of the lower parasequence (Kelly, 2004; Dumoulin and others, 2023). Other sections that we studied show a similar progression of lithofacies, with phosphatic hardground textures generally best developed, and overall phosphorus contents highest, at the top of the lowest parasequence (figs. 4, 6).

# Middle Carbonate-Chert Unit 1

MCC1 (fig. 2) (Whidden and others, 2018) encompasses the lower part of the informal limestone and dolomite member of the Shublik Formation of Detterman and others (1975) and is partly equivalent to zone C of Kupecz (1995). MCC1 was studied and sampled at 10 outcrop localities (figs. 1, 7–9; table 1) and consists mainly of calcareous quartz siltstone to fine-grained sandstone, lesser limestone, and a significant interval of HPS (including phosphorite) that is the thickest and most continuous phosphatic interval seen anywhere in the Shublik. MCC1 differs from LC1 in containing limestone beds and more abundant calcareous fossils (especially the flat clam *Daonella* sp., which is a common constituent through much of the unit) and in being less pervasively bioturbated.

Fossils indicate that much of MCC1 is Ladinian (late Middle Triassic), though the upper part may be Carnian (early Late Triassic) in age. The middle Ladinian index species *Daonella frami* (McRoberts, 2010) was recognized in several beds within MCC1 at Fire Creek (Detterman and others, 1975) and has also been identified in sections on the Kavik and Echooka Rivers (Detterman and others, 1975; C. McRoberts, State University of New York at Cortland, written commun., 2014). The upper beds of MCC1 at Fire Creek contain foraminifera that indicate a Carnian age (identification by M. Mickey in Kelly, 2004).

## Lithologies

### Main Belt

In the main outcrop belt, MCC1 is ~8 to 23 m thick (fig. 7) and it is thickest in the east. The unit generally consists of a phosphatic lower interval (fig. 8) and a more calcareous and quartz-rich upper interval (fig. 9). A distinctive lower interval of HPS (including phosphorite) as thick as 7 m is found in all main belt sections except Cobble Creek and

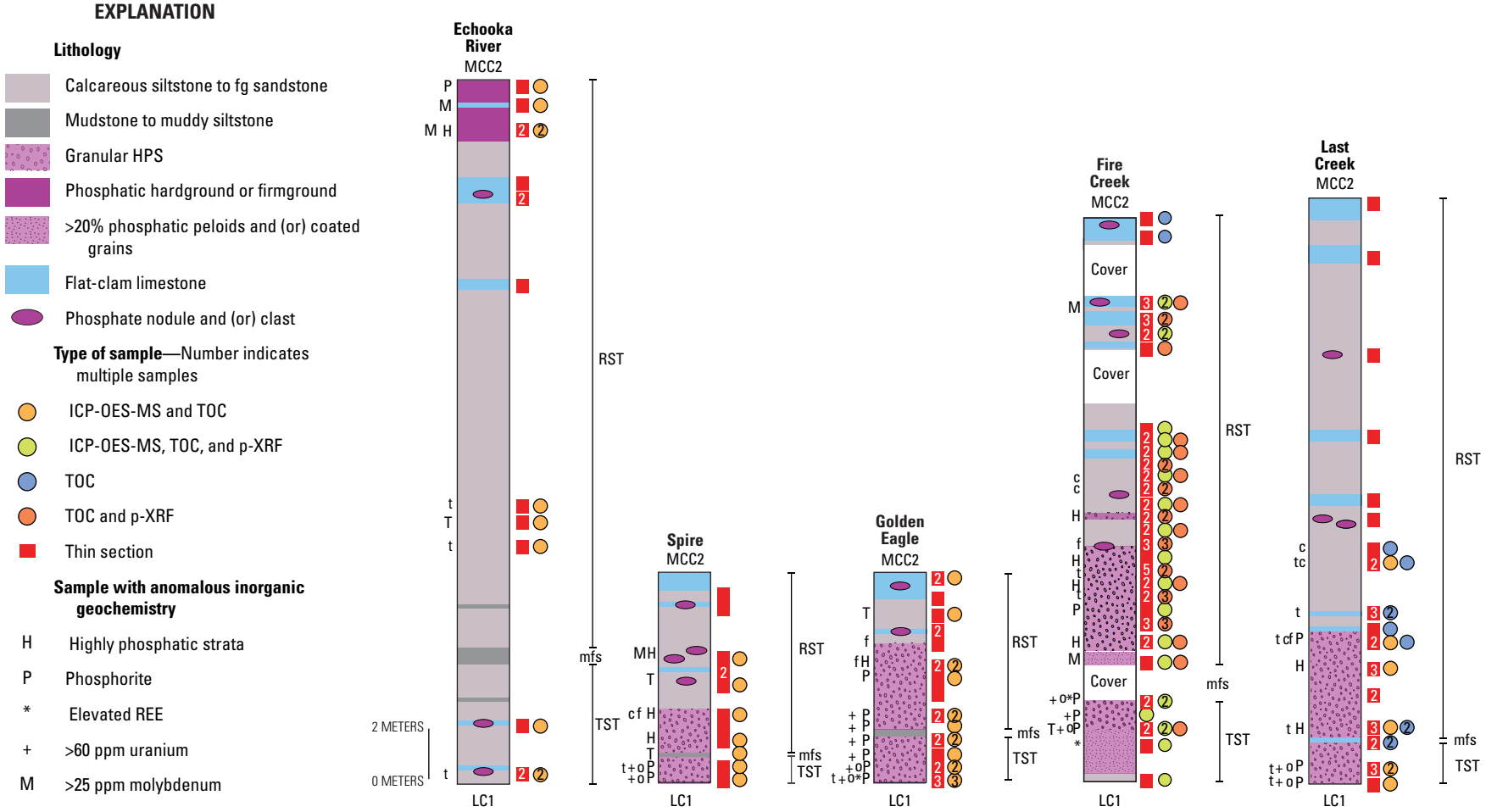


**Figure 7.** Stratigraphy of middle carbonate-chert unit 1 (MCC1) of the Triassic Shublik Formation, northeastern Alaska, in the most completely exposed sections measured for this study. Inorganic geochemical data are based on inductively coupled plasma-optical emission spectroscopy-mass spectroscopy (ICP-OES-MS) analyses (Dumoulin and others, 2023). The term "cover" indicates a part of the section that is poorly exposed or covered. Values shown for high-total-organic-carbon (TOC) samples are as given by analyst. See figure 1 and table 1 for locality information. fg, fine-grained; HPS, highly phosphatic strata; p-XRF, portable X-ray fluorescence; MCC2, middle carbonate-chert unit 2; RST, regressive systems tract; mfs, maximum flooding surface; TST, transgressive systems tract; LC1, lower clastic unit 1; %, percent; ppm, parts per million; m, meter. The informal LC1, MCC1, and MCC2 units are from Whidden and others (2018).

Aichilik River, where covered zones ≤10 m and 4.5 m thick, respectively, occur above the highest exposures of LC1. The phosphatic interval, which includes the sandy phosphorite facies described by Kelly and others (2007) at Fire Creek, can be found through 110 km of outcrop, spanning from Kemik Creek in the southwest to Last Creek in the northeast (fig. 1). This interval consists mostly of granular phosphorites (≥7.86 percent phosphorus) made of sand-sized phosphate grains (fig. 8*C–D*) in a matrix of phosphate, calcite, or silica cement. Subordinate interbeds of granular HPS with 4.84–7.67 percent phosphorus (fig. 8*E*; table 3; Dumoulin and others, 2023) and phosphatic siltstone to sandstone with 1.52–3.95 percent phosphorus (fig. 8*B*) contain phosphate grains intermixed with silt- to sand-sized quartz, chert, and bioclasts (dominantly flat-clam fragments). The phosphate grains in these beds are clearly transported: strata show grading, cross-bedding, and parallel lamination (figs. 3*E*, 8*B*).

The phosphatic interval is petrographically and chemically distinctive. Basal beds contain detrital quartz and common, multi-layered phosphatic ooids with quartz centers (figs. 7, 8*B–C*); some beds are composed entirely of ooids and include coated grains with unconformity-bounded internal surfaces (fig. 8*C*) (Pufahl and Grimm, 2003). The most phosphatic beds consist of tightly packed phosphatic peloids and little matrix (fig. 8*D*). Phosphate content and grain packing decrease upward within the interval, whereas calcite increases, occurring both as grains (mainly flat-clam fragments) and cement. Phosphate-coated flat-clam fragments are abundant in the beds near, and just above, the top of the phosphate interval (figs. 7, 8*E*).

The upper part of MCC1 in the main outcrop belt consists of siltstone to fine-grained sandstone made up of carbonate, quartz, and phosphate clasts in various proportions (fig. 9*A–B*), interbedded with and grading into flat-clam packstone to grainstone (fig. 9*C–D*). Most carbonate clasts are fossil (particularly flat-clam) fragments, and most phosphate clasts are simple peloids. Flat-clam-rich beds increase in thickness and abundance upward and typically resemble the transported flat-clam facies of Whidden and others (2019b), with small, thin, broken shell fragments, minor quartz silt, and locally chaotic microtextures (fig. 9*D*). Phosphate nodules, most ellipsoidal and ≤1 cm in size, occur irregularly through the upper part of MCC1 (fig. 9*A*).

Bioturbation is less evident in MCC1 than in LC1, but some bed surfaces have small, horizontal burrows. Shell layers, especially in the upper part of MCC1, show local, sub-millimeter scale bioturbation swirls and whorls (Whidden and others, 2019b) produced by meiofauna.

Calcareous forms that are likely large, calcite-replaced *Tasmanites* algal cysts (fig. 8*F*) (compare figs. 8*B*, *F–G* of Dumoulin and others, 2022) are a notable component of several beds near the middle of MCC1 in sections at Kavik River and Cobble Creek, and at Spire, and Fire and Last Creeks (fig. 7). Other fossils identified in MCC1 at Fire Creek include the pecten *Camptonectes* sp., the bivalve *Lima* sp., and spiriferid brachiopods (Detterman and others, 1975) as well as various ostracodes (Sohn, 1987). Fossils observed in thin section as minor constituents of this unit include agglutinated and calcareous foraminifera, calcareous sponge spicules, and echinoderm and bryozoan fragments. Radiolarians, coated or replaced by phosphate, are found as discrete grains in sandy beds and within phosphate nodules, and are replaced by calcite in flat-clam-rich beds.

Micrite (calcite crystals ≤4 micrometers [µm] in diameter) (Folk, 1959) is rare in the Shublik Formation, and most beds classed there as wackestones or packstones contain a mud matrix made largely of non-carbonate material (clay and [or] organic material). True micrite does occur in MCC1 as peloids found in a few flat-clam packstone and grainstone beds at Last Creek and Aichilik River.

### Echooka River

In the Echooka River section, MCC1 is 27 m thick and differs in several ways from coeval strata in the main outcrop belt (fig. 7). MCC1 in this section consists largely of siltstone made up of various proportions of quartz, bioclasts (flat-clam fragments), and phosphatic peloids. These beds resemble the siltstone to fine-grained sandstone that makes up most of the upper part of MCC1 in the main outcrop belt. Resistant beds near the base and in the upper part of MCC1 at Echooka River are limestones with subordinate phosphate peloids, phosphate nodules as long as 3 cm, and patchy phosphate cement. Granular calcite spar cement partly obliterates the original depositional textures in a few samples, but some beds contain pavements of well-preserved *Daonella frami* (Detterman and others, 1975) that appear to have accumulated in situ, showing little post-mortem disturbance (fig. 9*E*) (compare Whidden and others, 2019b). Other beds, especially those higher in the section, have broken shells and chaotic textures indicating transport and redeposition. HPS predominate in the upper 2 meters of the unit; these beds contain abundant phosphate nodules and peloids, along with flat clams, echinoderm fragments, calcitized and phosphatized radiolarians, and rare foraminifera. Phosphate cements much of this interval and fills vertical burrows as much as 8 cm long; complex microtextures indicate that this interval, which we interpret as a hardground, underwent multiple cycles of phosphate formation, erosion, and redeposition (fig. 9*F–G*).

## Geochemistry

### Total Organic Carbon Data

TOC values are generally somewhat higher in MCC1 than in LC1. Most samples previously reported from this interval at the Fire Creek section (Detterman, 1970; Kelly, 2004) contain 1–2 weight percent TOC. New samples analyzed from Fire Creek and nine other sections ($n$=117)

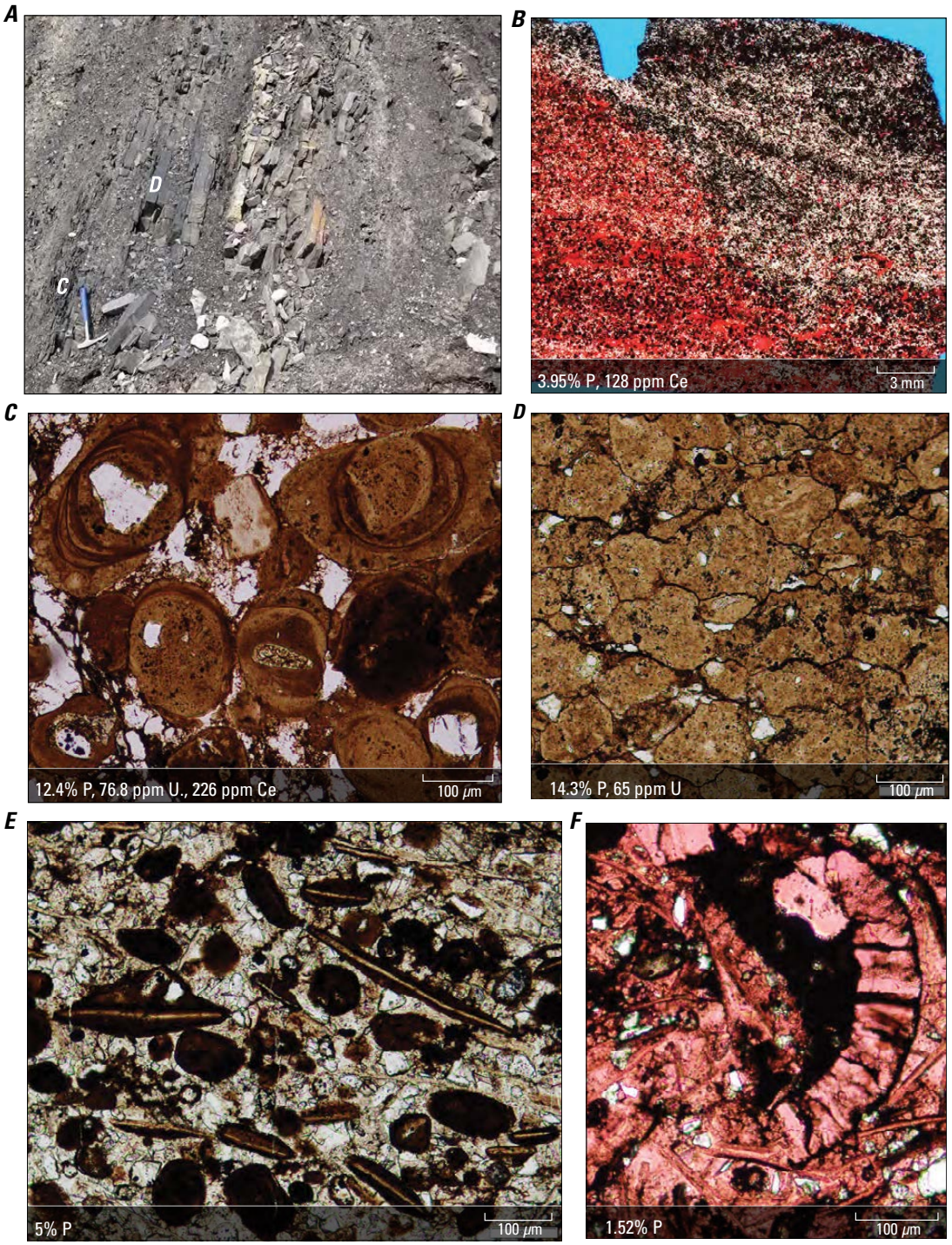


**Figure 8.** Images of sedimentary and biogenic features of the lower to middle part of middle carbonate-chert unit 1 (MCC1) of Whidden and others (2018) in the Triassic Shublik Formation, northeastern Alaska. *A*, Outcrop at the Golden Eagle locality of the lower phosphatic part of MCC1. Letters indicate the sample sites for parts *C* and *D*. *B*, Thin section scan from the Fire Creek locality of cross-bedded phosphatic quartz-calcite siltstone. Calcite is stained red in the lower left quadrant. *C*, Photomicrograph of sample taken near the base of MCC1 at Golden Eagle, showing phosphorite with abundant ooids and detrital quartz. Most ooids are characterized by unconformity-bounded internal surfaces (Pufahl and Grimm, 2003). *D*, Photomicrograph of sample taken near the base of MCC1 at Golden Eagle, showing tightly packed phosphatic peloids with little matrix. *E*, Photomicrograph from the Spire locality of abundant phosphate-coated flat-clam fragments in granular highly phosphatic strata (HPS). *F*, Photomicrograph from Fire Creek of a calcite-replaced fragment of a large *Tasmanites* algal cyst; calcite is stained pink. See figure 1 and table 1 for locality information. Geochemical data (Dumoulin and others, 2023) shown in inset box where available. %, percent; P, phosphorus; Ce, cesium; U, uranium; ppm; parts per million; mm, millimeter, μm, micrometer. Photographs by J.A. Dumoulin, U.S. Geological Survey.

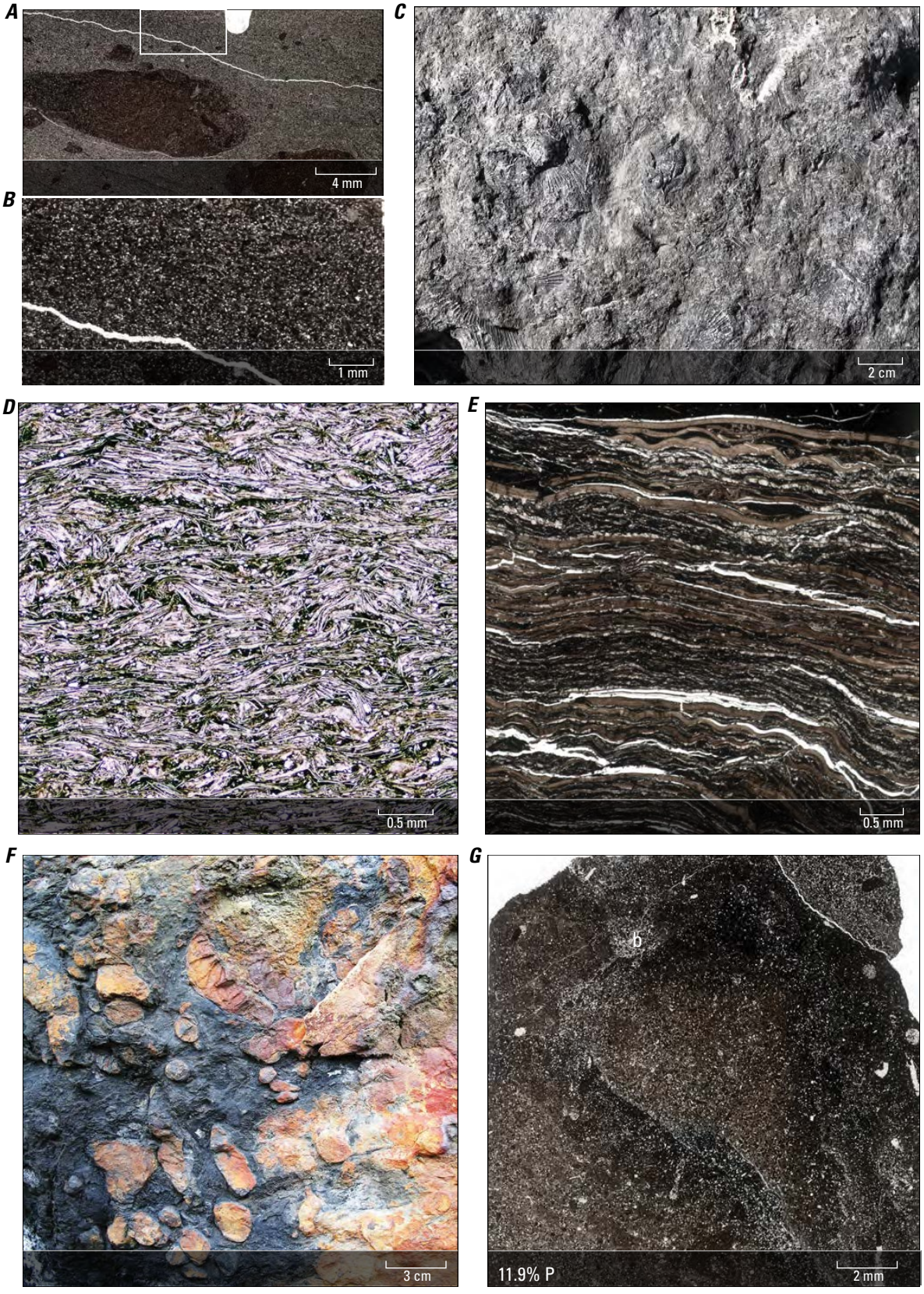
A
4 mm
B
1 mm
C
2 cm
D
0.5 mm
E
0.5 mm
F
3 cm
G
b
11.9% P
2 mm

**Figure 9 (page 18).** Images of sedimentary and biogenic features of the middle to upper part of the middle carbonate-chert unit 1 (MCC1) of Whidden and others (2018) in the Triassic Shublik Formation, northeastern Alaska. *A*, *B*, Thin section scan from the Fire Creek locality showing quartz-carbonate-phosphate siltstone with small flat-clam fragments, phosphatic nodules, and peloids. Box in *A* shows the extent of part *B*, which provides a closer view of siltstone texture. *C*, *D*, Flat-clam limestone with small, thin shell fragments and locally chaotic microtexture, seen in outcrop at the Spire locality (*C*) and in a photomicrograph from the Golden Eagle locality (*D*). *E*, Thin section scan from the Echooka River locality showing a daonellid limestone with larger, more complete shells than those in part *D*. *F*, Photograph of outcrop at Echooka River of hardground made up of highly phosphatic strata (HPS) . *G*, Thin section scan from the HPS outcrop in part *F* showing phosphatized burrow (b) and complex microtextures that suggest multiple cycles of phosphatization. See figure 1 and table 1 for locality information. Geochemical data (Dumoulin and others, 2023) shown in inset box where available. %, percent; P, phosphorus; cm, centimeter; mm, millimeter. Photographs by J.A. Dumoulin, U.S. Geological Survey.

(table 3) (Dumoulin and others, 2023) largely fall into this range, but about half of our samples (excluding limestones) contain >1.6 weight percent TOC, and one-quarter of this group have >2 weight percent TOC. The limestones have uniformly low values (generally <1 weight percent TOC), whereas the highest TOC values (3–4.06 weight percent, *n*=5) were found in thin beds of mudstone and muddy siltstone, mainly in the lower half of MCC1 at Golden Eagle, Spire, Fire Creek and Echooka River (fig. 7).

## Inorganic Geochemical Data

Geochemical data demonstrate that high phosphorus values are found in the lower part of MCC1 throughout the main outcrop belt. These data also document other distinctive features of these strata (fig. 7; table 3) (Dumoulin and others, 2023). Our findings confirm and expand on previous findings of high phosphorus content in this part of the Shublik Formation at Fire Creek (Detterman, 1970; Kelly, 2004).

**Table 3.** Geochemical data (Dumoulin and others, 2023) from the middle carbonate-chert unit 1 (MCC1) of Whidden and others (2018) in the Shublik Formation, northeastern Alaska.

[See figure 1 for locality map and table 1 for locality details. See (Dumoulin and others, 2023) for complete geochemical data; samples from MCC1 that were analyzed only for total organic carbon (TOC) (Fire Creek, number of samples [*n*]=30; Kavik River, *n*=1; Last Creek, *n*=11) are not included below. Localities: A, Aichilik River; Co, Cobble Creek; D, Dodo Creek; E, Echooka River; F, Fire Creek; G, Golden Eagle; K, Kavik River; Ke, Kemik Creek; L, Last Creek; S, Spire. Other abbreviations: Al, aluminum; Ca, calcium; cc, calcareous; HPS, highly phosphatic strata; lms; limestone; m, mudstone; Mo, molybdenum; P, phosphorus; ph, phosphatic; ppm, parts per million; pte, phosphorite; s., sample(s); Si, silicon; sltst, siltstone; sst, sandstone; U, uranium; %, percent; —, not applicable; /, to]

| Lithology | Localities | TOC (weight percent) | Concentration | | | | | |
|---|---|---|---|---|---|---|---|---|
| | | | Al (%) | Ca (%) | Si (%) | P (%) | Mo (ppm) | U (ppm) |
| m | S (*n*=1) | 3.63 | 4.19 | 18.6 | 15.3 | 1.61 | 17 | 16.2 |
| sltst/sst | E, F, G | 0.63–3.27 | 1.1–3.36 | 3.07–22.9 | 13–39.9 | 0.34–0.83 | 4–13 | 5.94–9.22 |
| | (*n*=4) | (2 s. >1.6) | — | — | — | — | — | — |
| ph cc sltst/sst | Co, D, E, F, L, S | 0.59–4.06 | 0.45–3.83 | 11.4–30.2 | 6.65–23.7 | 1.06–3.95 | 3–29 | 7.02–28.1 |
| | (*n*=14) | (7 s. >1.6) | — | — | — | — | (1 s. >10) | — |
| HPS | Co, D, F, G, L, S | <0.02–2.12 | 0.6–2.61 | 16.9–29.8 | 7.49–20.1 | 4.84–7.67 | 2–27 | 10.9–47.2 |
| | (*n*=14) | (4 s. >1.6) | — | — | — | — | (1 s. >17) | — |
| | E (*n*=2) | 0.89, 1.87 | 1.53, 1.9 | 23.7, 26.7 | 8.52, 9.95 | 5.84, 6.77 | 21, 49 | 23.8, 30.2 |
| pte | D, F, G, K, Ke, L, S (*n*=27) | 0.85–2.79 | 0.46–1.96 | 21.6–34 | 4.15–18.2 | 7.9–14.9 | 2–14 | 16.5–123 |
| | | (16 s. >1.6) | — | — | — | (18 s. >10) | — | (20 s. >60) |
| | E (*n*=1) | 1.33 | 0.93 | 28.6 | 8.48 | 11.9 | 21 | 41.2 |
| lms | A, E, F, G | 0.11–1.31 | 0.14–1.63 | 21.9–37.8 | 1.76–10.2 | 0.02–2.46 | <2–52 | 0.99–26.1 |
| | (*n*=12) | — | — | — | — | — | (2 s. >25) | — |

Forty-one samples of HPS (including 27 phosphorites) were analyzed from 8 sections (table 3) using ICP-OES-MS; 18 of these samples contain >10 percent phosphorus, with a maximum value of 14.9 percent (34 percent phosphorus pentoxide). Sixteen HPS samples from the Fire Creek section analyzed using p-XRF yielded similar results (Dumoulin and others, 2023). Basal beds with detrital quartz and notable phosphatic ooids have elevated REE values in several sections (fig. 7). For example, several phosphorites at the base of the Golden Eagle section contain 226–269 ppm cerium, 65–76 ppm dysprosium, and 760–958 ppm yttrium (Dumoulin and others, 2023). Uranium values are high in the lower part of the phosphorite interval, producing a pronounced GR response on well logs (Rouse and others, 2020). Twenty-one phosphorite samples analyzed for this study contained >60 ppm uranium, with the highest contents (108–123 ppm) found near the base of MCC1 in the Spire, Golden Eagle, and Fire Creek sections (fig. 7; table 3) (Dumoulin and others, 2023).

HPS from the Echooka River section differ in texture and stratigraphic position from those in the main outcrop belt, and ICP-OES-MS data indicate geochemical differences as well. All three samples of HPS (including 1 phosphorite) from Echooka River have higher molybdenum values (21–49 ppm) than all but one HPS sample from the main outcrop belt (fig. 7). Uranium values at Echooka River are only moderately elevated, with no values >60 ppm (table 3).

All lithologies in MCC1 contain less silicon and more calcium than their counterparts in LC1, reflecting the increase in carbonate clasts and cement as well as the concomitant decrease in quartz silt and sand. Molybdenum contents are generally low, but slightly to moderately elevated values of 27–52 ppm molybdenum were found in two silty beds at Fire Creek and in a limestone bed at Echooka River (Dumoulin and others, 2023).

## Depositional Setting

Sedimentologic, faunal, and geochemical data indicate that MCC1 accumulated in a deeper and less oxygenated submarine environment than did LC1. In the main outcrop belt, granular phosphorites and related strata (fig. 8*A–E*) (condensed phosphate of Föllmi [1996]) were deposited and reworked in middle-ramp settings characterized by high productivity (Pufahl and Groat, 2017). Flat clams (including *Daonella*) were opportunistic benthic bivalves suited to oxygen-deficient settings (McRoberts, 2010); their predominance in MCC1, along with limited evidence of bioturbation, suggests that dysoxic bottom waters were common during deposition of this unit. The moderately elevated molybdenum values (25–100 ppm) found in several MCC1 samples may be due to episodic euxinic bottom-water conditions (Scott and Lyons, 2012). Concentrations of prasinophyte algae such as *Tasmanites* are thought to occur in temperate- to cool-water environments with periods of dysoxia to anoxia and high nutrient availability (fig. 8*F*) (Prauss, 2007; Vigran and others, 2008). We interpret the greater abundance and thickness of limestone event beds in the upper part of MCC1 as evidence for a shallowing-upward environment (figs. 7, 9*C–D*).

Granular phosphorites in the main outcrop belt appear to have formed in a "sweet spot" in space and time (Pufahl and Groat, 2017) where clastic input was reduced and phosphogenesis was enhanced. Coeval, more proximal strata to the northwest (South Barrow 3 and Simpson 1 wells) (fig. 1) and more distal strata to the south (Echooka River) both contain *Daonella frami* (Detterman and others, 1975; R. Blodgett, Robert B. Blodgett and Associates, written commun., 2019), but both lack granular phosphorites. We suggest that phosphogenesis at the onset of MCC1 was concentrated in the middle shelf environment where sections of the main outcrop belt accumulated, a setting less affected by siliciclastic influx than that of the proximal sections, but more subject to reworking and redeposition than the distal Echooka River site.

The lithologic differences between MCC1 in the Echooka River section and in the main outcrop belt (fig. 7) are due to a somewhat deeper-water setting for the former, consistent with its more distal position in the basin (fig. 1). We suggest that the lack of granular phosphorites and the presence of flat-clam pavement beds (fig. 9*E*) at Echooka River reflect a quiet submarine environment affected by few high-energy episodes. Limestone event beds are confined to the upper part of the section, which we interpret to have formed in shallowing-upward conditions. The phosphatic hardground that caps MCC1 at Echooka River (fig. 9*F–G*) is like the hardgrounds found at the tops of shallowing-upward successions in LC1 (fig. 6*F–G*) and, like those beds, likely records an interval of slow deposition or nondeposition.

## Sequence Stratigraphy

MCC1 constitutes the T-R sequence 2 (S2) of Whidden and others (2018) and Rouse and others (2020) (fig. 2). In the main outcrop belt, the TST of this sequence consists mainly of granular HPS that contain common phosphatic ooids and have high uranium contents and locally high REEs (fig. 8*B*). These strata are capped by a thin bed of mudstone, lime mudstone, or, at the Fire Creek section, a thin, covered interval (fig. 7) that we interpret as the mfs. Granular HPS, which make up the lower part of the RST (fig. 8*A,C–E*), grade upwards into variously phosphatic and calcareous siltstone to very fine grained sandstone that typically contains 1–4 percent phosphorus (as peloids and nodules) (fig. 9*A–B*). Limestone event beds (fig. 9*C–D*) increase in thickness and abundance upward. The succession at Echooka River is generally similar, but the TST and lower RST there lack HPS and contain more abundant thin beds of mudstone and fine-grained limestone, and the RST is capped by a phosphatic hardground (figs. 7, 9*E–G*). This phosphatic hardground formed during the

depositional hiatus that marks the transition from marine regression (top of S2) to transgression (base of T-R sequence 3 [S3], as defined by Whidden and others [2018] and Rouse and others [2020]). In the main outcrop belt, a change from limestone event beds to poorly exposed mudstones records this transition.

# Middle Carbonate-Chert Unit 2

MCC2 (fig. 2) (Whidden and others, 2018) is equivalent to the middle part of the limestone and dolomite member of Detterman and others (1975) and the lower part of zone B of Kupecz (1995). In outcrop, the unit was examined in eight complete to nearly complete sections and five partial sections (figs. 1, 10–12; table 1). MCC2 consists of limy siltstone, silty limestone, limestone, and subordinate mudstone. Coquinas containing pelecypods and other fossils are a characteristic feature of the upper part of this unit in the main outcrop belt. Overall, MCC2 is the least phosphatic part of the Shublik Formation in outcrop, although sparse to moderately common phosphate nodules occur in many sections and limited occurrences of HPS were found in a few western outcrops. Two coarsening- and thickening-upward sequences, defined by an increase in the abundance and thickness of pelecypod-bearing limestone layers, constitute the upper part of MCC2 at Fire Creek (Whidden and others, 2018). A similar pattern characterizes other sections in our study (fig. 10).

Fossils, mainly halobiid flat clams and ammonites, indicate an age of Carnian to early Norian for MCC2. Detterman and others (1975) report Carnian collections from strata we assign to this unit at Fire Creek and Echooka River. Carnian or younger calcareous dinoflagellates occur near the base of the unit at Golden Eagle (J. Self-Trail, USGS, written commun., 2019). Conodonts were found near the top of the unit in the Fire and Cobble Creek sections and indicate a Norian age (M. Orchard, Geological Survey of Canada, written commun., 2017).

## Lithologies

### Main Belt

Complete sections of MCC2 are ~13 to 28 m thick in the main outcrop belt (fig. 10), but the lower part of the unit is often poorly exposed or covered (for example, Whidden and others, 2018). The higher, well-exposed part of the unit consists of calcite-cemented quartz-carbonate±phosphate siltstone to fine-grained sandstone (fig. 11*A*) interbedded with (and grading into) silty pelecypod wackestone, packstone, and grainstone (fig. 11*F–G*). Bioclasts in halobiid-bearing beds are locally bored and are typically broken and abraded. Textures indicate that most limestone beds of MCC2 have affinities with the transported flat-clam facies of Whidden and others (2019b), but some intervals, especially in the lower part of the unit, contain in situ concentrations of halobiid bivalves interlayered with calcareous and (or) siliceous radiolarite (fig. 11*B–E*). Both displaced and in situ phosphatic masses occur in MCC2; many beds contain minor amounts of phosphatic peloids, nodules, and (or) clasts. Phosphatic steinkerns and phosphate-filled burrows are locally notable in this unit, and phosphate-coated flat-clam (halobiid) fragments are found in upper beds of some sections (figs. 10, 11*F–G*). HPS are rare and confined to a few thin beds rich in displaced phosphate clasts, seen chiefly in the upper part of the Spire (figs. 3*C*, 10) and Kemik Creek sections. Thin, discontinuous phosphatic hardgrounds occur near the top of the unit at the Mesa (fig. 10), Kemik Creek (fig. 12*F–G*), and Cache Creek localities.

The uppermost part of MCC2 is faunally and lithologically distinctive. It consists of 1–3 m of coarse-grained bivalve coquina interbedded with calcareous siltstone to fine-grained sandstone (fig. 12*A–E*). The coquina layers, which are 1–25 cm thick, coarsen and thicken upward within the interval; their bed bases are sharp and scoured, and some of the siltstone interbeds are internally laminated or cross-laminated (fig. 12*A–C*, *E*). Horizontal and vertical burrows are abundant (fig. 12*A–C*, *E*). Shell fragments, largely derived from thick-shelled bivalves such as *Gryphaea* sp. (with few definitive flat-clam pieces), are loosely to tightly packed in a matrix of quartz siltstone or calcite spar cement (fig. 12*D–G*). Phosphatic pebbles and steinkerns occur within, or are concentrated along the bases of, some beds (fig. 12*D–G*); siltstone rip-up clasts as long as 4 cm occur locally.

Echinoderm fragments (including echinoid spines) (fig. 11*A*, *F*) are a common constituent of both siltstone and limestone beds throughout MCC2. Phosphatized and calcitized radiolarians and sponge spicules occur mainly in phosphate nodules and clasts; calcitized (and rare silica-filled) radiolarians are also found disseminated or concentrated into thin layers within halobiid-bearing limestone intervals (fig. 11*B–E*). Fossils identified in MCC2 at Fire Creek include several species of *Halobia*, other bivalves (*Leptochondria nationalis*, *Gryphaea* sp., and *Lima* sp.), arcestid ammonites, rhynchonellid brachiopods, and gastropods (Detterman and others, 1975), as well as several species of ostracodes (Sohn, 1987). Halobiid pelecypod fragments and spiriferid and rhynchonellid brachiopods (Tourtelot and Tailleur, 1971) occur in correlative strata at Cache Creek. Other fossils seen in thin section include bryozoan fragments, vertebrate bone fragments (fig. 12*G*), and rare foraminifera.

### Echooka River

MCC2 in the Echooka River section is ~18 m thick; the lower fifth of the unit is mostly covered (fig. 10). Like MCC1, MCC2 at Echooka River has similarities and differences with coeval strata in the main outcrop belt. Identical species of *Halobia* and similar arcestid ammonites occur in MCC2 at Fire Creek and Echooka River (Detterman and others, 1975),

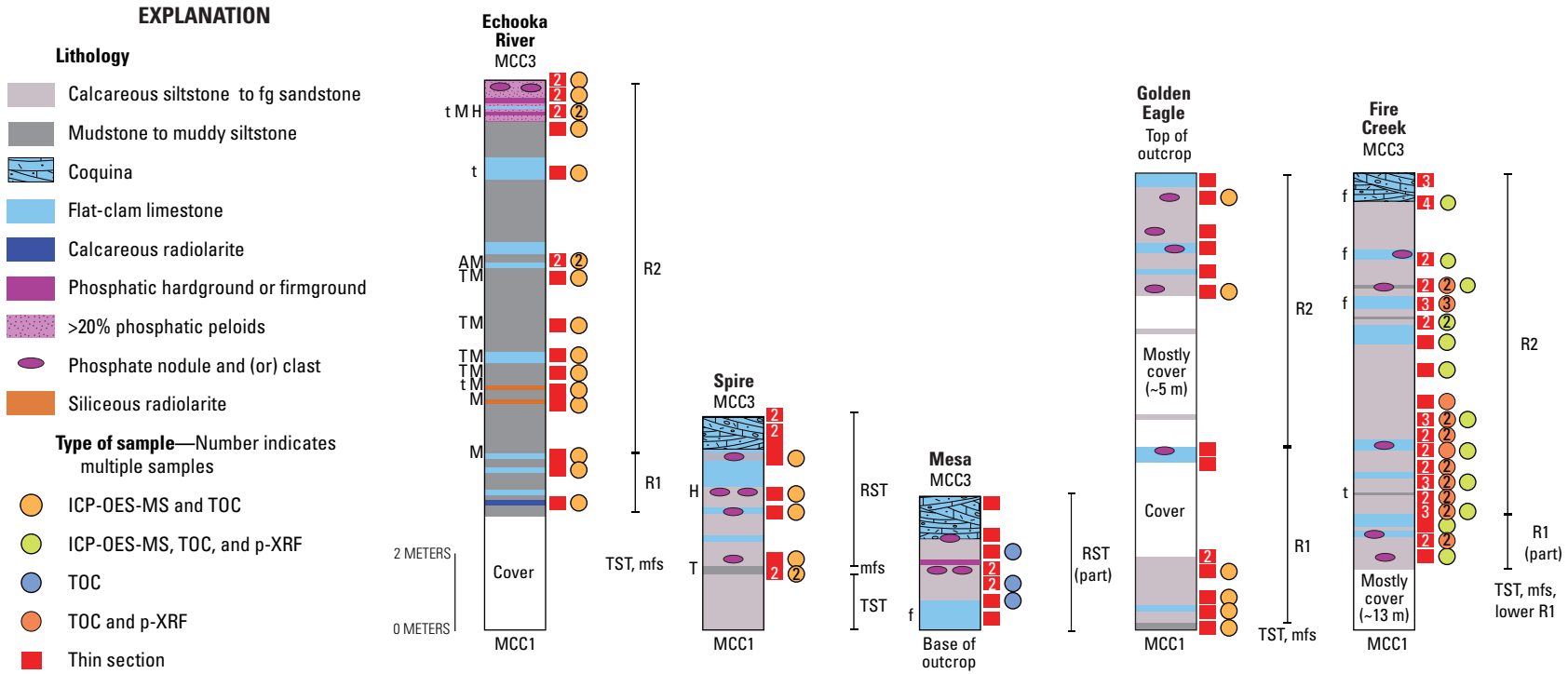


**Figure 10.** Stratigraphy of middle carbonate-chert unit 2 (MCC2) of the Triassic Shublik Formation, northeastern Alaska, in the most completely exposed sections measured for this study. Outcrop evidence indicates that the Spire section has been shortened by faulting, and only the upper part of MCC2 is exposed at the Mesa section. Inorganic geochemical data are based on inductively coupled plasma-optical emission spectroscopy-mass spectroscopy (ICP-OES-MS) analyses (Dumoulin and others, 2023). The term "cover" indicates a part of the section that is poorly exposed or covered. See figure 1 and table 1 for locality information. R1 and R2 denote regressive parasequences within the regressive systems tract (RST). Other abbreviations: fg, fine-grained; TOC, total organic carbon; p-XRF, portable X-ray fluorescence; MCC3, middle carbonate-chert unit 3; TST, transgressive systems tract; mfs, maximum flooding surface; MCC1, middle carbonate-chert unit 1; %, percent; ppm, parts per million; m, meter. The informal MCC1, MCC2, and MCC3 units are from Whidden and others (2018).

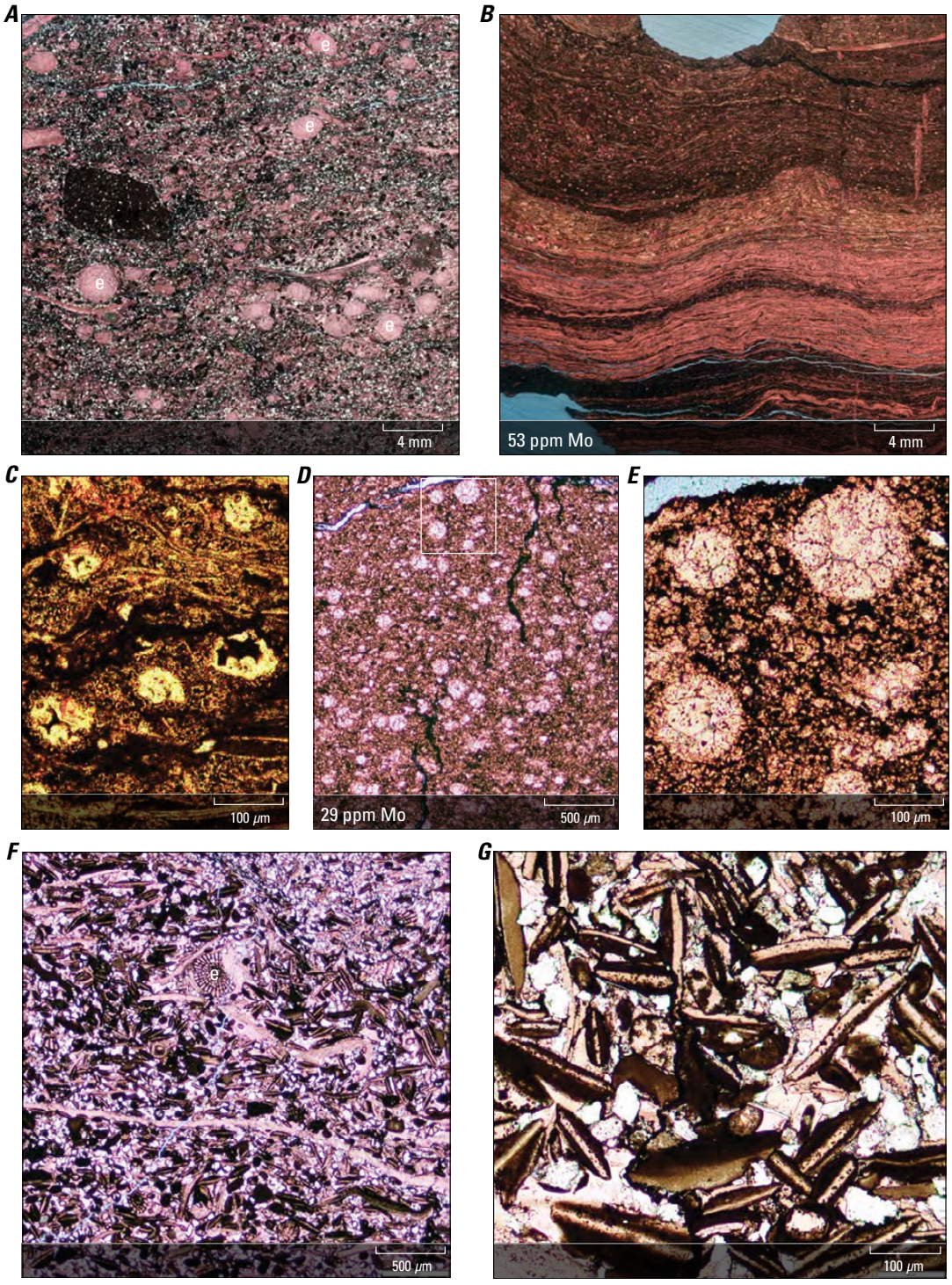


**Figure 11.** Images of sedimentary and biogenic features of middle carbonate-chert unit 2 (MCC2) of Whidden and others (2018) in the Triassic Shublik Formation, northeastern Alaska. *A*, Thin section scan from the Cobble Creek locality showing quartz-carbonate-phosphate siltstone with halobiid flat-clam fragments and locally abundant echinoderm debris, including echinoid spines (e). *B*, Thin section scan from the Aichilik River locality showing concentrations of thin-shelled halobiid flat clams and muddy interlayers that contain silica- (chalcedony-) filled radiolarians. *C*, Photomicrograph from Aichilik River showing the radiolarians in close view. *D*, *E*, Photomicrographs from Aichilik River of calcareous radiolarite. Box in *D* shows extent of part *E*. *F*, *G*, Photomicrographs from Cobble Creek of abundant, phosphate-coated halobiid fragments, an echinoid spine (e), and quartz silt (white grains) in a silty, phosphatic limestone bed (halobiid grainstone) near the top of MCC2. Calcite is stained pink in parts *A*–*G*. See figure 1 and table 1 for locality information. Geochemical data (Dumoulin and others, 2023) shown in inset box where available. Mo, molybdenum; ppm, parts per million; mm, millimeter µm, micrometer. Photographs by J.A. Dumoulin, U.S. Geological Survey.

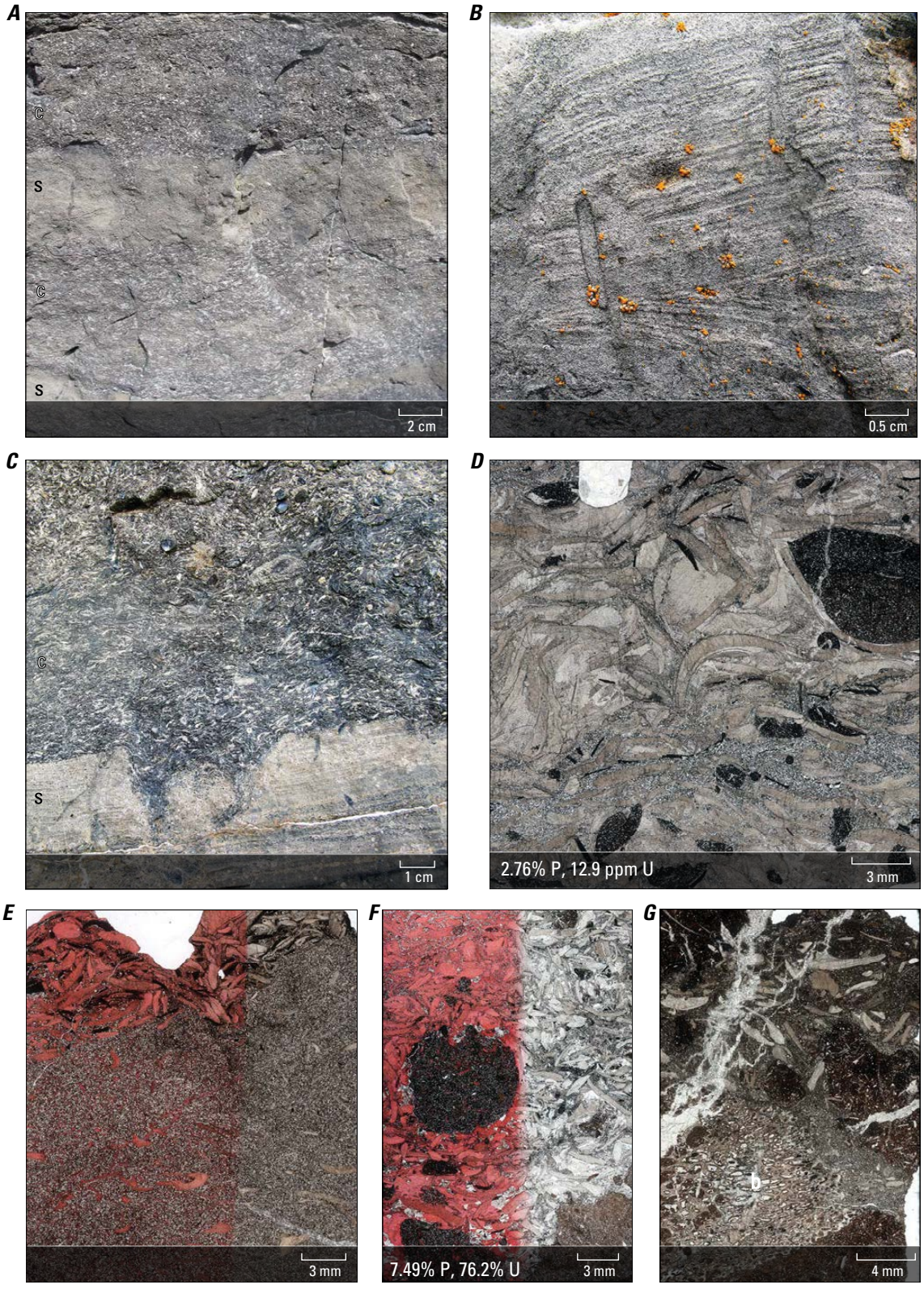
A
C
S
C
S
2 cm
B
0.5 cm
C
C
S
1 cm
D
2.76% P, 12.9 ppm U
3 mm
E
3 mm
F
7.49% P, 76.2% U
3 mm
G
b
4 mm

**Figure 12 (page 24).** Images of additional sedimentary and biogenic features of the upper part of middle carbonate-chert unit 2 (MCC2) of Whidden and others (2018) in the Triassic Shublik Formation, northeastern Alaska. *A*, Photograph of outcrop at the Camp 263 Creek locality showing coquina (c) interbedded with calcareous siltstone (s). *B*, Photograph of outcrop at Camp 263 Creek showing cross-bedded calcareous siltstone cut by vertical burrows. *C*, Photograph of outcrop at Camp 263 Creek showing coquina interbedded with calcareous siltstone; lower siltstone layer is cross-bedded and cut by vertical burrows. *D*, Thin section scan from Camp 263 Creek of coquina composed of robust bivalve fragments in a matrix of calcite spar and quartz siltstone with locally common phosphatic clasts and steinkerns. *E*, Thin section scan from the Spire locality of coquina similar to that in part *D* overlying siltstone. Calcite is stained pink on the left side. *F*, Thin section scan from the Kemik Creek locality showing coquina overlying phosphatic hardground. Calcite is stained pink on the left side. *G*, Thin section from Kemik Creek of coquina with bone fragment (b). See figure 1 and table 1 for locality information. Geochemical data (Dumoulin and others, 2023) shown in inset box where available. %, percent; P, phosphorus; U, uranium; ppm, parts per million; cm, centimeter; mm, millimeter. Photographs by J.A. Dumoulin, U.S. Geological Survey.

and two coarsening-upward sequences constitute the upper parts of both sections. However, at Echooka River, the fine-grained parts of the two sequences are mudstone to muddy siltstone with thin layers of calcareous and siliceous radiolarite (fig. 10), not siltstone to sandstone as seen in the main outcrop belt. Interbeds of halobiid wackestone to packstone increase upward in abundance and thickness in both of the coarsening-upward sequences at Echooka River. Mudstone, especially in the lower part of the upper sequence, is organic-rich, and non-carbonate mud forms the matrix of some halobiid-bearing beds. Granular calcite spar cement obliterates the original depositional textures in other limy layers near the top of both sequences. Where preserved, the original textures indicate that the flat-clam beds there, as in the main outcrop belt, represent a range in degree of post-mortem transport. Quartz silt is largely absent from limestones throughout MCC2 at Echooka River, and phosphate is found mainly near the top of the upper sequence, where fine- to coarse-sand-sized phosphatic clasts are concentrated at the base of some limy beds. Thin, undulatory layers there that are locally heavily phosphatized are likely discontinuous hardgrounds (fig. 10).

As in the main outcrop belt, echinoderm debris is abundant throughout MCC2 at Echooka River and is the main bioclast in some limestones. Ammonites occur at several horizons in the upper coarsening-upward sequence, most notably at the top of a 20-cm-thick bed that overlies 3.5 m of organic-rich mudstone (fig. 10). A dozen specimens, 1–5 cm in diameter, were found on the upper bedding surface, which also contains abundant halobiid flat clams. The ammonites identified from this bed consist of *Arctosirenites* cf. *A. canadensis* Tozer, *Juvavites* sp., and *Arcestes* sp. (Detterman and others, 1975). Ostracodes are a minor component of some wacke-packstone intervals, and scattered fragments of brachiopods and robust bivalves are found in limy layers at the top of the unit.

## Geochemistry

### Total Organic Carbon Data

TOC values determined in this study for MCC2 are generally low, with a few exceptions, and the patterns match those previously reported from this interval at Fire Creek by Detterman (1970) and Kelly (2004). More than two-thirds of our samples from 12 complete and partial sections of this unit (table 4) ($n$=103) (Dumoulin and others, 2023) contain <1.6 weight percent TOC. The lowest values occur in limestones in the upper half of the unit. The highest values (3.19–6.33 weight percent, $n$=8) occur mainly in mudstones and muddy siltstones in the lower part of the unit at Spire and near the middle of the Echooka River section (fig. 10). Five samples from Echooka River contain >4.7 weight percent TOC, including a sample of HPS near the top of the unit (fig 10).

### Inorganic Geochemical Data

Mudstone, siltstone, and limestone in MCC2 are less phosphatic but otherwise similar geochemically to those lithologies in MCC1 (tables 3, 4) (Dumoulin and others, 2023). HPS are less common in MCC2 than in any other part of the Shublik Formation and occur only as rare event beds near the top of the section at Spire, Echooka River (fig. 10), and Kemik Creek. Less than half of all samples analyzed by ICP-OES-MS from MCC2 contained >1 percent phosphorus, and less than one-fifth of the samples contained >2 percent phosphorus (Dumoulin and others, 2023). Analysis by p-XRF of closely spaced samples from the Fire Creek section show similar chiefly low phosphorus abundances (Dumoulin and others, 2023) and compare well with compositional data previously reported by Detterman (1970) and Kelly (2004).

**Table 4.** Geochemical data (Dumoulin and others, 2023) from the middle carbonate-chert unit 2 (MCC2) of Whidden and others (2018) in the Triassic Shublik Formation, northeastern Alaska.

[See figure 1 for locality map and table 1 for locality details. See (Dumoulin and others, in 2023) for complete geochemical data; samples from MCC2 that were analyzed only for total organic carbon (TOC) (Cache Creek, number of samples [*n*]=5; Camp 263, *n*=9; Fire Creek, *n*=27; Mesa, *n*=3; North Sadlerochit, *n*=3) are not included below. Localities: A, Aichilik River; Co, Cobble Creek; 2, Camp 263 Creek; D, Dodo Creek; E, Echooka River; F, Fire Creek; G, Golden Eagle; Ke, Kemik Creek; S, Spire. Other abbreviations: Al, aluminum; Ca, calcium; cc, calcareous; HPS, highly phosphatic strata; lms, limestone; m, mudstone; md, muddy; Mo, molybdenum; P, phosphorus; ppm, parts per million; rad, radiolarian-rich strata; s., sample(s); Si, silicon; sil, siliceous; sltst, siltstone; sst, sandstone; U, uranium; %, percent; —, not applicable; /, to]

| Lithology | Localities | TOC (weight percent) | Concentration | | | | | |
|---|---|---|---|---|---|---|---|---|
| | | | Al (%) | Ca (%) | Si (%) | P (%) | Mo (ppm) | U (ppm) |
| m/md sltst | F, G, S | 0.97–3.21 | 3.51–4.21 | 7.44–18.9 | 14.9–29.6 | 0.64–2.89 | 10–20 | 8.52–24.3 |
| | (*n*=5) | (2 s. ≥3.1) | — | — | — | (1 s. >1) | — | — |
| | E | 1.69–6.33 | 1.76–3.5 | 7.77–24.8 | 11.5–27.3 | 0.03–1.48 | 53–183 | 5.86–32.3 |
| | (*n*=5) | (4 s. >3.2) | — | — | — | (1 s. >1) | — | — |
| sil rad | A, E (*n*=3) | 1.07–1.96 | 0.59–0.71 | 16.2–19.2 | 22.6–25.3 | 0.04–0.05 | 35–53 | 6.03–9.01 |
| cc rad | A (*n*=2) | 0.51, 2.04 | 0.47, 0.6 | 33.7, 35.8 | 2.68, 2.9 | 0.02, 0.04 | 18, 29 | 3.78, 3.86 |
| cc sltst/sst | D, F, G, Ke, S | 0.29–1.64 | 1.16–2.98 | 14.6–24.8 | 12.3–29.6 | 0.34–2.7) | <2–9 | 4.87–22.7 |
| | (*n*=15) | — | — | — | — | (5 s. >1) | — | — |
| lms | A, Co, 2, D, F, G, Ke | 0.38–0.84 | 0.58–1.43 | 27.2–34.4 | 3.1–11.4 | <0.1–4.21 | 2–40 | 2.31–55.2 |
| | (*n*=14) | — | — | — | — | (10 s. >1) | (1 s. >21) | — |
| | E | 0.45–5.1 | 0.23–0.79 | 27.9–35.7 | 0.94–9.43 | 0.02–3.69 | 4–34 | 1.61–7.36 |
| | (*n*=9) | (3 s. >2) | — | — | — | (2 s. >1) | (2 s. >25) | — |
| HPS | Ke, S (*n*=3) | 0.88–1.12 | 1.07–1.33 | 22.8–30.3 | 8.91–16 | 4.65–7.49 | 4–8 | 19.2–146 |
| | E (*n*=1) | 4.8 | 1.37 | 21.3 | 12.7 | 5.21 | 40 | 17.5 |

Uranium values are generally low throughout MCC2, except for three samples of phosphatic limestone coquina and HPS at Kemik Creek that contain 55, 76, and 146 ppm uranium (table 4) (Dumoulin and others, 2023); these samples are within and adjacent to a phosphatic hardground near the top of the unit that has local fluorite cement (fig. 12*F–G*).

Elevated molybdenum contents (33–183 ppm) characterize much of MCC2 at Echooka River (fig. 10) and were also found in several radiolarian-bearing beds (fig. 11*B–E*) and one halobiid limestone in the Aichilik River section (table 4) (Dumoulin and others, 2023). Highest molybdenum values at Echooka River (175 and 183 ppm) occur in organic-rich, muddy siltstones that also contain high concentrations of vanadium (1,070 and 1,560 ppm) and zinc (582 and 677 ppm).

## Depositional Setting

In the main outcrop belt, lithofacies, faunal, and geochemical data from MCC2 indicate that deposition took place largely in middle- to inner-ramp settings similar to, and in part slightly shallower than, those posited for MCC1. The predominance of halobiid bivalves, which like *Daonella* were tolerant of low oxygen levels (McRoberts, 2010), imply that dysoxic conditions may have been common. However, increasing evidence of bioturbation in upper parts of MCC2 indicate increasing oxygenation with time. We interpret sequences of coarsening- and thickening-upward limestone event beds as shallowing-upward successions. The coquina beds that cap MCC2 contain coarser, more diverse shell fragments than those of limestone beds in any other part of the Shublik Formation in the main outcrop belt, and the fauna includes thick-shelled bivalves, including the oyster *Gryphaea* sp., that are typical of nearshore biofacies (R. Blodgett, Robert B. Blodgett and Associates, written commun., 2019). The coquina beds thus demonstrate input from shallow-water, high-energy (inner-ramp) environments. Reduced abundance of phosphate in MCC2 relative to underlying parts of the Shublik Formation suggests that deposition occurred in a less productive setting, a change that could reflect large-scale environmental shifts. An episode of global warming during the Carnian, the Carnian pluvial episode (for example, Dal Corso and others, 2018), may have affected oceanic circulation patterns, and thus nutrient availability and phosphate cycling, in the Arctic Alaska basin.

The differences between MCC2 at Echooka River and in the main outcrop belt likely reflect the deeper-water, more distal setting of the former locality. These differences include the overall finer grain size and higher organic content of the Echooka River section. Coarse-grained coquina beds are

lacking in MCC2 at Echooka River, although the highest limy beds do contain a few robust bivalve fragments. Elevated molybdenum contents (33–183 ppm) occur throughout the section and imply that low-oxygen conditions were more prevalent at Echooka River; values >25 ppm and >100 ppm have been interpreted to indicate intermittently and persistently euxinic conditions, respectively (Scott and Lyons, 2012).

### Sequence Stratigraphy

MCC2 makes up the entirety of S3 of Whidden and others (2018) and Rouse and others (2020) (fig. 2). At Fire Creek, the TST, mfs, and lower RST of this sequence are mainly poorly exposed calcareous mudstone and siltstone (see fig. 9*B* of Whidden and others, 2018) (fig. 10). Limestone event beds, which are more abundant in the upper, better-exposed part of the unit at Fire Creek, define two coarsening- and thickening-upward parasequences (Whidden and others, 2018; Rouse and others, 2020). Similar patterns characterize other sections in the main outcrop belt and at Echooka River (fig. 10). The coquina beds at the top of the unit are the coarsest-grained limestones seen in any exposures of the Shublik Formation. MCC2 at Echooka River is finer grained overall than coeval strata in the main outcrop belt, and the uppermost beds contain more phosphatic clasts and fewer robust bivalve fragments. Thin, phosphatic hardgrounds found near the top of the unit at Echooka River and in several main belt outcrops reflect depositional hiatuses during the culmination of the RST.

## Middle Carbonate-Chert Unit 3

MCC3 (fig. 2) (Whidden and others, 2018) is equivalent to the upper part of the limestone and dolomite member of Detterman and others (1975) and the upper part of zone B of Kupecz (1995). In 6 of the 10 studied outcrop sections, the unit appears to be complete or nearly so (figs. 1, 13–15; table 1). MCC3 is typically the most calcareous part of the Shublik Formation and contains the least amount of siliciclastic detritus. Although HPS occur in virtually all the MCC3 sections we examined, they are more heterogeneous in form and discontinuous in vertical and lateral extent than those in MCC1; phosphate is most abundant in the upper half of MCC3. As in MCC2, two coarsening-upward sequences form the upper part of MCC3 in complete sections, but the upper sequence of MCC3 is finer grained overall than the lower sequence.

Flat clams occur widely in MCC3, but few precise age determinations have been published for the strata bearing them. However, fossil constraints from underlying and overlying units indicate an age of early to middle Norian for MCC3. The most constrained ages come from the Phoenix 1 well, 200 km northwest of the outcrop belt (fig. 1), where four distinct species of *Halobia* denote early and middle Norian ages (McRoberts and others, 2020) for strata that we assign to MCC3. At Fire Creek, near the middle of MCC3, *Eomonotis* sp. indet. and *Halobia* sp. indet. occur together and indicate an age of middle to late middle Norian (*Columbianus* ammonoid zone) (identification by C. McRoberts in Whidden and others, 2018). A similar co-occurrence of halobiids and monotids (likely eomonotids) at Bathtub ridge (fig. 1; table 1) (identification by N. Silberling in Camber, 1994), indicates a comparable age for these strata. Late Triassic foraminifera are reported by Bergquist (1966) from beds we include in MCC3 at Dodo Creek. Carnian or younger calcareous dinoflagellates occur near the middle of the unit at Spire (J. Self-Trail, USGS, written commun., 2019). Poorly preserved palynomorphs of Middle to Late Triassic age occur in mudstone near the base of the unit at the Mesa section (J. Bujak, Bujak Research International, written commun., 2015).

### Lithologies

#### Main Belt

Complete sections of MCC3 in the main outcrop belt range from ~15 to 21.5 m thick (fig. 13). The lower part of the unit consists mainly of mudstone, siltstone, and (or) flat-clam limestone. Thin interbeds of calcareous radiolarite occur at Fire Creek, where many closely spaced samples were taken from these lower beds (fig. 13).

The middle part of MCC3 consists largely of flat-clam packstones (fig. 14*A–B*) and grainstones that form a coarsening- and thickening-upward succession (fig. 13). Microtextures such as broken shells and chaotic shell orientation (fig. 14*B*) denote that the flat-clam fossils in many beds have undergone some transport, but other layers contain well-ordered accumulations of thin and delicate but intact shells, which likely accumulated primarily in situ (fig. 14*A*). Sub-millimeter scale bioturbation whorls occur locally. Phosphate, which forms in situ nodules, displaced clasts (including steinkerns) (fig. 14*B*), and in situ and displaced peloids, is most abundant in the upper part of the succession, which is capped by one or more intervals of HPS (phosphate-rich event beds and phosphatic hardgrounds) (figs. 13, 14*B*).

The upper part of MCC3 is mainly lime mudstone (fig. 14*E–F*) to wackestone with subordinate interlayers of calcareous radiolarite and flat-clam packstone to grainstone (fig. 13). Petrographic study and geochemical analyses indicate that mudstones and wackestones in MCC3 are generally more calcareous than texturally equivalent strata in underlying units; the matrix is largely microspar (20- to 30-µm calcite crystals) (fig. 14*F*) (Folk, 1965). Beds coarsen and thicken upwards, and the flat-clam accumulations display various degrees of post-mortem transport. Phosphate types and patterns of occurrence are like those seen in the middle part of the unit (figs. 3*F*, 13, 14*C–D*). Phosphate is especially abundant at the top of MCC3, where it forms crusts, firmgrounds, and hardgrounds with complex microtextures that record multiple cycles of phosphate deposition and reworking (fig. 15*A–C*). These strata contain locally abundant pyrite (fig. 15*A–B*) and have distinctive geochemical characteristics.

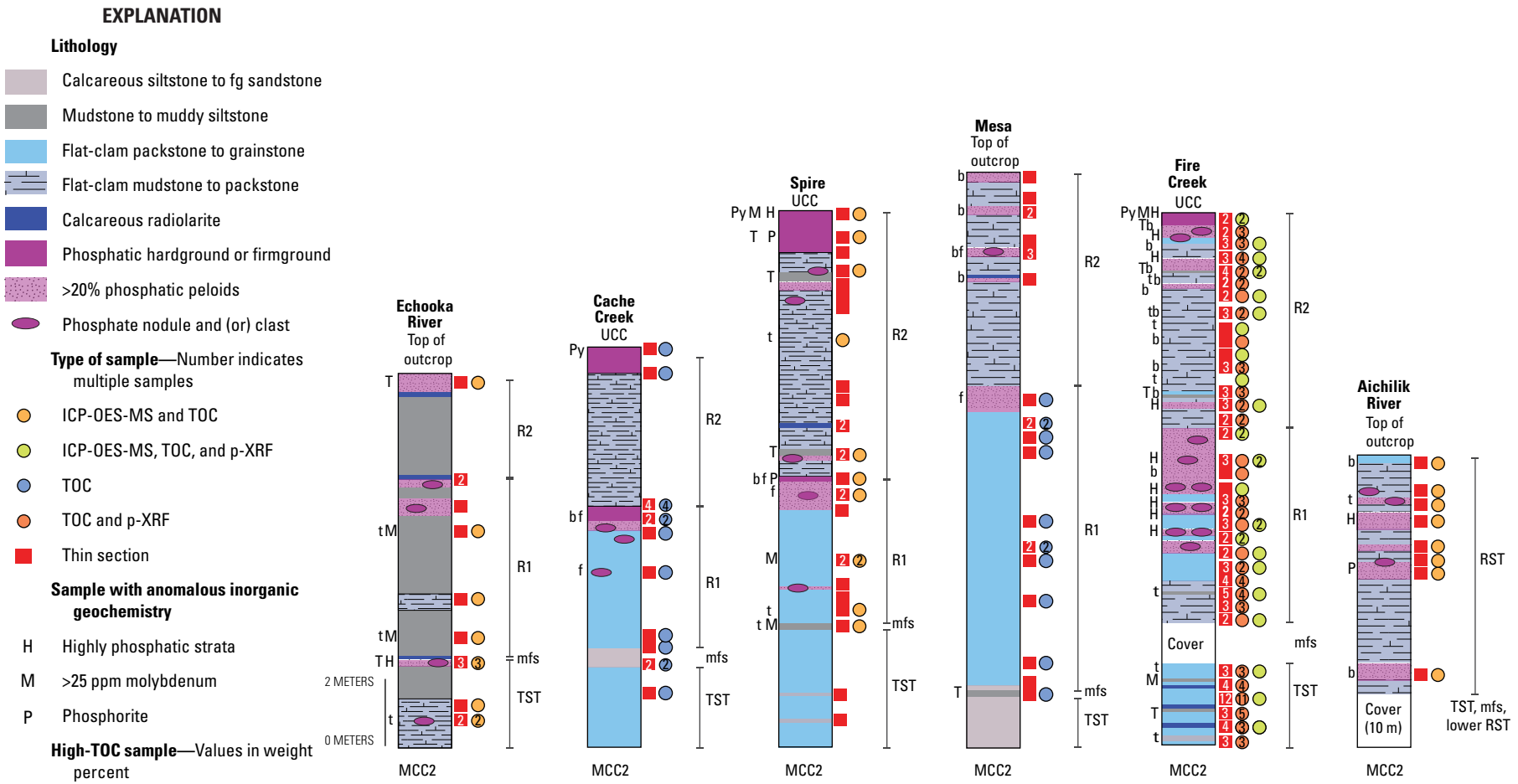


**Figure 13.** Stratigraphy of middle carbonate-chert unit 3 (MCC3) of the Triassic Shublik Formation, northeastern Alaska, in the most completely exposed sections measured for this study. The term "cover" indicates a part of the section that is poorly exposed or covered. Inorganic geochemical data (Dumoulin and others, 2023) are based on inductively coupled plasma-optical emission spectroscopy-mass spectroscopy (ICP-OES-MS) analyses. See figure 1 and table 1 for locality information. R1 and R2 denote regressive parasequences within the regressive systems tract (RST). Other abbreviations: fg, fine-grained; TOC, total organic carbon; p-XRF, portable X-ray fluorescence; mfs, maximum flooding surface; TST, transgressive systems tract; MCC2, middle carbonate-chert unit 2; UCC, upper clastic-carbonate unit; %, percent; ppm, parts per million; m, meter. The informal MCC2, MCC3, and UCC units are from Whidden and others (2018).

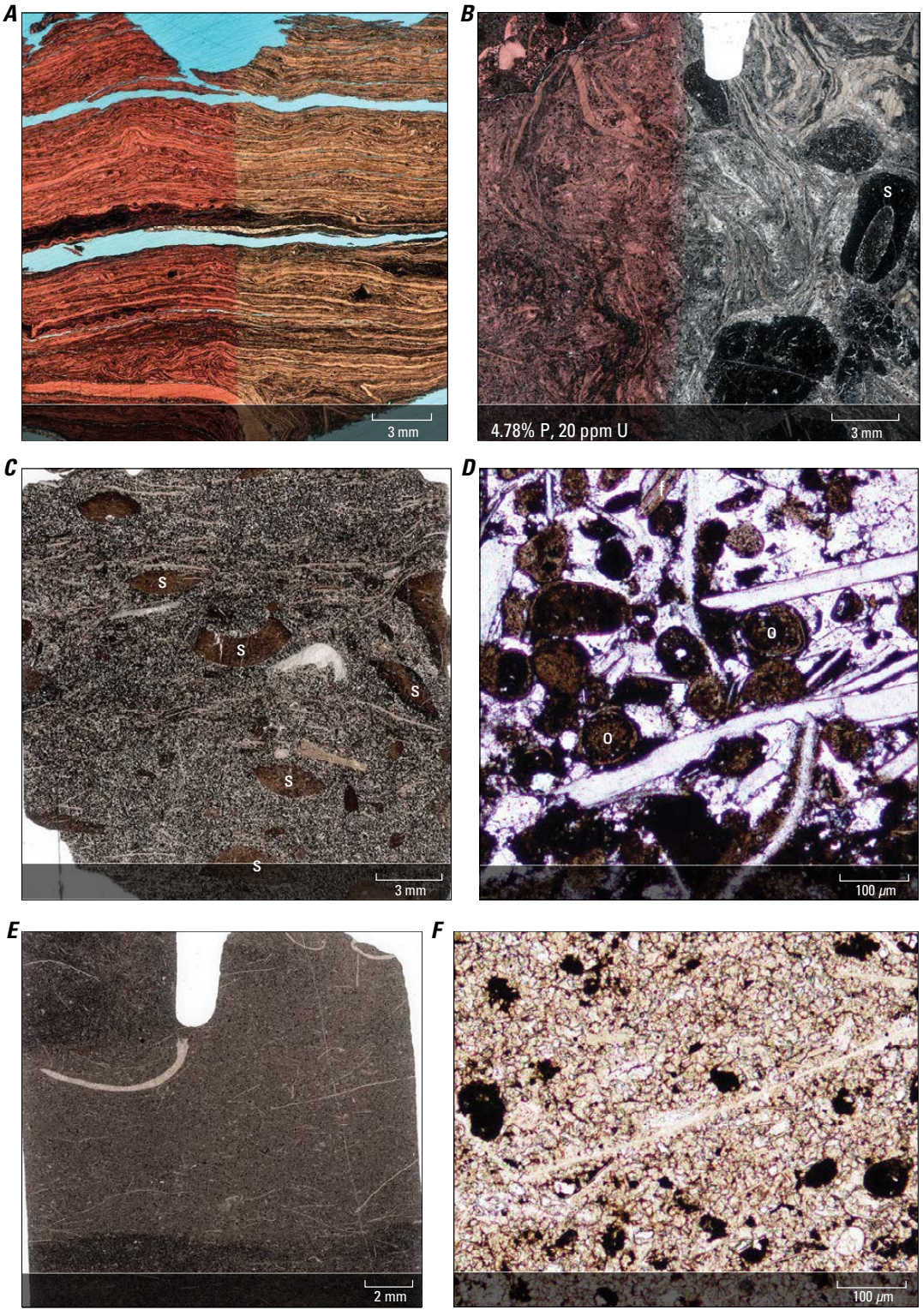


**Figure 14.** Images of sedimentary and biogenic features of middle carbonate-chert unit 3 (MCC3) of Whidden and others (2018) in the Triassic Shublik Formation, northeastern Alaska. *A*, Thin section scan from the Mesa locality showing tightly packed flat-clam packstone in the lower parasequence. *B*, Thin section scan from the Dodo Creek locality showing event bed from near the top of the lower parasequence that contains chaotically arranged flat-clam shells and displaced phosphatic clasts, including steinkerns (s). *C*, Thin section scan from Mesa showing event bed from near the top of the upper parasequence that contains abundant phosphatic peloids and steinkerns. *D*, Photomicrograph from Mesa showing event bed from near the top of the upper parasequence that contains phosphatic clasts including ooids (o), and phosphate-coated flat clams (f). *E*, *F*, Thin section scan (*E*) and photomicrograph (*F*) from Mesa, sampled from the upper parasequence, of lime mudstone with sparse, mainly very thin flat-clam shells and minor phosphatic peloids in a matrix of microspar. See figure 1 and table 1 for locality information. Geochemical data (Dumoulin and others, 2023) shown in inset box where available. %, percent; P, phosphorus; U, uranium; ppm, parts per million; mm, millimeter; µm, micrometer. Images by J.A. Dumoulin, U.S. Geological Survey

The sand-sized phosphate grains found throughout MCC3 are mainly simple peloids (figs. 3*F*, 15*D*), but phosphatic ooids occur in minor amounts near the tops of both coarsening-upward successions (fig. 14*D*). Phosphate-coated flat-clam fragments were also seen in the upper beds of both successions (figs. 13, 14*D*). Fluorite cements some phosphate-rich beds in the lower coarsening-upward interval.

Belemnoid rostrums have distinctive cross sections in thin section view (see figs. 70, 71 of Adams and MacKenzie, 1998) and were seen exclusively in samples from MCC3 (fig. 13). These rostrum cross sections are rounded to ovoid and 0.4–1.25 mm in diameter (fig. 15*D*). They occur in numerous beds in the upper half of the unit at Fire Creek (figs. 13, 15*D*) and were also seen in MCC3 samples from the

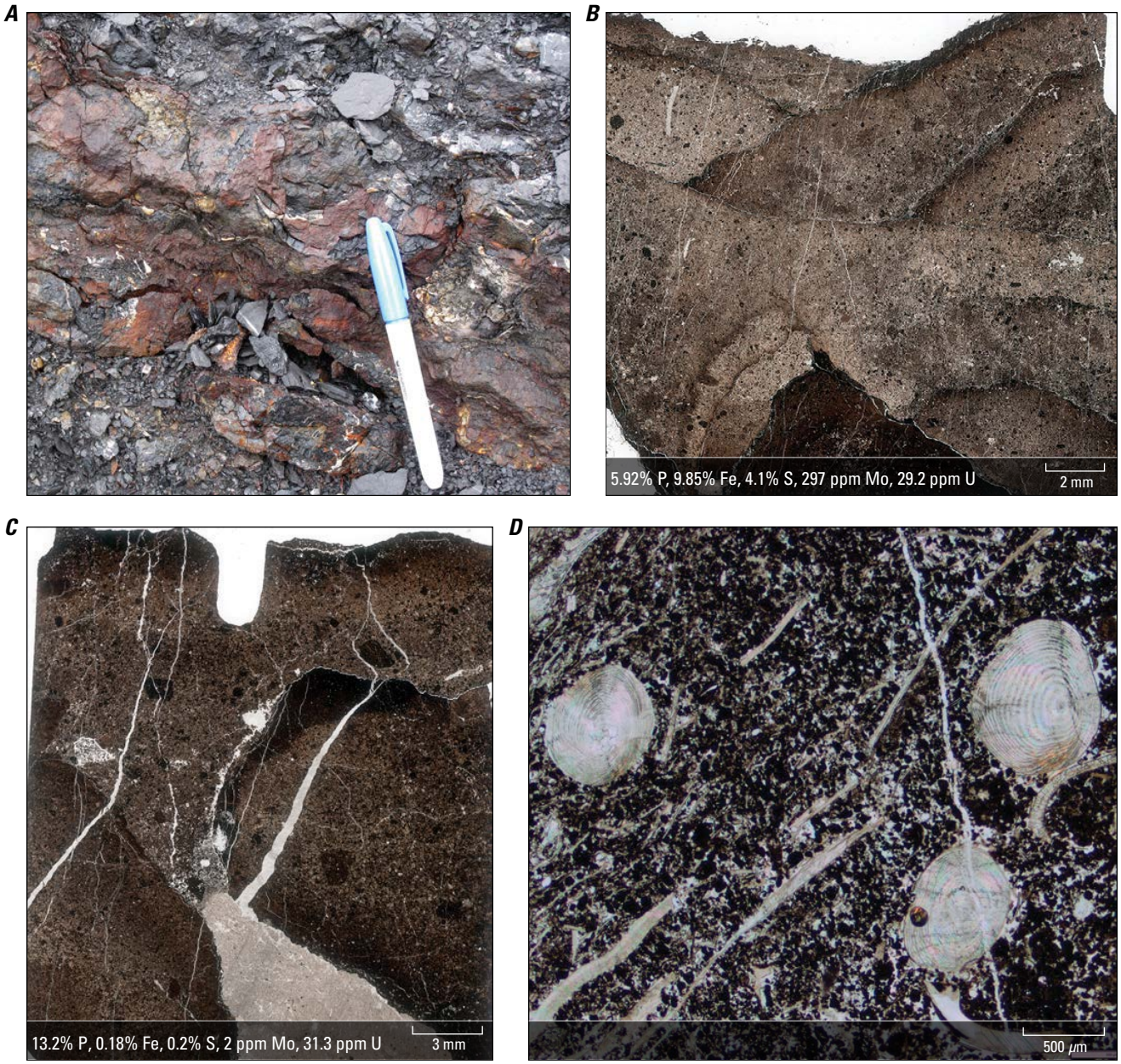


**Figure 15.** Images of additional sedimentary and biogenic features of middle carbonate-chert unit 3 (MCC3) of Whidden and others (2018) in the Triassic Shublik Formation, northeastern Alaska. *A*, Photograph of outcrop at the Spire locality showing a thick phosphatic hardground with complex microtextures at the top of MCC3; the upper part of this hardground is highly pyritic. *B*, *C*, Thin section scans of the phosphatic hardground shown in part *A* showing complex microtextures; sample at top of hardground (*B*) is pyritic and less phosphatic than sample near base (*C*). *D*, Photomicrograph from the Fire Creek locality showing belemnoid rostrums in flat-clam limestone with abundant phosphatic peloids. See figure 1 and table 1 for locality information. %, percent; P, phosphorus; Fe, iron; S, sulfur; Mo, molybdenum, U, uranium; ppm, parts per million; mm, millimeter; µm, micrometer. Geochemical data (Dumoulin and others, 2023) shown in inset boxes where available. Images by J.A. Dumoulin, U.S. Geological Survey.

Mesa (fig. 3*F*), Dodo Creek, Cache Creek, Spire, and Aichilik River sections, a partial section of MCC3 at Camp 263 Creek, and an isolated locality of probable MCC3 in the USGS Arctic D-4 quadrangle. Echinoderm fragments are notably rarer in MCC3 than in MCC2 and occur mainly in flat-clam beds near the tops of the coarsening-upward cycles. Radiolarians are locally abundant in thin layers of calcareous radiolarite (fig. 13) and are common in most phosphate-rich intervals, where they are replaced by phosphate, calcite, or pyrite within phosphate nodules, clasts, and hardgrounds. Fossils previously reported from beds we assign to MCC3 include various ostracodes (Sohn, 1987), the ammonite *Sirenites* sp. at Fire Creek (Detterman and others, 1975), and rhynchonelloid and spiriferid brachiopods at Bathtub ridge (identified by N. Silberling in Camber, 1994). Bryozoans, gastropods (fig. 3*F*), foraminifera, and sponge spicules are minor faunal components seen in thin sections from MCC3.

### Echooka River

MCC3 at Echooka River is at least 14 m thick (fig. 13); the uppermost beds of the Shublik Formation are not exposed at this locality. The section overall is finer grained, less calcareous, less phosphatic, and more organic-rich than equivalent strata in the main outcrop belt. The main lithology is noncalcareous to weakly calcareous mudstone to muddy siltstone. Lime mudstone to fine-grained wackestone is found mainly in the lower part of the section, and thin layers of calcareous radiolarite occur locally (fig. 13). The lowest of these layers overlies a thin interval of very fine grained, organic-rich HPS with abundant phosphatic peloids and phosphate-filled radiolarians. Coarser beds of flat-clam wackestone to packstone with abundant phosphatic peloids and nodules occur in the upper third of the section (fig. 13). Detterman and others (1975) report halobiid flat clams, brachiopods (including the rhynchonellid *Psioidea* sp.), and indeterminate ammonites from these beds.

## Geochemistry

### Total Organic Carbon Data

Previously reported TOC values from MCC3 at Fire Creek are mostly <2 weight percent (Detterman, 1970; Kelly, 2004). New data that we obtained from MCC3 in eight sections ($n$=170) are similar but include higher values from several parts of the unit (table 5) (Dumoulin and others, 2023). Mudstones and muddy siltstones with 2.05–4.23 weight percent TOC occur in the lower part of the unit at Spire, Mesa, and Fire Creek; similar beds in the upper part of the unit at Spire and Fire Creek have 2.99–4.76 weight percent TOC (fig. 13). Higher TOC also characterizes our MCC3 samples from the Echooka River section, where eight of ten samples contained 2.18–3.91 weight percent TOC (fig. 13) (Dumoulin and others, 2023). Limestone with sparse to abundant flat clams, a lithology that makes up much of MCC3, typically has low (<1.6 weight percent) TOC (table 5); highest TOC contents were found at Spire and Aichilik River, in clam-rich packstones with textures indicating in situ bivalve accumulations.

**Table 5.** Geochemical data (Dumoulin and others, 2023) from the middle carbonate-chert unit 3 (MCC3) of Whidden and others (2018) in the Triassic Shublik Formation, northeastern Alaska.

[See figure 1 for locality map and table 1 for locality details. See (Dumoulin and others, 2023) for complete geochemical data; samples from MCC3 that were analyzed only for total organic carbon (TOC) (Cache Creek, number of samples [$n$]=15; Fire Creek, $n$=78; Mesa, $n$=12) are not included below. Localities: A, Aichilik River; B, Bathtub Ridge; D, Dodo Creek; E, Echooka River; F, Fire Creek; S, Spire. Other abbreviations: Al, aluminum; Ca, calcium; HPS, highly phosphatic strata; lms; limestone; m, mudstone; Mo, molybdenum; P, phosphorus; ppm, parts per million; pte, phosphorite; s., sample(s); Si, silicon; sltst, siltstone; U, uranium; %, percent; —, not applicable; /, to]

| Lithology | Localities | TOC (weight percent) | Concentration | | | | | |
|---|---|---|---|---|---|---|---|---|
| | | | Al (%) | Ca (%) | Si (%) | P (%) | Mo (ppm) | U (ppm) |
| m/sltst | F, S | 1.59–4.76 | 1.09–1.98 | 24.5–28.9 | 7.56–11 | 0.06–3.59 | 7–97 | 6.1–32 |
| | ($n$=5) | — | — | — | — | (2 s. >1) | (2 s. >25) | — |
| | E | 2.47–3.61 | 1.26–2.81 | 15.5–25.6 | 12.3–20 | 0.33–3.62 | 5–80 | 8.68–13.2 |
| | ($n$=5) | — | — | — | — | (3 s. >1) | (2 s. >25) | — |
| lms | A, B, F, S | <0.2–2.92 | 0.06–1.25 | 28.2–38.4 | 0.27–7.78 | 0.01–4.38 | 2–62 | 0.82–51.7 |
| | ($n$=35) | (29 s. <1.6) | — | — | — | (23 s. >1) | (3 s. >25) | — |
| | E | 1.38–2.55 | 0.42–0.58 | 27.6–35.8 | 1.78–6.24 | 0.26–1.73 | 3–6 | 2.62–5.52 |
| | ($n$=4) | — | — | — | — | (2 s. >1) | — | — |
| HPS | A, D, E, F, S | 0.92–3.91 | 0.38–1.09 | 21.8–37.2 | 2.21–8.07 | 4.66–7.63 | 2–297 | 12–29.3 |
| | ($n$=11) | — | — | — | — | — | (2 s. >25) | — |
| pte | A, D, S | 0.8–3.34 | 0.47–1.36 | 30.8–36.7 | 2.71–5.26 | 8.59–14.6 | 2–33 | 31.3–72.6 |
| | ($n$=5) | — | — | — | — | — | (1 s. >7) | — |

### Inorganic Geochemical Data

Inorganic geochemical data align with petrographic data indicating that MCC3 is the most calcareous and least siliceous part of the Shublik Formation in the outcrop sections we studied (table 5) (Dumoulin and others, 2023). Most samples analyzed are limestones with 28–38 percent calcium and <8 percent silicon; mudstones, siltstones, and HPS contain more calcium and less silicon than equivalent lithologies in underlying units. Our data indicate that HPS (including phosphorites) are more common in MCC3 than in MCC2 but less common than in MCC1. HPS occur in the upper parts of both coarsening-upward sequences, and the highest phosphorus values are at the top of MCC3 (figs. 13, 15*C*) (Dumoulin and others, 2023), a pattern also found by Detterman (1970) and Kelly (2004) in their data from Fire Creek.

Molybdenum is elevated (39–97 ppm) in mudstones, muddy siltstones, and a few limestones in the lower to middle part of the unit at Spire, Fire Creek, and Echooka River (fig. 13), and in poorly exposed beds that we assign to this unit at Bathtub ridge (table 5) (Dumoulin and others, 2023). P-XRF analysis of closely spaced samples from Fire Creek found numerous samples, almost all in the lower third of the unit, with elevated molybdenum (28–117 ppm) (Dumoulin and others, 2023). Elevated to very high molybdenum values (33, 84, and 297 ppm) occur in the pyritic hardground at the top of the unit at Spire, Dodo Creek, and Fire Creek (fig. 15*B*; table 5) (Dumoulin and others, 2023).

Uranium values are moderately elevated (26.1–51.7 ppm) in HPS and some phosphatic limestones at Spire (fig. 15*C*), Fire Creek, and Aichilik River. Elevated uranium values also characterize the pyritic hardground at the top of the section at Spire (fig. 15*B*), Dodo Creek, and Fire Creek. Kelly (2004) reported 108 ppm from this interval at Fire Creek, whereas our highest values for this hardground were 71.9 and 72.6 ppm from two samples at Dodo Creek (Dumoulin and others, 2023). High levels of barium (1,520–6,550 ppm) were found in this hardground at Spire, as well as in several samples of HPS and phosphatic limestone from Aichilik River and Fire Creek, one of which contained patchy barite cement in thin section.

### Depositional Setting

Sedimentologic, faunal, and geochemical data suggest that MCC3 accumulated in middle-ramp settings that were slightly deeper and received less siliciclastic input than did those of MCC2. As in MCC1 and MCC2, the flat-clam-dominated biota is consistent with common dysoxia, but local evidence of bioturbation and generally low molybdenum values imply that anoxia was rare and (or) transient. We interpret the coarsening-upward successions as having formed in shallowing-upward environments characterized by increasingly abundant event beds. These beds contain various proportions of redeposited flat-clam fragments and reworked and redeposited phosphatic material, but they lack fragments of robust bivalves such as *Gryphaea* sp., which are common in the event beds at the top of MCC2. This suggests that MCC3 event beds accumulated in and were sourced by settings with slightly deeper water and lower energy than event beds in MCC2. Upper parts of both shallowing-upward successions in MCC3 contain phosphatic hardgrounds, indicating periods of slow or nondeposition. These hardgrounds are especially well developed at the top of the unit. The predominance of lime mudstone and wackestone in the upper succession, versus packstone and grainstone in the lower one, denotes a deeper- and (or) quieter-water environment for the former succession. The greater abundance of phosphate in MCC3 compared to MCC2 indicates a return to more productive environmental conditions, though this could also reflect increased periods of little or no sediment deposition during which phosphate was concentrated through diagenetic processes and (or) physical reworking.

As posited for underlying units, differences between MCC3 at Echooka River and in the main outcrop belt are likely due to deposition of the former in a more distal, deeper, and quieter water setting. At Echooka River, the event beds are fewer and generally finer grained, flat-clam packstones and grainstones are less common than wackestones and mudstones, and the section overall is more organic-rich (table 5) (Dumoulin and others, 2023).

### Sequence Stratigraphy

MCC3 constitutes T-R sequence 4 (S4) of Whidden and others (2018) and Rouse and others (2020) (fig. 2). An interval ~2 to 6 m thick at the base of the unit consists of one or more thin, fining-upward cycles of limestone, lesser siltstone, and (or) mudstone that we interpret as the TST and mfs of this sequence (fig. 13). Two coarsening- and thickening-upward parasequences make up the RST of S4 in complete sections examined for this study (fig. 13). Limy event beds, most with abundant phosphate, become more common upward within both parasequences. Phosphatic crusts, firmgrounds, and hardgrounds also occur in the upper parts of both parasequences but are particularly well developed at the top of the unit (fig. 15*A–C*), indicating that a prolonged depositional hiatus marked the climax of the RST in S4.

## Upper Clastic-Carbonate Unit 1

UCC1 (fig. 2) (Whidden and others, 2018) encompasses the uppermost part of the Shublik Formation and is equivalent to the clay shale member of Detterman and others (1975) and zone A of Kupecz (1995). UCC1 is poorly exposed through much of the outcrop belt but was sampled at six localities. The most complete exposures are at Dodo, Fire, and Cache Creeks, where the unit consists of calcareous shale interbedded with more resistant lime mudstone (figs. 1, 16; table 1). The unit is not exposed at Echooka River. Kelly (2004) reported a thickness of ~50 m for strata we assign to UCC1 at Fire Creek.

Tourtelot and Tailleur (1971) measured ~30 m of equivalent strata at Cache Creek, and we estimate that UCC1 is ~35 m thick at Aichilik River.

Although UCC1 is abundantly fossiliferous at many localities, precise, published ages come mainly from subsurface sections. The unit is most tightly dated in the Phoenix 1 well (fig. 1), where species of *Halobia*, *Eomonotis*, *Monotis* (*Entomonotis*), and *Gryphaea* demonstrate that it ranges from late middle to late Norian (McRoberts and others, 2020). Middle to early late Norian flat clams (halobiids and monotids) and *Gryphaea* sp. occur in UCC1 at Fire Creek (Tourtelot and Tailleur, 1971; Detterman and others, 1975). Microfossils provide broader ages for UCC1 at several localities. Diverse foraminifera of Late Triassic age (fig. 16*F*), as well as echinoid spines, gastropod molds, and ostracodes, are reported from this unit at Dodo Creek (Bergquist, 1966), Fire Creek (Sohn, 1987; identified by M. Mickey in Kelly, 2004), and Cache Creek (J. Bujak, Bujak Research International, written commun., 2015); one of the Cache Creek samples also contains a curved, conical tooth of a possible

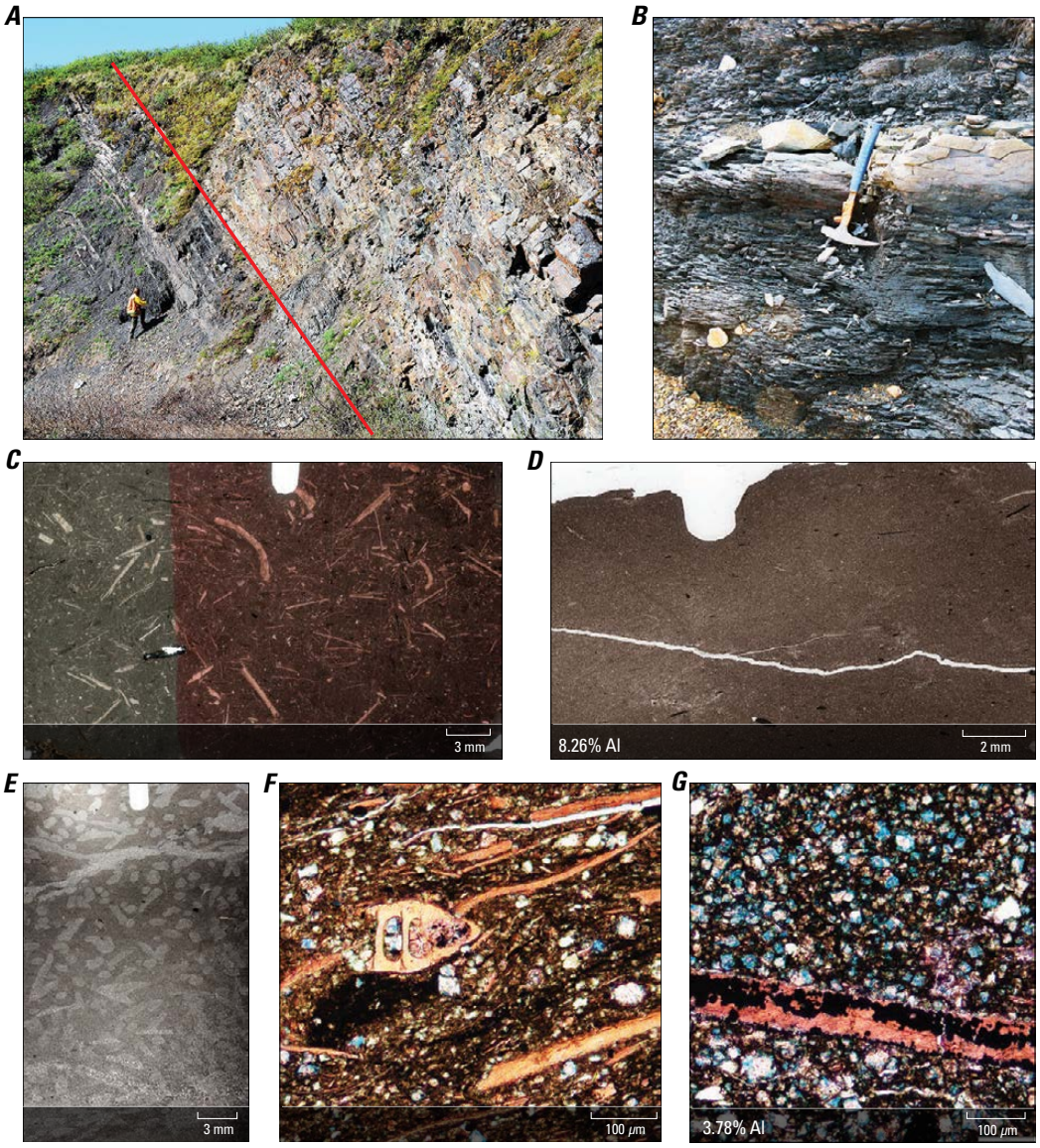


**Figure 16.** Images of sedimentary and biogenic features of upper clastic-carbonate unit 1 (UCC1) of Whidden and others (2018) in the Triassic Shublik Formation, northeastern Alaska. *A*, Photograph of outcrop of the upper part of UCC1 at the Aichilik River locality, showing interbedded calcareous shale (dark gray) and carbonate mudstone (beige); the line marks the contact with the overlying Karen Creek Sandstone. *B*, Photograph of outcrop at the Dodo Creek locality showing interbedded calcareous shale and carbonate mudstone in the upper part of UCC1. *C*, Thin section scan from the Spire locality of carbonate wackestone that contains small flat-clam fragments, some of which are partly replaced by pyrite [black (opaque)]. Calcite is stained pink on the right side. *D*, Thin section scan from Dodo Creek of calcareous shale that contains sparse, small bioclasts (most are pyritized and appear black in the image) and scattered quartz silt (white specks). *E*, Thin section scan from Dodo Creek of carbonate mudstone with abundant microburrows (white). *F*, Photomicrograph from Dodo Creek of carbonate mudstone to wackestone that contains small flat-clam fragments, dolomite rhombs, a calcareous foraminifer, pyrite nodules and crystals (black) and quartz silt. Ferric dolomite is stained blue; calcite is stained pink. *G*, Photomicrograph from Dodo Creek of carbonate mudstone to wackestone that contains a small flat-clam fragment that is partly replaced by pyrite (black crystals), abundant dolomite rhombs, and minor quartz silt. Ferric dolomite is stained blue; calcite is stained pink. See figure 1 and table 1 for locality information. Geochemical data (Dumoulin and others, 2023) shown in inset box where available. %, percent; Al, aluminum; ppm, parts per million; mm, millimeter; µm, micrometer. Photograph in *A* by D.W. Houseknecht, U.S. Geological Survey (USGS); photographs in *B*–*G* by J.A. Dumoulin, USGS.

marine reptile. Poorly preserved palynomorphs; common ostracodes; small, agglutinated foraminifera; and a single calcareous benthic foraminifer occur in strata that may be part of UCC1 at the upper Mesa section (table 1); this assemblage is of Middle(?) to Late Triassic age (J. Bujak, Bujak Research International, written commun., 2015).

## Lithologies

The exposures of UCC1 examined for this study consist chiefly of recessive calcareous shale interbedded on a scale of centimeters to decimeters with more resistant lime mudstone to flat-clam wackestone and rare packstone (fig. 16*A–B*). Shaly intervals grade to silty shale and quartz siltstone, whereas limestone forms nodular beds and lenses. Illite makes up the clay component of the unit at Cache Creek (Tourtelot and Tailleur, 1971). Carbonate material in both the shale and limestone beds includes calcareous microspar and subordinate ferric and non-ferric dolomite rhombs (≤40 µm) (fig. 16*F–G*). Microbioturbation is evident in a few beds (fig. 16*E*). Scattered fossils are mainly minute, very thin flat-clam fragments (fig. 16*C*, *F–G*); locally abundant calcareous and agglutinated foraminifera (fig. 16*F*); and minor ostracodes and echinoderm debris. A few coarser shell pieces (brachiopods and *Gryphaea*? sp.) were seen in the basal beds of UCC1 at Spire, Dodo Creek, and Cache Creek; trace amounts of glauconite occur locally in this basal interval. Pyrite is found throughout the unit as small, disseminated grains, nodules as large as a few centimeters in diameter, and partly to completely replaced fossil fragments (fig. 16*C–D*, *F–G*). A few sand-sized phosphatic clasts occur at Spire, and phosphatic steinkerns of monotid flat clams and other fossils are found at Fire Creek (Tourtelot and Tailleur, 1971; Kelly, 2004).

## Geochemistry

### Total Organic Carbon Data

New TOC values from UCC1 at four locations (table 6) (*n*=28) (Dumoulin and others, 2023) range from 0.37 to 2.85 weight percent; one third of our samples contain ≥1.6 weight percent TOC and three values are >2.5 weight percent. Previous analyses from this unit at Fire Creek found similar results, with a TOC range of <1 to 2.2 weight percent (Detterman, 1970; Kelly, 2004). In the Phoenix 1 well (fig. 1), programmed pyrolysis analyses indicate that organic matter in UCC1 is of a different type and (or) is less well-preserved (less hydrogen-rich) than the organic matter in the underlying MCC units (Whidden and others, 2019a). However, pyrolysis data are not currently available to test if this difference also characterizes UCC1 within the outcrop belt.

### Inorganic Geochemical Data

A limited suite of inorganic geochemical data from UCC1 at Dodo Creek (table 6) (Dumoulin and others, 2023) supports our petrographic observations and agrees with previously published data from this unit at Fire Creek (Detterman, 1970; Kelly, 2004). The shaly beds contain more aluminum, more silicon, and less calcium than the lime mudstones and wackestones (compare fig. 16*D*, *G*). Aluminum values in this unit are notably higher than those in the underlying MCC units. Phosphorus is low (<0.2 percent) in all our samples and in most previously analyzed samples, but a few higher values (1–3 percent phosphorus pentoxide) are reported from the upper part of the unit at Fire Creek (Detterman, 1970; Kelly, 2004). Molybdenum and uranium are low (≤3 ppm and <5 ppm, respectively) in all our samples.

**Table 6.** Geochemical data (Dumoulin and others, 2023) from the upper clastic-carbonate unit 1 (UCC1) of Whidden and others (2018) in the Triassic Shublik Formation and the Karen Creek Sandstone, northeastern Alaska.

[See figure 1 for locality map and table 1 for locality details. See (Dumoulin and others,2023) for complete geochemical data; samples from UCC1 that were analyzed only for total organic carbon (TOC) (Cache Creek, number of samples [*n*]=10; Fire Creek, *n*=3; Mesa, *n*=9) are not included below. Localities: A, Aichilik River; C, Cache Creek; D, Dodo Creek; F, Fire Creek. Other abbreviations: Al, aluminum; Ca, calcium; HPS, highly phosphatic strata; m, mudstone; Mo, molybdenum; P, phosphorus; ppm, parts per million; s., sample; Si, silicon; sltst, siltstone; U, uranium; %, percent; —, not applicable; /, to]

| Lithology | Localities | TOC (wt. pct) | Concentration | | | | | |
|---|---|---|---|---|---|---|---|---|
| | | | Al (%) | Ca (%) | Si (%) | P (%) | Mo (ppm) | U (ppm) |
| Upper clastic-carbonate unit 1 | | | | | | | | |
| m/sltst | D (*n*=6) | 0.47–1.19 | 1.42–8.37 | 24.5–28.9 | 4.71–24.8 | 0.04–0.17 | <2–3 | 1.84–4.89 |
| Karen Creek Sandstone | | | | | | | | |
| sltst | A, C (*n*=3) | 0.28–1.27 | 0.95–4.02 | 0.7–23.8 | 8.94–38.8 | 0.09–0.66 | <2–11 | 4.36–5.33 |
| HP | C, F (*n*=4) | 0.32–0.61 — | 0.97–1.77 — | 11.6–27.6 — | 9.49–27.8 — | 4.7–10.1 (1 s. >7.2) | <2, 2 — | 28.4–180 — |

## Depositional Setting

Sedimentologic and faunal data suggest middle- (to outer?-) ramp settings for UCC1, with increased siliciclastic input relative to the underlying MCC3 unit. The predominantly fine size of sediment and fossils found in UCC1 are consistent with deposition in moderately deep, quiet water. The microfauna of foraminifera and ostracodes at Cache Creek imply a middle- to outer-shelf environment with normal values of salinity and oxygen content (J. Bujak, Bujak Research International, written commun., 2015); low molybdenum values also denote normal oxygenation (Scott and Lyons, 2012). Scarcity of phosphate may reflect less productive oceanographic conditions, more rapid deposition, and (or) increased dilution by fine-grained siliciclastic input.

## Sequence Stratigraphy

UCC1 makes up most of T-R sequence 5 (S5) of Whidden and others (2018) and Rouse and others (2020) (fig. 2). On the basis of GR data, these authors interpret the basal meter of UCC1 at Fire Creek as the TST and mfs of this sequence; they assign the rest of UCC1, as well as much of the overlying Karen Creek Sandstone, to the RST at this locality. The generally poor exposures characteristic of UCC1 obscure any finer-scale subdivisions, such as parasequences, that may exist within this part of S5. The Karen Creek Sandstone is further discussed below (see the "Karen Creek Sandstone" section).

# Other Sections of the Shublik Formation

The Shublik Formation was examined at three sites within the area of the USGS Arctic 1:250,000-scale quadrangle (Helicopter ridge, Porcupine Lake West, and Arctic D–4 quadrangle localities; ~40 km southeast of the Echooka River locality) and at one site in the Philip Smith Mountains 1:250,000-scale quadrangle (Philip Smith Mountains locality; ~50 km southwest of the Echooka River locality) (fig. 1; table 1). These strata have been deformed (strongly folded and faulted) and are locally foliated, partly recrystallized, and cut by numerous stylolites and veins of calcite and quartz. Available age and lithologic data indicate that MCC strata are present at all four localities, but subdivisions within MCC cannot be distinguished on the basis of lithology. However, fossils seen in thin section from the Arctic D–4 locality indicate that strata equivalent to MCC3 are present there. Lithofacies at the Philip Smith Mountains locality indicate that the lower part of that section represents LC1.

## Lithologies and Geochemistry

### Helicopter Ridge

We examined two short sections, 8 and 18 m thick (fig. 1; table 1), at Helicopter ridge, where Brosgé and others (2001) reported an ammonite of Middle Triassic or younger age in strata they mapped as the Shublik Formation (their fossil locality [loc.] 22 in their unit Trs). The Ivishak Formation, also exposed there, yielded an ammonite of middle Early Triassic (Smithian) age (fossil loc. 22 in unit TrPs of Brosgé and others [2001]); the contact between these units is not exposed. The Shublik at Helicopter ridge consists of more-resistant layers and lenses of limestone and mudstone intercalated with less-resistant papery shale. Where original textures are best preserved, lithologies include lime mudstone and lesser flat-clam wackestone to packstone. The flat clams are generally small, thin, and some are partly dissolved or recrystallized. Some beds contain calcitized radiolarians, calcareous and siliceous sponge spicules, and local crinoid fragments. Phosphate forms rare lenses and nodules a few millimeters to several centimeters thick that are elongated parallel to bedding and appear to have formed in situ (fig. 3*A*); well-preserved radiolarians, filled with calcite and (or) quartz, occur in some of the nodules. TOC values ($n$=28) range from 0.26 to 3.6 weight percent, with 36 percent of these values ≥2 weight percent (Dumoulin and others, 2023).

### Porcupine Lake West

About 30 m of section were studied at this locality (fig. 1; table 1), which yielded pelecypods of Carnian age (fossil loc. 15 in unit Trs of Brosgé and others [2001]). The strata at Porcupine Lake West are like those at Helicopter ridge, but the original textures are less well preserved at Porcupine Lake West, where limy mudstone and papery shale predominate. Only a few samples contain recognizable fossils, which are mainly sparse flat-clam fragments. Phosphate was not observed. The TOC content ($n$=7) ranges from 0.42 to 3.19 weight percent, with five of the values >2 weight percent (Dumoulin and others, 2023).

### Arctic D–4 Quadrangle

Poorly exposed rubble of black, sooty limestone at this locality (fig. 1; table 1) contained pelecypods of Carnian or early Norian age (fossil loc. 26 in unit Trs of Brosgé and others [2001]). A thin section shows flat clams and a belemnoid rostrum in a recrystallized calcite matrix. Belemnoid rostrums elsewhere were seen only in MCC3, suggesting that these strata correlate with that unit.

### Philip Smith Mountains

About 20 m of Shublik Formation is discontinuously exposed at this locality (fig. 1; table 1) but the section is folded and cleaved, so the true stratigraphic thickness is uncertain but probably less than 10 m. The lower beds are quartz siltstone to very fine grained sandstone with subordinate carbonate rhombs, phosphatic peloids and nodules as large as 3 cm in diameter, and centimeter-scale pyrite nodules. Phosphate nodules are made up of phosphatic peloids and subordinate detrital quartz in a matrix of ferric dolomite and calcite cement; some nodules contain phosphatized and calcitized radiolarians with well-preserved test structures. These beds

likely represent LC1. Upper beds that we consider equivalent to MCC are sooty limestone with sparse to common flat clams and possible calcitized radiolarians.

## Depositional Setting

Available data indicate that the Shublik Formation at these four southern localities accumulated largely in middle- to outer-shelf settings, although a shallower environment is possible for strata tentatively assigned to LC1 at the Philip Smith Mountains locality. The four sections are generally fine grained and the fossils, which are largely small, thin flat-clam fragments, are sparse. TOC data, available from two sites, show a higher proportion of samples with ≥2 weight percent TOC than is seen in MCC in the main belt (36 and 70 percent of Helicopter Ridge and Porcupine Lake West samples, respectively, versus <20 percent of main belt locality samples), but values from the USGS Arctic 1:250,000 quadrangle localities are not as high as the highest values from the Echooka River section. Phosphate, rare overall, was observed only as small, in situ nodules in mudstone at the Helicopter ridge locality, and in strata likely equivalent to LC1 at the Philip Smith Mountains locality. The lithofacies and geographic positions of these four sites suggest that they are the most distal localities sampled in the study. Features diagnostic of the Otuk Formation (most notably radiolarian chert), however, were not observed in any of these sections.

# Karen Creek Sandstone

The Upper Triassic Karen Creek Sandstone (fig. 2), defined by Detterman and others (1975), crops out largely along the north front of the Brooks Range (between the Kavik River and Aichilik River localities) and in an area to the north (approximately between our Cache Creek and Dodo Creek localities). Its southeastern, mountain front exposures are thicker (as thick as 38 m) and unfossiliferous, whereas those in the northern area are thinner and contain more carbonate and locally abundant fossils (Detterman and others, 1975). We studied the Karen Creek at one of the mountain front exposures (the Aichilik River locality), where it is ~35 m thick, as well as at four northern area localities (the Cache Creek, Mesa, Fire Creek and Dodo Creek localities), where it is ≤6 m thick (figs. 1, 16*A*, 17; table 1). A rubbly interval at Echooka River also likely represents this unit.

Pelecypods (*Monotis ochotica ochotica* and *Gryphaea keilhaui*) indicate that the lower part of the Karen Creek Sandstone at Fire Creek is of late Norian age, but the higher beds in this unit have not been dated (Detterman and others, 1975). *M. ochotica* is the youngest monotid species found in northern Alaska, where it is of middle late to late late Norian age (Silberling and others, 1997). Monotids of this or slightly older age are reported from beds that we consider to be Karen Creek Sandstone at Cache Creek (Tourtelot and Tailleur, 1971) and Echooka River (Detterman and others, 1975); the Cache Creek fauna also includes *Gryphaea* sp. and finely ribbed pectenacid pelecypods. *Monotis (Entomonotis) ochotica* occurs (McRoberts and others, 2020) in strata assigned by Whidden and others (2018) to the upper part of UCC1 in the Phoenix 1 well, indicating that the lower part of the Karen Creek Sandstone may be coeval with the upper part of UCC1 in the subsurface (fig. 2).

## Lithologies

The Karen Creek Sandstone at the Aichilik River locality (figs. 1, 16*A*, 17*A*) typifies the mountain front outcrop belt of this unit that was described by Detterman and others (1975). The Aichilik section consists of quartz siltstone to very fine grained sandstone in massive to tabular beds that are 30–50 cm thick; more recessive beds are typically finer grained. Bioturbation has obscured primary structures; *Zoophycos* was seen in float. Subordinate clast types include chert, white mica, plagioclase, and rare glauconite. A sample taken near the middle of the section contains abundant dolomite rhombs and a small shell fragment. A bed at the base of the section contains 5–7 percent rounded to irregular, outsized glauconite pellets and a reworked, coarse-sand-sized phosphate clast; cm-scale phosphate nodules also occur at this locality (Tourtelot and Tailleur, 1971). Other exposures of the Karen Creek Sandstone in the mountain front outcrop belt include the type section, which was described in detail by Reed (1968) and is located ~70 km southwest of the Aichilik River section. The type section is generally like the Aichilik River section, with scattered phosphate nodules as large as 8 cm in diameter (Reed, 1968).

**Figure 17 (page 37).** Images of sedimentary and biogenic features of the Upper Triassic Karen Creek Sandstone, northeastern Alaska. *A*, Photograph of outcrop at the Aichilik River locality showing the massive to tabular beds of quartz siltstone to very fine grained sandstone that typify the mountain front outcrop belt. *B*, Thin section scan from the Cache Creek locality (part of the northern outcrop belt, in which lithologies are more heterogeneous than in the mountain front outcrop belt) showing bioturbated, very fine grained quartz sandstone above a phosphate nodule with sparse small fossil fragments (white). *C*, Photograph of outcrop at the Fire Creek locality (northern outcrop belt) showing bioturbated, sandy limestone with phosphate nodules and abundant fossil debris. *D*. Photomicrograph from Fire Creek showing concentration of phosphatic coated grains, some of which have unconformity-bounded internal surfaces (u). *E*, Photomicrograph from Fire Creek showing a phosphatic coated grain with an extinction cross under crossed polars, the presence of which indicates partial replacement of originally calcitic ooids. See figure 1 and table 1 for locality information. Geochemical data (Dumoulin and others, 2023) shown in inset box where available. %, percent; P, phosphorus; U, uranium; ppm, parts per million; mm, millimeter; µm, micrometer. Photograph in *A* by D.W. Houseknecht, U.S. Geological Survey (USGS); photographs in *B*–*E* by J.A. Dumoulin, USGS.

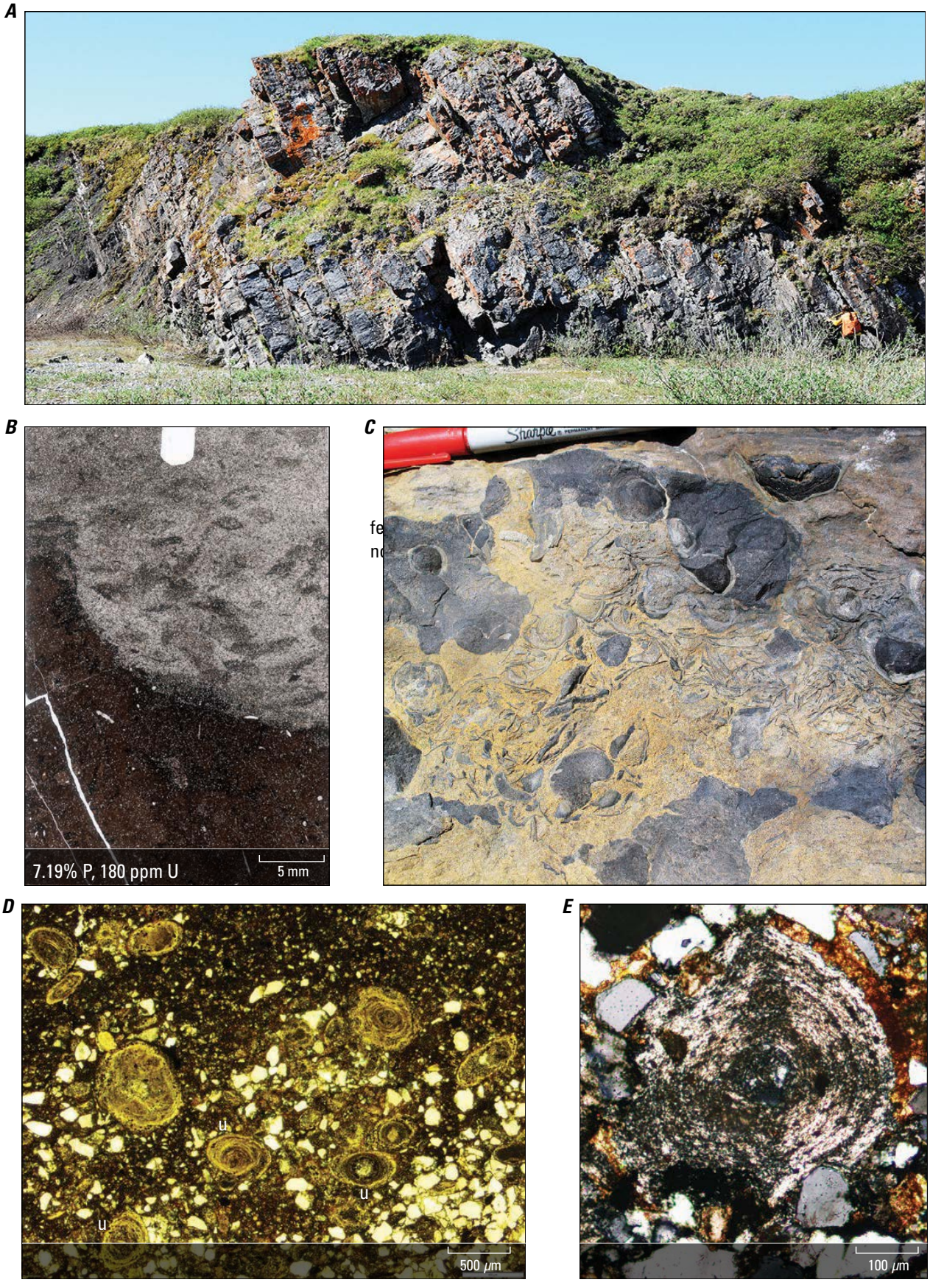
A
B
7.19% P, 180 ppm U
5 mm
C
Sharpie
D
u
u
u
500 μm
E
100 μm

Exposures of the Karen Creek Sandstone in the northern outcrop belt are more heterogenous than those along the mountain front (fig. 17*B–E*). The beds range from thin (≤10 cm) to thick (>50 cm) and are blocky to irregular. Fossils and phosphate nodules are locally abundant, especially in the lower to middle parts of the unit (fig. 17*B–C*). At Fire and Cache Creeks, quartz siltstone to fine-grained sandstone is interbedded with, and grades into, silty to sandy limestone with robust pelecypod fragments; some limy layers include rare to abundant disseminated rhombs of dolomite and (or) siderite. At Dodo Creek (and Echooka River), silty to sandy limestone predominates throughout the unit. A rubbly exposure near the upper Mesa locality is primarily quartz siltstone to very fine grained sandstone with 5–10 percent outsized glauconite grains. Bioturbation is common in the northern outcrop belt (fig. 17*B*); a distinctive layer of vertical (*Skolithos*-type) burrows, each ~0.5 cm wide and 3 cm long, occurs near the top of the Karen Creek Sandstone at Fire Creek (see fig. 6*D* of Kelly and others, 2007). Fossils are generally broken and abraded, and pelecypod shells in several samples are intensively bored. Other bioclasts include ostracodes and brachiopod and echinoderm fragments. Lenses of HPS, especially notable at Fire and Cache Creeks, contain numerous round to irregular phosphate nodules as long as 7 cm in diameter (fig. 17*B*), as well as local pyrite nodules.

The phosphate in the Karen Creek Sandstone is distinctive, as noted by previous authors (Reed, 1968; Tourtelot and Tailleur, 1971; Detterman and others, 1975). Most of the phosphate masses appear to have formed in place, and some fill burrows or shells (fig. 17*C*). Many nodules contain irregular, medium to very coarse sand sized, coated grains made up of anisotropic phosphate, which contrasts with the isotropic phosphate typical of the Shublik Formation (figs. 17*D–E*) (Reed, 1968; Tourtelot and Tailleur, 1971). Some of these coated grains show a distinct extinction cross under crossed polars, which indicate that the phosphate in these grains has partly replaced calcite (fig. 17*E*), since calcite ooids are characterized by an extinction cross (for example, Tucker, 2011). A few coated grains contain unconformity-bounded internal surfaces (fig. 17*D*) (Pufahl and Grimm, 2003). Coated grains are found in both the mountain front outcrop belt (Reed, 1968) and the northern outcrop belt of the Karen Creek Sandstone (fig. 17*D–E*). These grains are more irregular in size and shape than most phosphatic ooids found in the Shublik during our study, and they occur loosely disseminated within and adjacent to phosphatic nodules (fig. 17*D*). Phosphatic ooids in the Shublik, in contrast, are concentrated in laminated layers and event beds, along with similarly sized quartz sand and bioclasts (figs. 8*C*, 14*D*). Phosphate-replaced calcite ooids occur in several wells in the northern part of the Prudhoe Bay Oil Field area (Hulm, 1999) in strata that we interpret as the upper part of MCC3. The microfabrics of these ooids were not described, but the grains illustrated (see fig. 12*B* of Hulm, 1999) appear more regular in form than many of the coated grains in the Karen Creek Sandstone (fig. 17*D*).

# Geochemistry

## Total Organic Carbon Data

TOC values previously published from the Karen Creek Sandstone are rare and uniformly low (<1 weight percent) (Tourtelot and Tailleur, 1971). The new values reported herein are similarly low. Three siltstone samples and four HPS samples were analyzed from the sections at Fire Creek, Cache Creek, and Aichilik River; all contain less than 1.3 weight percent TOC (table 6) (Dumoulin and others, 2023).

## Inorganic Geochemical Data

The same samples that were analyzed for TOC were also analyzed for inorganic geochemistry (table 6) (Dumoulin and others, 2023). The results agree with our petrographic observations and strengthen the geochemical findings reported for the Karen Creek Sandstone in previous studies (Tourtelot and Tailleur, 1971; Kelly, 2004). The wide range of silicon and calcium values aligns with the lithologic heterogeneity we observed; silicon is highest (≥38 percent) and calcium lowest (<1 percent) in two siltstone samples from the mountain front outcrop belt (Aichilik River locality). Three samples of HPS (including one phosphorite) from Fire Creek and another HPS sample from Cache Creek have elevated uranium (28.4–180 ppm; 3 values >40 ppm). All molybdenum values are low (≤11 ppm; ≤2 ppm in all but one sample).

High values of chromium were previously noted in the Karen Creek Sandstone at Fire Creek; our study confirms and expands on these findings. Most Shublik Formation and Karen Creek Sandstone samples contain <250 ppm chromium (Tourtelot and Tailleur, 1971; Kelly, 2004; Dumoulin and others, 2023). However, three Karen Creek Sandstone samples reported by Tourtelot and Tailleur (1971) contained 1,000–1,500 ppm chromium, and two samples listed in Kelly (2004) had 621 and 2,360 ppm chromium. A sample of HPS (with irregular coated grains) analyzed for our study from Fire Creek contains 1,030 ppm chromium, and a siltstone sample from the base of the Karen Creek at Aichilik River has 645 ppm chromium. Even higher values of chromium (as much as 11,700 ppm) occur in subsurface samples of the Shublik, mainly from UCC1 in the South Barrow 3 and Northstar 1 wells (fig. 1). Based on paleontologic and GR correlations, these subsurface Shublik samples are coeval with to slightly older than our Karen Creek samples. Analyses of several subsurface samples using micro X-ray fluorescence indicate that the chromium resides primarily in small, detrital grains of chromite (K. Pfaff, Colorado School of Mines, written commun., 2021); a similar residence is assumed for chromium in the Karen Creek Sandstone.

Chromium values as high as 1,540 ppm were reported from phosphorites of the Permian Phosphoria Formation (Hiatt and Budd, 2003) and attributed to deposition in anoxic and euxinic settings. Chromium in these samples resides in phosphate (francolite) grains, however, and is accompanied

by elevated amounts of cadmium (as much as 385 ppm) and nickel (540 ppm). The Karen Creek Sandstone samples with elevated chromium that were reported by Kelly (2004) and analyzed for this study did not contain elevated cadmium and nickel (maximum values of 1.7 ppm and 39 ppm, respectively, *n*=4) (Dumoulin and others, 2023).

## Depositional Setting

Sedimentologic and faunal data indicate moderately shallow-water, inner- to middle-ramp settings for the Karen Creek Sandstone. The formation records an influx of siliciclastic sand that contrasts with the underlying mud-dominated UCC1 unit of the Shublik Formation. This influx is especially pronounced in the mountain front outcrop belt of the Karen Creek Sandstone, in which strata are thicker overall and contain a higher proportion of quartz sand and silt than sections in the northern outcrop belt. Robust, abraded fossil fragments in the northern outcrop belt imply shallow-water, high-energy settings; calcitic ooids (likely precursors for some of the phosphatic coated grains in the Karen Creek) also denote such an environment. Pervasive bioturbation and low molybdenum values indicate oxygenated bottom-water conditions. The presence of phosphate may reflect increased productivity and (or) slower or more episodic sedimentation relative to UCC1.

## Sequence Stratigraphy

Sequence stratigraphic interpretation of the Karen Creek Sandstone is complicated by a paucity of age control for this unit and, consequently, uncertain correlations with the subsurface Sag River Sandstone. Although the lowermost beds of the Karen Creek Sandstone contain late Norian fossils at Fire Creek, the uppermost beds there are undated, as is the entire unit throughout the mountain front outcrop belt. The Sag River Sandstone section contains fossils of both Norian and Rhaetian age (Whidden and others, 2018). Whidden and others (2018) and Rouse and others (2020) provisionally assigned the lower part of the Karen Creek Sandstone to the RST of S5, and the upper part of the Karen Creek Sandstone to T-R sequence 6 (S6) (fig. 2). Support for this interpretation is provided by phosphate distribution in the Karen Creek, well documented in the Fire Creek section (Kelly, 2004; Kelly and others, 2007; this study). There, phosphate occurs chiefly in the lower two-thirds of the unit and is most abundant at the top of this interval, where nodules coalesce to form a probable hardground layer like those that cap LC1 and MCC3 in the Shublik Formation. As in the MCC3 unit, HPS in this layer contain notable pyrite and uranium (fig. 17*B*). Coated grains are concentrated in and just above this layer. We suggest that this phosphatic hardground marks a depositional hiatus at the end of S5 and that the remainder of the Karen Creek Sandstone was deposited during the subsequent S6. Detailed study of other Karen Creek Sandstone sections, as well as additional work on the biostratigraphy and lithostratigraphy of the Karen Creek and Sag River Sandstones, would test these interpretations.

# Facies Patterns

Facies within the Triassic Shublik Formation in northeastern Alaska vary across both space and time. This section summarizes facies patterns (focusing on spatial and temporal changes in carbonate, phosphate, and organic content) seen in our study sections and investigates factors controlling these variations. Our study expands and elaborates on the geographic and stratigraphic variations of the Shublik noted by previous authors.

Figure 1 shows the position of our study sites within the lithologic zones originally recognized by Parrish and others (2001a, b) and then modified by Kelly (2004) and Kelly and others (2007). Thirteen sites in our main Shublik Formation outcrop belt, as well as the distal Bathtub ridge locality, are within or on trend with the phosphatic zone. Five additional distal localities (Echooka River, Philip Smith Mountains, Helicopter ridge, Porcupine Lake West, and Arctic D–4 quadrangle) plot in or on trend with the organic-rich zone (fig. 1). The lithologic zones delineated by these authors broadly capture some of the lithologic variation we observed across our study area, but additional complexities are revealed when vertical facies changes are also considered.

Vertical lithologic changes within outcrop sections of the Shublik Formation were recognized by Detterman and others (1975), who divided the unit into two siliciclastic-dominated members separated by a carbonate-rich middle member. The LC1, MCC1, MCC2, MCC3, and UCC1 units used in this report (fig. 2) are a refinement of that scheme.

Geographic facies changes in the study area are most clearly seen by comparing facies within the main outcrop belt, which are laterally quite consistent, to those of the Echooka River section, the most complete and least deformed of the six distal localities (fig. 1). Vertical facies shifts are obvious within the main belt and at Echooka River.

## Carbonate Content

In the sections that we investigated, carbonate content in the Shublik Formation varies vertically in type and amount. These variations are generally similar in both the main outcrop belt and at Echooka River, with a few exceptions. Carbonate is least common in both areas in LC1, where it is absent to negligible through much of the unit. Some beds, however, contain as much as 10 percent calcite and (or) ferric dolomite as patchy cement and disseminated grains. Rare calcareous fossils were seen largely in upper parts of the unit in a few main belt sections.

Carbonate is an important component of all the MCC units. It occurs chiefly as fossils (predominantly flat clams), silt- to sand-sized detritus, and calcite cement. Different flat clams characterize each MCC unit, but the flat clams in all units show similar modes of occurrence. Many clams have been transported as part of event beds (figs. 9*D*, 14*B*), which are thicker and more numerous in the upper parts of the shallowing-upward regressive sequences found in all three MCC units. Other clams show little or no evidence

of post-mortem transport; such in situ flat-clam pavements are most abundant in the Echooka River section (fig. 9*E*) but are also found in the main outcrop belt, especially in MCC3 (fig. 14*A*).

Macrofaunal diversity in the study area is greatest in MCC2 (for example, Detterman and others, 1975). The pelecypod coquina at the top of MCC2 is a distinctive facies found only at that stratigraphic level and only within the main outcrop belt. It contains fragments of thick-shelled bivalves such as *Gryphaea* that are typical of near-shore settings, and denotes input from shallow-water, high-energy environments. Echinoderm fragments are more common in MCC2 than in any other part of the Shublik Formation.

Carbonate in UCC1 is mainly fine (silt-sized) detritus, calcareous microspar, and dolomite rhombs (fig. 16). Fewer flat-clam-rich beds are found in this unit than in the MCC units. Previous workers (Bergquist, 1966; Kelly, 2004) reported more foraminifera from UCC1 than from lower parts of the Shublik Formation, but this likely reflects processing issues; foraminifera are easier to obtain from the calcareous mudstones of UCC1 than from the calcite-cemented limestones of the MCC units (K. Bird, USGS emeritus, written commun., 2022). Foraminifera were seen in thin sections from all the MCC units in the main outcrop belt during this study.

## Phosphatic Strata

Three main types of HPS occur in the Shublik Formation in the study sections, and each has distinctive distribution patterns in space and time. Granular HPS are found only in the lower part of MCC1 in the main outcrop belt. The other two HPS types, which have wider temporal ranges, are seen in the main outcrop belt and at Echooka River. Event beds that contain enough phosphate to be classed as HPS occur in LC1 and MCC1 to MCC3 but are most numerous in MCC3. HPS interpreted as phosphatic hardgrounds are found in these four units and may occur in the Karen Creek Sandstone as well. In the main belt, hardgrounds are best developed at the tops of shallowing-upward (regressive) parasequences in LC1 and MCC3. Hardgrounds at Echooka River are found in similar settings in LC1, MCC1, and MCC2 (figs. 4, 7, 10, 13).

Granular HPS (fig. 8*A*, *C–E*) occur in the transgressive and early regressive parts of S2 (figs. 2, 7), where they form an interval as thick as 7 m that extends through 110 km of outcrop. This type of HPS also occurs in correlative subsurface intervals in the Alcor 1 and Merak 1 wells, 95 km northwest of the west edge of the outcrop belt (fig. 1) (Dumoulin and others, 2020). The granular HPS zone has the highest concentration of phosphate seen anywhere in the study area; it includes the most HPS, most phosphorites ($n$=27), highest values of phosphorus (as much as 14.9 percent, or 34 percent phosphorus pentoxide), and highest concentrations of REEs (Dumoulin and others, 2023). Consistently high uranium values (61–123 ppm) characterize the lower part of this interval, which contains more phosphatic ooids (fig. 8*C*) than any other part of the Shublik Formation. Phosphatic grains throughout the granular HPS interval show abundant evidence of transport in outcrop, hand sample, and thin section (figs. 3*E*, 8*B*). This interval has similarities to the idealized TST phosphorite illustrated in Pufahl and Groat (2017), as well as to Pliocene to Pleistocene phosphorite deposits on the Namibian shelf (Compton and Bergh, 2016). The main Namibian deposit is several meters thick, 70–90 km wide, and formed largely in middle shelf settings under the influence of the Benguela upwelling system. It is made up of sand-sized phosphate grains (some of which are concentrically banded), millimeter-scale phosphate pebbles, and coarser bivalve shells that increase upwards in abundance.

Highly phosphatic event beds in the Shublik Formation have three lithologic variants. The first is a subset of the chert- and phosphate-clast conglomerate that is found at the base of LC1 in several sections in the main outcrop belt (fig. 4), as well as in a few western and central North Slope well penetrations that include the Brontosaurus 1, Drew Point 1, and Merak 1 wells (fig. 1) (Dumoulin and others, 2020, 2022). Some of these beds contain sufficient phosphate to be classed as HPS; one such bed occurs at Kavik River (fig. 3*D*). The second variant, phosphatic sandstone, is found in the middle and upper parts of LC1 (figs. 3*G*, 4, 6*A*). The third, phosphatic limestone, occurs rarely in MCC2 (figs. 3*C*, 10) and is common in MCC3 (figs. 13, 14*B–D*). Phosphatic sandstone and limestone event beds are found in the main outcrop belt and at Echooka River (figs. 4, 10, 13), as well as in some subsurface sections (for example, Brontosaurus 1 and Ikpikpuk 1 wells) (fig. 1) (Dumoulin and others, 2020, 2022; Whidden and others, 2019a, b). All three event bed types contain displaced phosphate granules and pebbles (figs. 3*C–D*, 14*B–C*). Sand-sized phosphatic peloids are abundant in many sandstone and limestone event beds (figs. 3*F–G*, 14*C–D*) but phosphatic ooids are a minor component seen in only a few limestone event beds in MCC3 (fig. 14*D*). Geochemical data from all three phosphatic event bed variants indicate that most samples have <6 percent phosphorus, and all have low molybdenum (≤12 ppm) and low to moderate uranium (12–36 ppm) (Dumoulin and others, 2023). Phosphatic conglomerate occurs at the base of S1 (figs. 2, 4); other phosphatic event beds are found mainly in upper parts of regressive parasequences in S1 and S4 (figs. 2, 4, 13). These latter phosphatic event beds resemble the idealized RST phosphorite of Pufahl and Groat (2017), in which phosphate forms during transgression but is reworked and concentrated during regression.

All the phosphatic hardgrounds in the units that we studied have similar physical characteristics in outcrop and thin section but differ in other ways through time and space. Commonalities include complex internal textures, evidence for multiple cycles of phosphate reworking and redeposition, and phosphatized borings and burrows (figs. 6*D–G*, 9*F–G*, 15*A–C*). In all units, the hardgrounds occur at the tops of regressive parasequences. However, hardgrounds are widespread in S1 and S4 (figs. 4, 13), whereas they are

limited in extent in S2 and S3 (figs. 7, 10). ICP-OES-MS data indicate geochemical differences between the hardgrounds based on their spatial and stratigraphic positions. Phosphatic hardgrounds in LC1 throughout our study area have uniformly low molybdenum (≤10 ppm), but those in the main outcrop belt have notably lower uranium (<26 ppm) than do those in the distal sections at Echooka River and Bathtub ridge (43.5–86.7 ppm) (table 2). Hardgrounds with a similar signature of low molybdenum (≤8 ppm) and high uranium (41–180 ppm) are also seen in MCC2 at Kemik Creek in the main belt ($n$=2) and in the Karen Creek Sandstone ($n$=3; tables 4, 6:) (Dumoulin and others, 2023). Moderate molybdenum (21–49 ppm) and uranium (17.5–41.2 ppm) characterize the hardgrounds in MCC1 and MCC2 at Echooka River (tables 3, 4). Hardgrounds in MCC3 in the main belt are geochemically complex, with some samples having elevated molybdenum (84, 297 ppm) and moderate uranium (27, 29 ppm) whereas others have low or moderate molybdenum (2, 33 ppm) but elevated uranium (72, 73 ppm) (Dumoulin and others, 2023). Phosphatic hardgrounds commonly form during periods of prolonged sediment starvation and condensation (for example, Pufahl and Groat, 2017), which we suggest occurred between successive sequences and parasequences in many parts of the Shublik Formation and in the Karen Creek Sandstone. Phosphatic hardgrounds also occur in subsurface sections of the Shublik, for example, in the Northstar 1 well (fig. 1) (Dumoulin and others, 2020).

The geochemistry of phosphatic strata in the Shublik Formation invites further study. Rouse and others (2020) ascribed variation in GR values of Shublik phosphatic layers in the subsurface to variation in uranium content, noting low GR response throughout LC1, despite the presence of locally abundant phosphate, whereas phosphate in the MCC units was relatively uranium-rich and provided a robust GR response. Our outcrop geochemical data indicate a similar general pattern, but with additional nuances (for example, HPS in distal LC1 sections have elevated uranium). The reasons for differing uranium contents of Shublik HPS have not yet been established. Pufahl and Groat (2017) suggested that uranium in phosphates was concentrated under more oxic conditions, but this explanation doesn't fit the combined uranium and molybdenum abundance patterns we observed, wherein both uranium-poor and uranium-rich LC1 phosphates have equally low molybdenum values that are consistent with an oxygenated environment. There is also no obvious connection between uranium content and phosphate texture. For example, uranium contents are low in some phosphatic hardgrounds with complex layering that indicates multiple episodes of phosphatization (14.4 ppm) (fig. 6*F*), but high in others with comparable textures (43.5 ppm) (fig. 6*G*). Overall sedimentation rate may be a factor, with higher uranium content expected in settings with slower and (or) more sporadic deposition (J. Slack, USGS emeritus, written commun., 2021). This hypothesis is consistent with the elevated uranium content seen in LC1 phosphates in more distal, condensed sections, where lower and more intermittent sedimentation rates are likely.

## Organic-Rich Strata

Organic-rich strata, like carbonate content and HPS, are inconsistently distributed through time and space in the Shublik Formation sections that we studied. Our new data extend the maxima of reported TOC ranges from outcrop samples for all units of the Shublik and the Karen Creek Sandstone. These data also support the results of Whidden and others (2018) and Dumoulin and others (2022), who found that TOC values are generally higher in the MCC units relative to LC1 and UCC1, and higher in distal sections relative to more proximal ones. In the main outcrop belt, TOC values ≥2 weight percent are most abundant in MCC1 and MCC3 (18 and 15 percent of samples, respectively) (Dumoulin and others, 2023). The highest TOC values (3–5 weight percent) are in <0.5-m-thick mudstone and muddy siltstone beds. These beds are found chiefly in the lower parts of MCC1 and MCC3 (within the TST and mfs of S2 and S4), but they also occur in the TST and mfs of S3 (unit MCC2) and in the upper regressive parasequence of S4 (figs. 7, 10, 13). Organic-rich lithologies in S2 and S4 include some HPS.

Samples with elevated TOC are more abundant in the distal sections that we studied. For example, 36 percent and 70 percent of the samples from MCC-equivalent strata at the Helicopter ridge and Porcupine Lake West sections, respectively, contain ≥2 weight percent TOC (Dumoulin and others, 2023). The highest TOC contents of the study were found in the Echooka River section, where values ≥2 weight percent occur in 30–80 percent of samples collected (LC1, 57 percent; MCC1, 30 percent; MCC2, 55 percent; MCC3, 80 percent) (Dumoulin and others, 2023). Elevated TOC values (3.18–4.32 weight percent) are found in muddy, phosphatic siltstones, <0.5 m thick, in LC1, MCC1, and MCC3 (figs. 4, 7, 13) (Dumoulin and others, 2023), but an especially organic-rich zone occurs in MCC2, in the lower part of the upper regressive parasequence of S3 (fig. 10). There, a 4-m-thick interval of mudstone to muddy siltstone, with thin interbeds of radiolarite and limestone, contains consistently high TOC (2.17–6.33 weight percent) and molybdenum (33–183 ppm) (Dumoulin and others, 2023). Carnian ammonites at the top of this interval indicate it is coeval with similar organic- and molybdenum-rich strata at two localities in northwestern Alaska (Dumoulin and others, 2022; Slack and others, 2021). These two sites—a section transitional between the Shublik and Otuk Formations at Surprise Creek and an Otuk Formation section in the Red Dog Mine area (fig. 1)—also represent distal facies.

## Controls on Facies Patterns

Facies patterns in the Shublik Formation were shaped by a variety of factors, including latitudinal and geographic setting, as well as changes in sea level, climate, oceanic circulation, and regional tectonism. Paleolatitude likely influenced the carbonate content of the Shublik; its facies and biofacies resemble those of heterozoan carbonates (James, 1997; James and Jones, 2016), which typically form in temperate- to cool-water settings, accumulate relatively

slowly, and are easily swamped by siliciclastic input. The Shublik lacks reefs and other carbonate buildups; its biota is dominated by mollusks, along with locally abundant echinoderms, lesser bryozoans, and some foraminifera and ostracodes. Corals and calcareous algae are absent, and true micrite and calcareous ooids are rare. These attributes are consistent with the moderate- to high-latitude setting proposed for the Shublik by Colpron and Nelson (2011).

The paleogeographic setting of the Shublik Formation also affected its content of phosphate and organic matter. Global phosphorite deposition shifted into northern high latitudes during the Triassic (Trappe, 1994), likely in response to changes in ocean circulation associated with increased global temperatures. The Shublik Formation, which is the largest known phosphate deposit of Triassic age in the world (Cathcart, 1991; Trappe, 1994), formed at a paleolatitude of ~45 to 60° (Colpron and Nelson, 2011). Previous workers have suggested that the formation's deposition was shaped by a marine upwelling system (Parrish and others, 2001a, 2001b) that affected much of the northwestern Laurentian margin during the late Paleozoic and early Mesozoic (Grasby and others, 2016). Strata encompassed by this margin during the Permian and Triassic crop out in northern and western Canada, northern Alaska, and Svalbard (for example, Embry and others, 2002; Grasby and others, 2016). Data from the Sverdrup Basin in northern Canada indicate that upwelling along the margin ceased at the end of the Permian but resumed during the Middle Triassic in response to cooling ocean temperatures (Grasby and others, 2016). This timing matches well with data from the Shublik, where phosphate deposition began during or shortly before the early Middle Triassic (Detterman and others, 1975).

The Shublik Formation is part of a belt of phosphatic, organic-rich source rocks deposited along the northwestern Laurentian margin during the Triassic. Other units in this belt include the Doig Formation in western Canada, the Murray Harbour Formation in the Sverdrup Basin, and the Botneheia Formation in Svalbard (Riediger, 1997; Krajewski, 2008; Grasby and others, 2016). However, the phosphate of northern Alaska is more abundant and was deposited for a longer period than that in these other areas (in which phosphate is confined to the Middle Triassic) (Embry and others, 2002). Although the phosphate content of the Shublik dipped during the early Late Triassic (MCC2 deposits), it increased again during the Norian (MCC3 deposits). The dip may be linked to an episode of global warming during the Carnian (Dal Corso and others, 2018). Limited spatial resumption of Norian phosphogenesis along the northwestern Laurentian margin could reflect paleobathymetric changes that reduced or precluded upwelling in the Sverdrup and Svalbard areas (Parrish and others, 2002).

Other factors contributed to facies patterns in the Shublik Formation. The fossil and geochemical data indicate that dysoxic conditions were locally common during deposition of the Shublik and likely contributed to the concentration and preservation of organic matter. Regional tectonic events also influenced Triassic deposition in northern Alaska, producing influxes of siliciclastic detritus during the Early and latest Triassic (Ivishak Formation, UCC1, Karen Creek Sandstone, and Sag River Sandstone) (fig. 2). The main part of the Shublik (LC1 and MCC1 to MCC3) formed in a lull between these events during which slow and (or) episodic sedimentation predominated, allowing heterozoan carbonates, phosphate, and organic matter to accumulate with minimal dilution by other detritus. Uneven distribution of these components within the Shublik reflects various orders of sea-level change superimposed on other global and regional controls. TOC maxima formed chiefly during transgressive and early regressive parts of eustatic cycles, whereas carbonate content increased upward within regressive systems. Granular HPS are limited to the transgressive and early regressive parts of S2 within the main outcrop belt. Phosphatic event beds and phosphatic hardgrounds are more widely distributed in time and space than granular HPS and are found mainly in the upper parts of regressive sequences and parasequences.

## Conclusions

New sedimentologic, petrographic, and geochemical data from 19 outcrop localities in the northeastern Brooks Range of Alaska document facies changes within the Middle to Upper Triassic Shublik Formation. Thirteen sections were studied in the main outcrop belt (which extends from the Kemik Creek locality in the southwest to the Aichilik River site in the east and to the Golden Eagle locality in the north) along with six sites farther south that contained more distal facies. Five units are recognized in the Shublik in the main belt, each of which was deposited during a second order transgressive-regressive sequence. The basal unit, lower clastic unit 1 (LC1) (Anisian? to Ladinian), consists of locally phosphatic quartz siltstone to sandstone. In contrast, siliciclastic, carbonate, phosphatic, and organic material in various proportions make up three middle units (middle carbonate-chert unit 1, middle carbonate-chert unit 2, and middle carbonate-chert unit 3 [MCC1, MCC2, and MCC3, respectively]), all of which include concentrations of unit-specific flat clams. MCC1 (Ladinian to Carnian?) has a characteristic basal interval (≤7 m thick) of granular phosphorite that grades upward into phosphatic, calcareous siltstone and daonellid limestone. MCC2 (Carnian to lower Norian) is largely siltstone and halobiid limestone, has less phosphate than other parts of the Shublik in this area, and is capped by a distinctive pelecypod coquina. MCC3 (lower to middle Norian) is the most calcareous interval of the Shublik in the study area; this unit consists chiefly of halobiid and eomonotid limestone and lime mudstone, though it also includes locally abundant phosphatic event beds and hardgrounds. The uppermost unit, upper clastic-carbonate unit 1 (UCC1) (middle to upper Norian) is mainly calcareous shale and lime mudstone with negligible phosphate.

Lithofacies in the southern, distal sections of the Shublik Formation are best preserved at the Echooka River locality. These distal sections are generally finer grained,

more organic-rich, and less phosphatic than those in the main outcrop belt, and they record less energetic and more poorly oxygenated conditions overall.

In our sections, highly phosphatic strata (10–34 percent phosphorus pentoxide) are chiefly Ladinian (lower MCC1) and lower to middle Norian (MCC3). Phosphorites are most abundant and contain the most phosphorus in MCC1. Total organic content (TOC) is typically higher in the middle carbonate-chert units relative to LC1 and UCC1, and higher in distal sections relative to more proximal ones. TOC in the main belt reaches a maximum of 4.97 weight percent and is highest in muddy beds found mainly in the lower parts of the three MCC units. Highest TOC in any of our distal sections is 6.33 wt. pct in MCC2 at Echooka River.

The Shublik Formation is overlain by the Karen Creek Sandstone (upper Norian), which consists largely of quartz siltstone to sandstone. Sections of the Karen Creek Sandstone along the mountain front are thicker and unfossiliferous, whereas those to the north contain more carbonate, as well as locally abundant pelecypods and phosphate.

Controls on facies distribution within the Shublik Formation include geographic, oceanographic, and tectonic factors. The Shublik accumulated at moderate to high latitudes along the northwestern Laurentian margin during a period of relative tectonic quiescence and subdued siliciclastic influx. Upwelling of cool, nutrient-rich currents along this margin facilitated the development of heterozoan carbonate facies and the local concentration of phosphate and organic material. Large- and small-scale eustatic cycles contributed to further spatial and stratigraphic partitioning of Shublik facies.

## Acknowledgments

We thank the Energy Resources Program of the U.S. Geological Survey (USGS) for financial support, and we thank our USGS colleagues, especially David Houseknecht and Thomas Moore, for helpful discussions. Thanks also to Adam Boehlke, Palma Botterell, and Augusta Warden (all USGS) for geochemical data and insights, and to Robert B. Blodgett (Robert B. Blodgett and Associates), Jonathan Bujak (Bujak Research International), Chris McRoberts (State University of New York at Cortland), Michael Orchard (Geological Survey of Canada), John Repetski (USGS), and Jean Self-Trail (USGS) for paleontological analyses. Reviews by Ken Bird (USGS emeritus) and Robert B. Blodgett are much appreciated.

## References Cited

Adams, A.E., and MacKenzie, 1998, A color atlas of carbonate sediments and rocks under the microscope: London, Manson Publishing Ltd., 184 p.

Bergquist, H.R., 1966, Micropaleontology of the Mesozoic rocks of northern Alaska: U.S. Geological Survey Professional Paper 302–D, p. 93–227, 12 pl., https://doi.org/10.3133/pp302D.

Bird, K.J., 1988, Structure-contour and isopach maps of the National Petroleum Reserve in Alaska, chap. 16 *of* Gryc, G., ed., Geology and exploration of the National Petroleum Reserve in Alaska, 1974 to 1982: U.S. Geological Survey Professional Paper 1399, p. 355–377, 57 pl., https://doi.org/10.3133/pp1399.

Bird, K.J., Burruss, R.C., and Pawlewicz, M.J., 1999, Thermal maturity, chap. VR *of* ANWR Assessment Team, ed., The oil and gas resource potential of the Arctic National Wildlife Refuge 1002 area, Alaska: U.S. Geological Survey Open-File Report 98–34, p. VR1–VR64, https://doi.org/10.3133/ofr9834.

Bodnar, D.A., 1984, Stratigraphy, age, depositional environments, and hydrocarbon source rock evaluation of the Otuk Formation, north-central Brooks Range, Alaska: Fairbanks, University of Alaska Fairbanks, Master's thesis, 232 p.

Brosgé, W.P., Reiser, H.N., Dutro, J.T., Jr., Detterman, R.L., and Tailleur, I.L., 2001, Geologic map of the Arctic quadrangle: U.S. Geological Survey Geological Investigations Series I–2673, 2 sheets, scale 1:250,000, 38-p. pamphlet, https://doi.org/10.3133/i2673.

Camber, W., 1994, Stratigraphy and depositional environments of Lower Cretaceous strata, western Bathtub Ridge, northeastern Brooks Range, Alaska: Fairbanks, University of Alaska Fairbanks, Master's thesis, 158 p.

Cathcart, J.B., 1991, Phosphate deposits of the United States—Discovery, development; Economic geology and outlook for the future, *in* Gluscoter, H.J., Rice, D.D., and Taylor, R.B., eds., Economic geology, v. P–2 *of* The geology of North America: Boulder, Colo., Geological Society of America, p. 153–164, https://doi.org/10.1130/DNAG-GNA-P2.153.

Cole, F., Bird, K.J., Mull, C.G., Wallace, W.K., Sassi, W., Murphy, J.M., and Lee, M.W., 1999, A balanced cross section and kinematic and thermal model across the northeastern Brooks Range mountain front, Arctic National Wildlife Refuge, Alaska, chap. SM *of* ANWR Assessment Team, eds., The oil and gas resource potential of the Arctic National Wildlife Refuge 1002 area, Alaska: U.S. Geological Survey Open-file Report 98–34, p. SM-1–SM-60, https://doi.org/10.3133/ofr9834.

Colpron, M., and Nelson, J.L., 2011, A Palaeozoic NW passage and the Timanian, Caledonian and Uralian connections of some exotic terranes in the North American Cordillera, chap. 31 *of* Spencer, A.M., Embry, A.F., Gautier, D.L., Stoupakova, A.V., and Sørensen, K., eds., Arctic Petroleum Geology: Geological Society of London Memoirs, v. 35, no. 1, p. 463–484, https://doi.org/10.1144/M35.31.

Compton, J.S., and Bergh, E.W., 2016, Phosphorite deposits on the Namibian shelf: Marine Geology, v. 380, p. 290–314, https://doi.org/10.1016/j.margeo.2016.04.006.

Dal Corso, J., Gianolla, P., Rigo, M., Franceschi, M., Roghi, G., Mietto, P., Manfrin, S., Raucsik, B., Budai, T., Jenkyns, H.C., Reymond, C.E., Caggiati, M., Gattolin, G., Breda, A., Merico, A., and Preto, N., 2018, Multiple negative carbon-isotope excursions during the Carnian Pluvial Episode (Late Triassic): Earth-Science Reviews, v. 185, p. 732–750, https://doi.org/10.1016/j.earscirev.2018.07.004.

Detterman, R.L., 1970, Analysis of Shublik Formation rocks from Mt. Michelson quadrangle: U.S. Geological Survey Open-File Report 70–101, 1-p. pamphlet, 3 pl., https://doi.org/10.3133/ofr70101.

Detterman R.L., Reiser, H.N., Brosgé, W.P., and Dutro, J.T., Jr., 1975, Post-Carboniferous stratigraphy, northeastern Alaska: U.S. Geological Survey Professional Paper 886, 46 p., https://doi.org/10.3133/pp886.

Dumoulin, J.A., Burruss, R.C., and Blome, C.D., 2013, Lithofacies, age, depositional setting, and geochemistry of the Otuk Formation in the Red Dog District, northwestern Alaska, *in* Dumoulin, J.A., and Dusel-Bacon, C., eds., Studies by the U.S. Geological Survey in Alaska, 2011: U.S. Geological Survey Professional Paper 1795–B, 32 p., https://doi.org/10.3133/pp1795B.

Dumoulin, J.A., Whidden, K.J., and Rouse, W.A., 2020 Triassic phosphatic rocks of northern Alaska—Spatial and temporal depositional patterns on a high-latitude, low-angle ramp, northwest Laurentian margin (abs.), *in* Cordilleran Tectonics Workshop, Anchorage, Alaska, February 21–23, 2020, Program and Abstracts: p. 16–17, accessed June 13, 2023, at https://cordillerantectonics.com/wp-content/uploads/2020/02/ctw2020_program_abstracts-1.pdf.

Dumoulin, J.A., Whidden, K.J., Rouse, W.A., and DeVera, C., 2023, Geochemical data from selected Triassic rock samples in northeastern Alaska: U.S. Geological Survey data release, https://doi.org/10.5066/P9FAGE8O.

Dumoulin, J.A., Whidden, K.J., Rouse, W.A., Lease, R., Boehlke, A., and O'Sullivan, P., 2022, Biosiliceous, organic-rich, and phosphatic facies of Triassic strata of northwest Alaska—transect across a high-latitude, low-angle continental margin, *in* Aiello, I.W., Barron, J.A., and Ravelo, A.C., eds., Understanding the Monterey Formation and similar biosiliceous units across space and time: Boulder, Colo., Geological Society of America Special Paper 556, p. 243–271, https://doi.org/10.1130/2022.2556(11).

Embry, A.F., Krajewski, K.P., and Mørk, A., 2002, A Triassic upwelling zone—The Shublik Formation, Arctic Alaska, U.S.A.—Discussion: Journal of Sedimentary Research, v. 72, no. 5, p. 740–741, https://doi.org/10.1306/032102720740.

Folk, R.L., 1959, Practical petrographic classification of limestones: American Association of Petroleum Geologists Bulletin, v. 43, no. 1, p. 1–38, https://doi.org/10.1306/0BDA5C36-16BD-11D7-8645000102C1865D.

Folk, R.L., 1965, Some aspects of recrystallization in ancient limestones, *in* Pray, L.C., and Murray, L.C., eds., Dolomitization and limestone diagenesis—A symposium: SEPM The Society for Sedimentary Geology Special Publication 13, p. 14–38, https://doi.org/10.2110/pec.65.07.0014.

Föllmi, K.B., 1996, The phosphorus cycle, phosphogenesis and marine phosphate-rich deposits: Earth-Science Reviews, v. 40, no. 1–2, p. 55–124, https://doi.org/10.1016/0012-8252(95)00049-6.

Grasby, S.E., Beauchamp, B., and Knies, J., 2016, Early Triassic productivity crises delayed recovery from world's worst mass extinction: Geology, v. 44, no. 9, p. 779–782, https://doi.org/10.1130/G38141.1.

Haq, B.U., and Schutter, S.R., 2008, A chronology of Paleozoic sea-level changes: Science, v. 322, no. 5898, p. 64–68, https://doi.org/10.1126/science.1161648.

Hiatt, E.E., and Budd, D.A., 2003, Extreme paleoceanographic conditions in a Paleozoic oceanic upwelling system—Organic productivity and widespread phosphogenesis in the Permian Phosphoria Sea, *in* Chan, M.A., and Archer, A.W., eds., Extreme depositional environments—Mega end members in geologic time: Boulder, Colo., Geological Society of America Special Paper 370, p. 245–264, https://doi.org/10.1130/0-8137-2370-1.245.

Homza, T.X., Fillerup, M.A., and Gardner, D.W., 2020, Toward a better understanding of northern Alaska's petroleum systems—Deconstructing the Barrow arch: American Association of Petroleum Geologists Bulletin, v. 104, no. 8, p. 1793–1816, https://doi.org/10.1306/04072019139.

Hosford Scheirer, A., and Bird, K.J., 2020, A lateral well in the Shublik Formation, Alaska North Slope, with implications for unconventional resource potential: Interpretation, v. 8, no. 2, p. SJ35–SJ49, https://doi.org/10.1190/INT-2019-0186.1.

Houseknecht, D.W., 2019, Evolution of the Arctic Alaska sedimentary basin, chap.18 *of* Miall, A.D., ed., Sedimentary basins of the United States and Canada (2d ed.): Elsevier, p. 719–745, https://doi.org/10.1016/B978-0-444-63895-3.00018-8.

Houseknecht, D.W., Rouse, W.A., Garrity, C.P., Whidden, K.J., Dumoulin, J.A., Schenk, C.J., Charpentier, R.R., Cook, T.A., Gaswirth, S.B., Kirschbaum, M.A., and Pollastro, R.M, 2012, Assessment of potential oil and gas resources in source rocks of the Alaska North Slope: U.S. Geological Survey Fact Sheet 2012–3013, 2 p., https://doi.org/10.3133/fs20123013.

Hubbard, R.J., Edrich, S.P., and Rattey, R.P., 1987, Geologic evolution and hydrocarbon habitat of the 'Arctic Alaska Microplate': Marine and Petroleum Geology, v. 4, no. 1, p. 2–34, https://doi.org/10.1016/0264-8172(87)90019-5.

Hulm, E.J., 1999, Subsurface facies architecture and sequence stratigraphy of the Eileen Sandstone, Shublik Formation, and Sag River Sandstone, Arctic Alaska: Fairbanks, University of Alaska Fairbanks, Master's thesis, 105 p.

Hutton, E.M., 2014, Surface to subsurface correlation of the Shublik Formation—Implications for Triassic paleoceanography and source rock accumulation: Fairbanks, University of Alaska Fairbanks, Master's thesis, 113 p, accessed June 13, 2023, at http://hdl.handle.net/11122/4565.

James, N.P., 1997, The cool-water carbonate depositional realm, *in* James, N.P., and Clarke, J.A.D., eds., Cool-water carbonates: SEPM Society for Sedimentary Geology Special Publication, v. 56, p. 1–20, https://doi.org/10.2110/pec.97.56.0001.

James, N.P., and Jones, B.G., 2016, The cool-water neritic realm, chap. 11 *of* James, N.P., and Jones, B.G., eds., Origin of carbonate sedimentary rocks: John Wiley & Sons, American Geophysical Union, p. 135–149.

Kelly, L.N., 2004, High resolution sequence stratigraphy and geochemistry of Middle and Upper Triassic sedimentary rocks, northeast and central Brooks Range, Alaska: Fairbanks, Alaska, University of Alaska, Master's thesis, 224 p., accessed June 13, 2023, at http://hdl.handle.net/11122/6013.

Kelly L.N., Whalen, M.T., McRoberts, C.A., Hopkin, E., and Tomsich, C.S., 2007, Sequence stratigraphy and geochemistry of the upper Lower through Upper Triassic of northern Alaska—Implications for paleoredox history, source rock accumulation, and paleoceanography: State of Alaska Department of Natural Resources, Division of Geological and Geophysical Surveys Report of Investigations 2007-1, 46 p., https://doi.org/10.14509/15773.

Knox, A.R., 2018, Petrographic and microfacies analysis of the Shublik Formation, northern Alaska—Implications for an unconventional resource system: Fairbanks, University of Alaska Fairbanks, Master's thesis, 109 p., accessed June 13, 2023, at http://hdl.handle.net/11122/9669.

Krajewski, K.P., 2008, The Botneheia Formation (Middle Triassic) in Edgeøya and Barentsøya, Svalbard—Lithostratigraphy, facies, phosphogenesis, paleoenvironment: Polish Polar Research, v. 29, no. 4, p. 319–364, accessed June 13, 2023, at https://citeseerx.ist.psu.edu/document?repid=rep1&type=pdf&doi=8ab1828c4f15c775b9df05ab69600a31490b9a34.

Kupecz, J.A., 1995, Depositional setting, sequence stratigraphy, diagenesis, and reservoir potential of a mixed lithology, upwelling deposit—Upper Triassic Shublik Formation, Prudhoe Bay, Alaska: American Association of Petroleum Geologists Bulletin, v. 79, no. 9, p. 1301–1319, https://doi.org/10.1306/7834D4AE-1721-11D7-8645000102C1865D.

Leffingwell, E., 1919, The Canning River region, northern Alaska: U.S. Geological Survey Professional Paper 109, 6 sheets, scale variable, 251-p. pamphlet, https://doi.org/10.3133/pp109.

McRoberts, C.A., 2010, Biochronology of Triassic bivalves, *in* Lucas, S.G., ed., The Triassic Timescale: Geological Society of London Special Publications 334, no. 1, p. 201–219, https://doi.org/10.1144/SP334.9.

McRoberts, C.A., Blodgett, R.B., and Bird, K.J., 2020, Middle and Upper Triassic bivalve biostratigraphy of the Shublik Formation from the Tenneco Phoenix #1 well, offshore central North Slope, Arctic Alaska, *in* Lucas, S.G., Hunt, A.P., and Lichtig, A.J., eds., Fossil Record 7, New Mexico Museum of Natural History and Science Bulletin 82, p. 259–274, accessed June 13, 2023, at http://faculty.cortland.edu/paleo-lab/wp-content/uploads/sites/39/2021/10/McRoberts_etal_2021_sm.pdf.

Moore, T.E., 1999, Balanced cross section, Bathtub syncline to Beaufort Sea through Niguanak structural high, Arctic National Wildlife Refuge (ANWR), northeastern Alaska, chap. BC *of* ANWR Assessment Team, ed., The oil and gas resource potential of the Arctic National Wildlife Refuge 1002 area, Alaska: U.S. Geological Survey Open-file Report 98–34, p. BC-1–BC-61, https://doi.org/10.3133/ofr9834.

Moore, T.E., Wallace, W.K., Bird, K.J., Karl, S.M., Mull, C.G., and Dillon, J.T., 1994, Geology of northern Alaska, *in* Plafker, G., and Berg, H.C., eds., The geology of Alaska, v. G-1 *of* The geology of North America: Boulder, Colo., Geological Society of America p. 49–140, https://doi.org/10.1130/DNAG-GNA-G1.49.

Ogg, J.G., Chen, Z.-Q, Orchard, M.J., and Jiang, H.S, 2020, The Triassic Period, *in* Gradstein, F.M., Ogg, J.G., Schmitz, M.D. and Ogg, G.M., eds., Geologic time scale 2020: Elsevier, 903–953, https://doi.org/10.1016/B978-0-12-824360-2.00025-5.

Parrish, J.T., Droser, M.L., and Bottjer, D.J., 2001a, A Triassic upwelling zone—The Shublik Formation, Arctic Alaska, U.S.A.: Journal of Sedimentary Research, v. 71, no. 2, p. 272–285, https://doi.org/10.1306/052600710272.

Parrish, J.T., Droser, M.L., and Bottjer, D.J., 2002, A Triassic upwelling zone—the Shublik Formation, Arctic Alaska, U.S.A.—Reply: Journal of Sedimentary Research, v. 72, no. 5, p. 742–743, https://doi.org/10.1306/032102720742.

Parrish, J.T., Whalen, M.T., and Hulm, E.J., 2001b, Shublik Formation lithofacies, environments, and sequence stratigraphy, Arctic Alaska, U.S.A., *in* Houseknecht, D.W., ed., Petroleum plays and systems in the National Petroleum Reserve—Alaska (NPRA): Society for Sedimentary Geology Core Workshop 21, p. 89–110, https://doi.org/10.2110/cor.01.01.0089.

Patton, W.W., Jr., and Matzko, J.J., 1959, Phosphate deposits in northern Alaska: U.S. Geological Survey Professional Paper 302–A, 17 p., 4 pl., https://doi.org/10.3133/pp302A.

Peters, K.E., Magoon, L.B., Bird, K.J. Valin, Z.C., and Keller, M.A., 2006, North Slope, Alaska—Source rock distribution, richness, thermal maturity, and petroleum charge: American Association of Petroleum Geologists Bulletin, v. 90, no. 2, p. 261–292, https://doi.org/10.1306/09210505095.

Prauss, M.L., 2007, Availability of reduced nitrogen chemospecies in photic-zone waters as the ultimate cause for fossil prasinophyte prosperity: Palaios, v. 22, no. 5, p. 489–499, https://doi.org/10.2110/palo.2005.p05-095r

Pufahl, P.K., and Grimm, K.A., 2003, Coated phosphate grains—Proxy for physical, chemical, and ecological changes in seawater: Geology, v. 31, no. 9, p. 801–804, https://doi.org/10.1130/G19658.1.

Pufahl, P.K., and Groat, L.A., 2017, Sedimentary and igneous phosphate deposits—Formation and exploration—An invited paper: Economic Geology v. 112, no. 3, p. 483–516, https://doi.org/10.2113/econgeo.112.3.483.

Reed, B. L., 1968, Geology of the Lake Peters area, northeastern Brooks Range: U.S. Geological Survey Bulletin 1236, 132 p., 4 pl., scale variable, https://doi.org/10.3133/b1236.

Riediger, C.L., 1997, Geochemistry of potential hydrocarbon source rocks of Triassic age in the Rocky Mountain Foothills of northeastern British Columbia and west-central Alberta: Bulletin of Canadian Petroleum Geology, v. 45, no. 4, p. 719–741.

Rouse, W.A., Whidden, K.J., Dumoulin, J.A., and Houseknecht, D.W., 2020, Surface to subsurface correlation of the Middle–Upper Triassic Shublik Formation within a revised sequence stratigraphic framework: Interpretation, v. 8, no. 2, p. SJ1–SJ16, https://doi.org/10.1190/INT-2019-0195.1. [Correction available at https://doi.org/10.1190/INT-2020-0521-ERRATUM.1.]

Scotese, C.R., 2002, PALEOMAP Project: C.R. Scotese, accessed October 28, 2022, at http://www.scotese.com.

Scott, C., and Lyons, T.W., 2012, Contrasting molybdenum cycling and isotopic properties in euxinic versus non-euxinic sediments and sedimentary rocks–Refining the paleoproxies: Chemical Geology, v. 324–325, p. 19–27, https://doi.org/10.1016/j.chemgeo.2012.05.012.

Sherwood, K.W., Johnson, P.P., Craig, J.D., Zerwick, S.A., Lothamer, R.T, Thurston, D.K., and Hurlbert, S.B., 2002, Structure and stratigraphy of the Hanna Trough, U.S. Chukchi Shelf, Alaska, *in* Miller, E.L., Grantz, A., and Klemperer, S.L., eds., Tectonic evolution of the Bering Shelf–Chukchi Sea–Arctic Margin and adjacent landmasses: Boulder, Colo., The Geological Society of America Special Paper 360, p. 39–66, https://doi.org/10.1130/0-8137-2360-4.39.

Silberling, N.J., Grant-Mackie, J.A., and Nichols, K.M., 1997, The Late Triassic bivalve *Monotis* in accreted terranes of Alaska: U.S. Geological Survey Bulletin 2151, 21 p.

Slack, J.F., McAleer, R.J., Shanks, W.C., III, and Dumoulin, J.A., 2021, Diagenetic barite-pyrite-wurtzite formation and redox signatures in Triassic mudstone, Brooks Range, northern Alaska: Chemical Geology, v. 585, https://doi.org/10.1016/j.chemgeo.2021.120568.

Sohn, I.G., 1987, Middle and Upper Triassic marine Ostracoda from the Shublik Formation, northeastern Alaska, chap. C *of* Yochelson, E.L., ed., Shorter contributions to paleontology and stratigraphy: U.S. Geological Survey Bulletin 1664, p. C1–C24, https://doi.org/10.3133/b1664.

Strasser, A., 2015, Hiatuses and condensation—An estimation of time lost on a shallow carbonate platform: The Depositional Record, v. 1, no. 2, p. 91–117, https://doi.org/10.1002/dep2.9.

Tourtelot, H.A., and Tailleur, I.L., 1971, The Shublik Formation and adjacent strata in northeastern Alaska; description, minor elements, depositional environments and diagenesis: U.S. Geological Survey Open File Report 71–284, 62 p, 1 pl., https://doi.org/10.3133/ofr71284.

Trappe, J., 1994, Pangean phosphorites—Ordinary phosphorite genesis in an extraordinary world?, *in* Embry, A.F., Beauchamp, B., and Glass, D.J., eds., Pangea—Global Environments and Resources: Canadian Society of Petroleum Geologists Memoir 17, p. 469–478.

Trappe, J., ed., 1998, Phanerozoic phosphorite depositional systems—A dynamic model for a sedimentary resource system, *in* volume 76 *of* Lecture notes in Earth sciences: Berlin, Springer-Verlag, 316 p., https://doi.org/10.1007/BFb0009673.

Tucker, M., 2011, Ooids, *in* Hopley, D., ed., Encyclopedia of modern coral reefs, structure form and process, part *of* Encyclopedia of Earth sciences series: Dordrecht, Springer, p. 752, https://doi.org/10.1007/978-90-481-2639-2_237.

Vigran, J.O., Mørk, A., Forsberg, A.W., Weiss, H.M., and Weitschat, W., 2008, *Tasmanites* algae—Contributors to the Middle Triassic hydrocarbon source rocks of Svalbard and the Barents Shelf: Polar Research, v. 27, no. 3, p. 360–371, https://doi.org/10.1111/j.1751-8369.2008.00084.x.

Walker, J.D., and Geissman, J.W., compilers, 2022, Geologic time scale v. 6.0: Boulder, Colo., Geological Society of America, https://doi.org/10.1130/2022.CTS006C.

Watts, K.F., Harris, A.G., Carlson, R.C., Eckstein, M.K., Gruzlovic, P.D., Imm, T.A., Krumhardt, A.P., Lasota, D.K., Morgan, S.K., Enos, P., Goldstein, R., Dumoulin, J.A., and Mamet, B., 1994, Analysis of reservoir heterogeneities due to shallowing-upward cycles in carbonate rocks of the Upper Mississippian and Pennsylvanian Wahoo limestone of northeastern Alaska—Final report: U.S. Department of Energy Technical Report DOE/BC/14471-11 under contract DE–AC22–89BC14471, prepared by the University of Alaska, Fairbanks, Tectonics and Sedimentation Research Group, Department of Geology and Geophysics, Geophysical Institute, 433 p.

Whidden, K.J., Birdwell, J.E., Dumoulin, J.A., Fonteneau, L.C., and Martini, B.A., 2019a, Integration of microfacies analysis, inorganic geochemical data and hyperspectral imaging to unravel mudstone depositional and diagenetic processes in two cores from the Triassic Shublik Formation, northern Alaska, *in* Unconventional Resources Technology Conference: Unconventional Resources Technology Conference Denver, Colo., July 22–24, 2019, https://doi.org/10.15530/urtec-2019-445.

Whidden, K.J., Dumoulin, J.A., and Rouse, W.A., 2018, A revised Triassic stratigraphic framework for the Arctic Alaska basin: American Association of Petroleum Geologists Bulletin, v. 102, no. 7, p. 1171–1212, https://doi.org/10.1306/0726171616517250.

Whidden, K.J., Dumoulin, J.A., Macquaker, J., Birdwell, J., Boehlke, A., and French, K.L., 2019b, Element cycling in the Middle to Upper Triassic Shublik Formation—Mineralization vs. recycling of biolimiting nutrients in an unconventional resource play, *in* 2019 Gussow Conference, New Directions in Geosciences for Unconventional Resources, Banff, Canada, October 15–17, 2019: Canadian Society of Petroleum Geologists, 11 p., accessed June 13, 2023, at https://www.cspg.org/common/Uploaded%20files/pdfs/documents/conference_website/gussow/archives/2019/Session%201/2-Whidden.pdf.

Wotzlaw, J.-F., Guex, J., Bartolini, A., Gallet, Y., Krystyn, L., McRoberts, C.A., Taylor, D., Schoene, B., and Schaltegger, U., 2014, Towards accurate numerical calibration of the Late Triassic: High-precision U-Pb geochronology constraints on the duration of the Rhaetian: Geology, v. 42, no. 7, p. 571–574, https://doi.org/10.1130/G35612.1.

Moffett Field Publishing Service Center, California
Manuscript approved April, 11, 2024
Edited by Claire Ashcraft and Phil Frederick
Layout by Kimber Petersen

ISSN 2330-7102 (online)
https://doi.org/10.3133/pp1814H